Title
Dysfunction of Circadian System in a Mouse Model of Rett Syndrome

Author
Li, Quan

Publication Date
2014

Peer reviewed|Thesis/dissertation

UNIVERSITY OF CALIFORNIA

Los Angeles

Dysfunction of Circadian System in a Mouse Model of Rett Syndrome

A dissertation submitted in partial satisfaction of the

requirements for the degree Doctor of Philosophy in

Molecular, Cellular and Integrative Physiology

by

Quan Li

2014

ABSTRACT OF THE DISSERTATION

Dysfunction of Circadian System in a Mouse Model of Rett Syndrome

By

Quan Li

Doctor of Philosophy in

Molecular, Cellular and Integrative Physiology

University of California, Los Angeles, 2014

Professor Christopher S. Colwell, Co-chair

Professor Yi E. Sun, Co-chair

Rett Syndrome (RTT) is a severe X-chromosome-linked neurological disorder and worldwide represents the second leading genetic cause of intellectual disabilities in females. The majority of RTT cases are caused by the mutations in *MECP2* gene encoding methyl-CpG-binding protein 2 (MeCP2) and sleep disturbances with abnormal sleep/wake cycles are prevalent in RTT patients indicating a deficit in their circadian timing system.

Hemizygous *Mecp2*$^{-/y}$ mice were examined to determine the disruption of circadian system and the potential underlying mechanisms caused by MeCP2 dysfunction. *Mecp2*$^{-/y}$ mice exhibited severe deficits in circadian rhythms of locomotor activity and temporal pattern of daily activity combined with extremely fragmented sleep behavior. Moreover, spontaneous electrical

activity and molecular core clock components were significantly attenuated within the SCN suggesting the weakened central clockwork. Peripheral organs also showed disrupted molecular core clock expression suggesting the disorganized peripheral oscillators. ChIP-qPCR study using *Mecp2*$^{-/y}$ MEFs revealed a loss of rhythmic binding pattern of histone markers at the clock gene promoter regions due to the loss of MeCP2. In addition, RTT individual fibroblasts exhibited abnormal core clock gene expression and *Mecp2*$^{-/y}$ mice were vulnerable due to the destabilized circadian system causing a shortened lifespan. These data strongly indicated an essential role of MeCP2 in circadian timing system and revealed the importance of stabilization of circadian system and sleep/wake cycles during the clinical care of RTT individuals.

Currently there is no cure for RTT patients. A small molecule, 7,8-Dihydroxyflavone (7,8-DHF) was recently identified to be a potent TrkB receptor agonist that mimicked BDNF functions as a potential therapeutic intervention for RTT treatment. Systematic administration of 7,8-DHF activated the phosphorylation of TrkB receptors and generated robust downstream Akt phorphorylation in wild-type mouse cortex and hippocampus tissues. Although systematic administration of 7,8-DHF did not significantly rescue the life span of the *Mecp2*$^{-/y}$ mutants, incubation of cortical slices with 7,8-DHF *in vitro* significantly increased the spontaneous firing rate of L5 pyramidal neurons of *Mecp2*$^{-/y}$ mutant mice. Taken together, these data suggested that 7,8-DHF rescued the physiological defect caused by the absence of MeCP2 and raised the possibility that it could be therapeutically useful for RTT treatment.

The dissertation of Quan Li is approved.

Gene D. Block

Carlos Portera-Cailliau

James Waschek

Christopher S. Colwell, Committee Co-chair

Yi E. Sun, Committee Co-chair

University of California, Los Angeles

2014

DEDICATIONS

To my parents, my husband, my sweet girl and lovely boy

Thanks for your endless love, belief, encouragement and unconditional support throughout my life

TABLE OF CONTENTS

LIST OF FIGURES

LIST OF TABLES

ACKNOWLEDGMENTS

Pursing a Ph.D was one of the most important decisions I have ever made and became the most challenging and greatest learning experience in my life so far. First of all, I'm incredibly thankful to my supervisor Dr. Yi Eve Sun, who has generously provided me this training opportunity in your lab for my graduate study. You have greatly inspired me with your passion for science, unusual creativity, enthusiasm and positive attitude during these past years. I have learned so much from you, not only in the scientific field, but also for my spiritual wellness. You have shared with us regarding the power originating from positive thinking that will gradually build inner strength and eventually facilitate people to achieve success in life. Hopefully I have really got to know how to practice it in my daily life so that I could always stay optimistically for future challenges.

I am tremendously thankful to Dr. Christopher Colwell as my mentor during the graduate training. This dissertation would not have been completed without your scientific guidance and constant encouragement. You're truly a great mentor and one of role models always having the positive influence on people around you. I'm so grateful for your continuous support both scientifically and emotionally for my graduate training. Also I'm especially thankful for you providing such a stimulating, interacting and friendly laboratory working atmosphere. It's truly been a great pleasure and wonderful experience to work with you.

I sincerely thank other members of my dissertation committee: Dr. Gene Block, Dr. Carlos Portera-Cailliau and Dr. James Waschek; for your interests, for valuable discussion at committee meetings, and for critical comments on this project. A special thank you goes to Carlos. I extremely appreciate your time, constant support and kind encouragement during the past year! I have learned and also benefited so much from your professional and personal advice.

This dissertation would not have been possible without the collaboration and contribution of many people from both the Colwell lab and Sun lab. I feel very fortunate to have worked together with Dr. Down Loh during my graduate career. We have had numerous conversations and exciting discussions sharing scientific ideas. Thank you for always being so patient to my endless questions, and I'm very grateful for your scientific knowledge, expertise and dedication to science as well as professional support. Other lab members have also contributed significantly with their work presented in this dissertation and provided their help along the way: Dr. Takashi Kudo (SCN electrophysiology), Danny Truong and Matthew Derakhshesh (behavior and sleep analysis), Zoë MacDowell Kaswan (immunohistochemistry), Dr. Rosemarie Tsoa and Dr. Yin Cheng (ChIP-qPCRs) as well as Dr. Weizheng Wei (electrophysiology in Chapter 3). Part of Chapter 2 is a version of manuscript: Quan Li*, Dawn H Loh*, Takashi Kudo, Danny Truong, Matthew Derakhshesh, Zoë MacDowell Kaswan, Rosemarie Tsoa, Yin Cheng, Yi Sun, Christopher S Colwell. Circadian rhythm disruption in a mouse model of Rett syndrome 2014 Submitted. Chapter 3 is a version of manuscript in preparation: Quan Li, Weizheng Wei, Yi E. Sun. Effect of 7,8-dihydroxyflavone in a mouse model of Rett Syndrome.

I must thank Dr. James Tidball, director of the Molecular, Cellular, and Integrative Physiology (MCIP) Program for offering me this incredible training opportunity and also for providing training grant and financial support for me during my early years within the program. Your guidance and vigorous efforts on leading student seminars and program retreats are very much appreciated as it's been a great learning and social experience to me for being part of it.

I would like to thank many of current and former members from the Sun lab and Colwell lab I have worked with for being part of this journey: Weihong Ge, Quan Lin, Volkan Coskun, Yin Cheng, Rosemarie Tsoa, Jun Kyoma, Bruno Blanchi, Dika Kuljis, Analyn Schroeder and

Tamara Cutler. In particular, the journal clubs of both labs are well organized with lots of discussion and I have definitely benefited a huge amount from them.

I would not be where I am at this moment without my family members and my best friends! I believe you should be proud of what we have accomplished together so far. Thanks my parents, Peizhi Zhao and Chengjun Li for endless love and support for no matter what my decisions would be. My deepest thanks go to my husband, Weizheng for all you've have done to help and support me during these past years. To my daughter, Katherine and my boy, Kelvin−You are really the foundation of my strength and have brought a lot of sunshine, laughter and happiness into my world. I am also very lucky to have such good friends in my life at LA: Shanping Chen, Katty Cai, Diancai Cai, Sophia Chang and Chunyan Liu. Thanks for your time, listening, sharing, encouragement, advice and moral support in every important moment. You're really part of my life and my heart is filled with joy and gratitude to all of you.

Vita

Education and Previous employment

2010--2014	Teaching assistant
	Life science Division & Departments of Physiological Science
	UCLA
2000--2008	Research associate
	Department of Physiological Science
	UCLA
2001--2003	Teaching assistant
	Summer course in Marine Biology Laboratory, Woodshole
1999	M.S., Neuroscience
	Tonji Medical University, Wuhan, Hubei, China
1994--1996	Lecturer
	Department of Physiology
	Tongji Medical University Wuhan, Hubei, China
1994	M.D., Clinical Medicine
	Tonji Medical University, Wuhan, Hubei, China

Awards

2008--2010	NIH institutional predoctoral fellowship in MCIP
2003	Nomination for UCLA Chancellor's Award for Research
2002	UCLA Fine Science Tools Postdoctoral Scholar Award

Publications

Li Q*, Loh DH*, Truong D, Kudo T, Derakhshesh M, Tsoa R, Cheng Y, Sun Y, Colwell CS. 2014 Dysfunction of circadian system in a mouse model of Rett Syndrome. Submitted

Li Q, Wei WZ, Sun Y. Effect of 7,8-dihydroxyflavone in a mouse model of Rett Syndrome. In preparation.

Villareal G*, Li Q*, Cai D, Fink A, Lim T, Bougie J, Sossin WS, Glanman DL 2009 Role of protein kinase C in the induction and maintenance of serotonin-dependent enhancement of the glutamate response in isolated siphon motor neurons of *Aplysia Californica*. *Journal of Neuroscience* 29: 5100-5107 (*The first two authors contribute equally)

Villareal G*, Li Q*, Cai D, Glanzman DL 2007 The Role of Rapid, Local Postsynaptic Protein Synthesis in Learning-Related Synaptic Facilitation in Aplysia. *Current Biology* 17:2073-2080 (*The first two authors contribute equally)

Li Q*, Roberts AC*, Glanzman DL 2005 Synaptic facilitation and behavioral dishabituation in Aplysia: dependence on release of Ca^{2+} from postsynaptic intracellular stores, postsynaptic exocytosis, and modulation of postsynaptic AMPA receptor efficacy. *Journal of Neuroscience* 25:5623-37

Chitwood RA*, Li Q*, Glanzman DL. 2001 Serotonin facilitates AMPA-type responses in isolated siphon motor neurons of Aplysia in culture. *Journal of physiology* 534:501-10 (*The first two authors contribute equally)

Li Q, Xiao H, Li A, Zhang Z 2002 Effect of Aluminium on the maintenance of LTP in Hippocampal CA3 Area of Rats. Journal of Huazhong University of Science and Technology• Health Sciences 31(5): 483-486 (In Chinese)

CHAPTER 1

General Review of Rett Syndrome and MeCP2 Function

1.1 Rett Syndrome

Rett Syndrome (RTT; MIM312750) is a pervasive postnatal neurological disorder (Hagberg et al 1985, Rett 1966) and worldwide represents the second leading genetic cause of severe intellectual disabilities in females. RTT primarily affects girls with an incidence of 1:10,000-15,000 live births, with rare cases reported in males (Moog et al 2003), and is characterized by severe mental retardation, language and learning disabilities, repetitive stereotyped hand movements and development regression. RTT is a considered a monogenic neurological disorder as more than 95% of RTT individuals carry loss-of-function mutations in the X chromosome-linked gene encoding methyl-CpG-binding protein 2 (*MECP2*) (Amir et al 1999).

RTT Symptoms

RTT symptoms can differ substantially among patients, ranging from classical RTT, showing the typical RTT phenotypes, to patients with only some RTT features (atypical RTT). Even in typical RTT cases, not all the symptoms occur initially, but rather appear over time (Chahrour & Zoghbi 2007, Liyanage & Rastegar 2014). RTT clinical phenotypes comprise four stages of manifestation (**Fig 1.1**). Typical RTT patients appear to have a normal prenatal and perinatal period with achievements of appropriate milestones for the first 6-18 months of life before the onset of stage I (developmental stagnation). Subsequently, RTT children fail to continue meeting psychomotor milestones and exhibit major RTT phenotypes indicating neurological involvement, such as deceleration of head growth and microcephaly (reduced brain/head size) that usually appears by the second year of life, growth retardation, weight loss and muscle hypotonia. Then their syndromes continue to progress into stage II (developmental

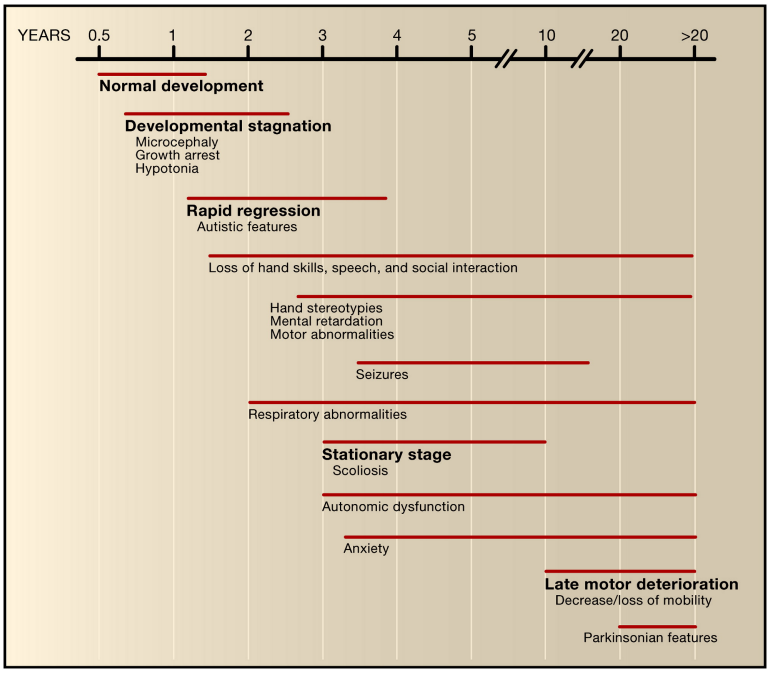

Figure 1.1 Onset and Progression of RTT Clinical Phenotypes

After a period of normal development, a healthy-looking baby girl falls into developmental stagnation, followed by rapid deterioration, loss of acquired speech, and the replacement of purposeful use of the hands with incessant stereotypies, a characteristic of the syndrome. Patients also develop social behavior abnormalities and are often misdiagnosed as having autism. The condition worsens with loss of motor skills and profound cognitive impairment. In addition, patients also suffer from anxiety, seizures, and a host of autonomic abnormalities.

Permission to reuse figure from Chahrour & Zoghbi 2007

regression). This regression phase appears evident by a loss of previously acquired skills such as purposeful hand function, spoken language and communication skills (Lee et al 2013). Affected patients develop certain hallmark traits including continuous stereotypic hand wringing and washing movements with a decline of purposeful hand use. Social withdrawal, behavior abnormalities and loss of language also develop and become apparent in addition to respiratory dysfunction, disturbed sleeping patterns, and seizures (Neul et al 2010).

Other autistic features also manifest, such as: social withdrawal, diminished eye contact and inconsolable crying (Lee et al 2013, Nomura 2005). The onset of mental deterioration is accompanied by loss of motor coordination and the development of ataxia and gait apraxia. Stage III is mainly defined as pseudo-stationary period that follows the regression phase. Certain skills such as communication skills may be recovered in some patients. However, RTT Patients still suffer from scoliosis, anxiety episode and additional autonomic abnormalities during this period. During stage IV (late motor deterioration period), most girls with RTT lose mobility and are often wheelchair-bound since teenage years. As patients get older, they often develop Parkinsonian features. These conditions reach a plateau and some patients could survive up to their sixty or seventieth yearof life in a severely debilitated physical condition (Roze et al 2007).

RTT exhibits certain hallmark of phenotypes that differentiate this disorder from other neurodevelopmental disorder, such as autism. Other common features include sleep alterations in RTT individuals. Patients have disturbances in maintaining their daily sleep and wake cycle. For example, RTT individuals may have difficulty falling sleep. They may also suffer from frequent awakening during the middle of night and stay awake during the day (Carotenuto et al 2013, Nomura 2005). These dysfunctions in timing of sleep have a major impact on daily life quality of RTT patients and on the family members who care for them.

RTT in Males

RTT does not normally run in families. 95% of the RTT cases are spontaneously occurring as both affected males and females are symptomatic and fail to reproduce. Since *MECP2* is an X-linked gene, RTT is mainly found and reported in females as the gene is

inactivated on one X-chromosome during dosage compensation in females (Adler et al 1995). RTT affects males much more severely than females due to hemizygosity. The RTT male patients produce a range of severe symptoms, including neonatal encephalopathy, motor abnormalities, respiratory dysfunction and early death within 2 years of birth (Schule et al 2008).

Neuropathology of RTT

Two hallmarks of typical RTT neuropathology are represented by: 1) a reduction in neuronal soma size with decreased dendritic complexity; 2) microcephaly in several brain regions including cerebral cortex, hypothalamus, midbrain and cerebellum in RTT patients (Armstrong 2001, Armstrong 2005, Reiss et al 1993, Saywell et al 2006). Typical RTT neurons are smaller and more densely packed. RTT brain weight is not only decreased but also disproportionately smaller in certain brain regions. Furthermore, RTT individuals showed an abnormal increase in the number of immature olfactory neurons and decrease in the number of terminally differentiated olfactory neurons (Ronnett et al 2003). There was a significant reduction in the density of dendritic spines and in the size and complexity of dendritic trees in pyramidal neurons of RTT frontal cortex and hippocampus CA1 region (Chapleau et al 2009). Neurochemical studies from RTT patient cerebrospinal fluid and brain tissues indicated abnormalities in the expression of various neurotransmitters and trophic factors including acetylcholine, dopamine, serotonin, glutamate substance P and nerve growth factor (Weng et al 2011a). However, any supporting evidence of neuronal or glial cell atrophy, degeneration or cell death, demyelination or neuronal migration defects has not been detected or identified. Therefore, RTT is not considered a neurodegenerative disease (Armstrong 2005). In addition to phenotypes in CNS, both human RTT patients and RTT mouse models showed symptoms in

other organs such as breathing abnormalities, impaired cardiac function resulting in sudden death and reduced life span, bone problems as well as difficulties in feeding and malnutrition (Guideri & Acampa 2005, Motil et al 2012, Ramirez et al 2013).

X-chromosome inactivation (XCI)

X-chromosome inactivation (XCI) is thought to impact the RTT pathology and clinical severity. The XCI causes uneven expression of wild type and mutant *MECP2* alleles within the brain. Usually, only one of the two X chromosomes is active in each cell and the choice of which X chromosome is active is usually random. Therefore, a female with a *MECP2* mutation is typically mosaic, whereby half of her cells express the wide-type *MECP2* allele and the other half express the mutant *MECP2* allele. However in exceptional situations, cells with wild-type *MECP2* allele grow and survive better than cells with the mutant copy, leading to a nonrandom pattern of XCI, which therefore ameliorates the RTT neurological phenotypes and leads to phenotypic variability in females. Some female patients can be mildly affected or are almost asymptomatic carriers of *MECP2* mutations owing to a highly favorable skewed ratio of XCI (Chahrour & Zoghbi 2007, Guy et al 2011). Mouse model studies also support a skewed XCI towards the wild-type *Mecp2* allele. Intriguingly, wild-type cells in both *Mecp2* mutant and knockout mice expressed lower levels of MeCP2 protein than in wild-type mice (Braunschweig et al 2004). Therefore, the variability of behavioral phenotypes in MeCP2 female mice and RTT females could be caused by the mosaic expression of mutant MeCP2, XCI unbalanced pattern and reduced normal MeCP2 levels in wild-type cells (Calfa et al 2011b).

Neurodevelopmental or neurological disorder?

Rett Syndrome was primarily discovered as a progressive neurodevelopmental disorder because of the late onset and the typical regression phase. However, studies have suggested MeCP2 could be dispensable during early growth and differentiation (Chen et al 2001, Guy et al 2001, Schule et al 2008). In the absence of MeCP2 in both humans and mouse models, brain structures and the overall number of neurons appeared normal soon after birth. In addition, MeCP2 expression increases dramatically within postmitotic neurons during synaptogenesis indicating a function of MeCP2 required in maintenance of neuronal function rather than in the initial developmental period. Although these evidences support a role for MeCP2 in synapse formation during brain development, MeCP2-deficient mouse models suggest otherwise. For example, experiments (Guy et al 2007) described that reactivation of the *Mecp2* gene even at later stages in severely symptomatic animals can reverse neurological phenotypes that resemble clinical RTT features. These data indicate that the absence of MeCP2 in the early development stage does not irreversibly damage brain structure and function suggesting RTT is not strictly a neurodevelopmental disorder.

Furthermore, recent studies from three independent labs (Cheval et al 2012, McGraw et al 2011, Nguyen et al 2012) showed that the absence of *Mecp2* during different developmental stages including postnatal brain (at the age of 5 weeks) and mature adult brain (at the age of 8-10 weeks) consistently caused the appearance of RTT-like phenotypes and shortened lifespan. Remarkably, the late deletion of *Mecp2* in both hemizygous males and heterozygous females during their adult stages caused brain to shrink resulting in higher than normal neuronal cell density (Nguyen et al 2012). It is highly plausible that MeCP2 function is required for stabilization and maintenance of mature neuronal networks and proper MeCP2 levels need to be

maintained throughout the lifetime. These adult RTT mouse models strongly imply that RTT is a neurological disorder rather than a strictly neurodevelopmental disorder (Bedogni et al 2014, Liyanage & Rastegar 2014).

1.2 MeCP2 structure and expression

MECP2/Mecp2 gene is an X-chromosome linked gene that spans around 76kB in the

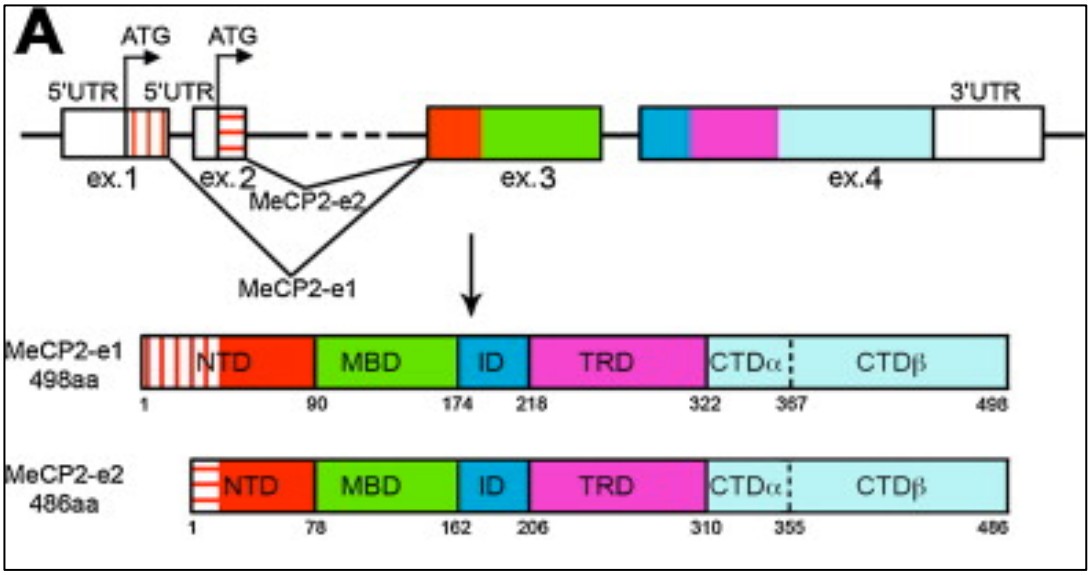

Fig 1.2 MeCP2 splicing and structure

Due to alternative splicing between exon 1 and exon 2, MeCP2 has two different isoforms (MeCP2-e1 and MeCP2-e2). MeCP2-e1 is 498 amino acids long and has 21 unique N-terminal residues (vertical red stripes). MeCP2-e2 is 486 amino acids long and has 9 unique residues (horizontal red stripes). The remaining protein sequence is common to both isoforms and can be divided in 6 domains: NTD (N-terminal domain), the MBD (methyl-CpG binding domain), the ID (intervening domain), the TRD (transcriptional repression domain), the CTDα and CTDβ (C-terminal domain).

Permission to reuse figure from Bedogni et al 2014

long arm of the chromosome (Xq28). MeCP2 (Methyl-CpG binding protein 2) is a basic nuclear protein with 486 residues belonging to Methyl-CpG Binding Protein (MBP) family that binds to methylated DNA sequence at cytosine 5'CpG through their Methyl-Binding Domain (MBD) (Lewis et al 1992). In both human and mouse, the *MECP2*/*Mecp2* gene comprises four exons (exon 1-4) and three introns (intron 1-3). MeCP2 protein structure (approximately 53 kDa in size **Fig. 1.2**) is composed of five major domains: N-terminal Domain (NTD); Methyl-CpG binding domain (MBD); Inter Domain (ID); Transcription Repression Domain (TRD) and C-terminal Domain (CTD).

MeCP2 Isoforms

Due to alternative splicing between exon 1 and 2, two different MeCP2 isoforms are generated: i) MeCP2e1, the longer isoform is encoded by exons 1,3 and 4 containing unique 21 amino acids residues at its N-terminus; ii) MeCP2e2 isoform; encoded by exons 2, 3 and 4 with 9 unique residues (Kriaucionis & Bird 2004). Except for their N-terminal regions, MeCP2 isoforms are similar and share the same functional domains, including MBD and TRD. Several studies suggested that both MeCP2 isoforms were very important in maintaining normal brain function and altered expression of both isoforms led to neurological complications (Jugloff et al 2008, Petel-Galil et al 2006). *Mecp2e1* is usually considered the major isoform in the adult mouse brain at mRNA level (Dragich et al 2007). Research studies with MeCP2 isoforms-specific antibodies suggested that MeCP2e1 was the major isoform in the brain (Zachariah et al 2012). Furthermore, there was relatively uniform in MeCP2e1 expression and differential enrichment expression in MeCP2e2 isoform within the same mouse brain regions including olfactory bulb, striatum, cortex, hippocampus, thalamus, and brainstem and cerebellum.

The same study also reported that in the adult female and male brain hippocampus, both MeCP2 isoforms were detected within the nucleus in neurons, astrocytes and oligodendrocytes (Olson et al 2014). These two isoforms have distinct expression patterns since MeCP2e1 is much more abundant than the e2 isoform in the postnatal brain. However, both isoforms are mainly considered functionally equivalent as RTT cases were not yet identified with mutations in the N-terminal regions (Itoh et al 2012, Shahbazian et al 2002b).

MeCP2 Expression

MeCP2 is widely expressed in many tissues, however appears to be most abundant in the brain (Shahbazian et al 2002b). As majority of RTT phenotypes are neurological, research studies are mainly focused on the brain-specific expression of MeCP2. In addition, brain-specific deletion of *Mecp2* at embryonic stage (E12) resulted in a phenotype identical to that of null mutation (Chen et al 2001, Guy et al 2001) indicating that the phenotype was caused by MeCP2 deficiency in the central nervous system (CNS) rather than in peripheral tissues. However, RTT symptoms from non-neuronal tissues including respiratory abnormalities, scoliosis and cardiac arrhythmia indicated the importance of MeCP2 expression and function outside the CNS (Guideri & Acampa 2005, Ogier & Katz 2008). Although MeCP2 was expressed in almost of all adult mouse brain regions including olfactory bulb, cortex, striatum, hippocampus, thalamus, cerebellum and brain stem, the highest expression was found in the cortex and cerebellum (Zachariah et al 2012). Furthermore, MeCP2 expression increased during brain development in several brain regions including cerebellum and olfactory bulb (Shahbazian et al 2002b). The neuronal MeCP2 level is relatively low during embryogenesis. Subsequently, it increases progressively during the postnatal stage of neuronal maturation (Kishi

& Macklis 2004, Skene et al 2010). Expression of MeCP2 develops progressively from deep cortical layers to superficial layers, suggesting a clear parallel between neuronal maturation and onset of MeCP2 expression increase.

MeCP2 Gain-of-Function and Duplication Syndrome

Recent RTT mouse models suggested that either overexpression or elimination of MeCP2 function had deleterious effects on synaptic and neuronal function. Loss- or gain-of-MeCP2 function affected dendrite formation and triggered bidirectional control in synaptic transmission in cortical and hippocampal regions of the brain (Na et al 2013). *In vitro* experiments showed that both overexpression and downregulation of MeCP2 levels in hippocampal and cortical cultures decreased dendritic arbor complexity and spine density (Chapleau et al 2009, Jiang et al 2013, Zhou et al 2006) although overexpression of MeCP2 was found to increase glutamatergic synapse number (Chao et al 2007). Miniature excitatory postsynaptic current (mEPSC) frequency was reported to be bidirectionally impacted by downregulated and upregulated MeCP2 expression with a positive correlation between levels of MeCP2 expression and spontaneous excitatory transmission (Na et al 2013). Finally, a tightly regulated expression of MeCP2 was found critically for neuronal homeostasis and long-term synaptic plasticity (Collins et al 2004, Na et al 2012). *MECP2* duplication syndrome was identified among male individuals (Ramocki et al 2010) and they appeared to correlate with the overexpression of MECP2 due to duplications of the Xq28 region (Na et al 2013). Thus, maintenance of MeCP2 in tightly defined concentration seems to be crucial for their proper function in CNS (Chao & Zoghbi 2012).

MeCP2 in Astrocytes and Microglia

Although earlier studies strongly indicated an exclusively role of MeCP2 underlying RTT pathogenesis, it was believed that other cells, such as glia, may play a major role in the disease. Astrocytes express less abundant MeCP2 relatively to neurons, however proper MeCP2 expression in astrocytes is essential for normal neuronal function. For example, the loss of MECP2 in glia negatively affected neurons in a non-cell-autonomous fashion. Furthermore, re-activation of MeCP2 expression only in astrocytes from constitutive MeCP2-deficient mice significantly improved locomotion and anxiety, restored respiratory dysfunction to a normal pattern, and greatly prolonged the lifespan compared to globally null mice (Ballas et al 2009). Re-expression of MeCP2 in the mutant astrocytes exerted non-cell-autonomous positive effects on mutant neurons *in vivo* and resulted in restoration of normal dendritic morphology (Lioy et al 2011). Moreover, researchers demonstrated that microglia cells affected the onset and progression of RTT phenotypes. The absence of MeCP2 in microglia caused neuronal excitotoxicity through release of abnormally high levels of glutamate (Maezawa & Jin 2010). To examine the impact of MeCP2 restoration in microglia during RTT pathophysiology, recent study showed that transplantation of either wild-type bone marrow or targeted expression of MeCP2 in bone marrow myeloid dramatically ameliorates typical RTT symptoms in MeCP2 null mice. These data have strongly supported the idea that wild-type MeCP2-expressing microglia within the context of RTT arrests the disease pathology (Derecki et al 2013, Derecki et al 2012). These research works strongly implicate astrocyte and microglia as major players in the pathophysiology of RTT and may open up a new avenue for RTT therapeutic treatments by targeting glia.

1.2 MeCP2 mutations and Rett Syndrome animals models

MeCP2 mutations

The majority of RTT cases occur generally by *de novo MECP2* mutations in the paternal origin of germ cells with extremely low risk of familial recurrence. More than 200 mutations in the *MECP2* gene have been identified in RTT individuals. These mutations are usually single point mutations in the coding sequences that result in a missense or nonsense mutant protein and cause a truncated form of the protein by altering a single amino acid. Eight of MECP2 mutations were commonly identified in RTT patients and occurred in regions that have been termed mutational "hotspots" (**Fig 1.3)**. These 8 mutation types (R106W, R133C, T158M, R168X, R255X, R270X R294Xnand R306C) caused by C>T transitions account for approximately 65% of *MECP2* mutations (Adkins & Georgel 2011, Percy & Lane 2005).

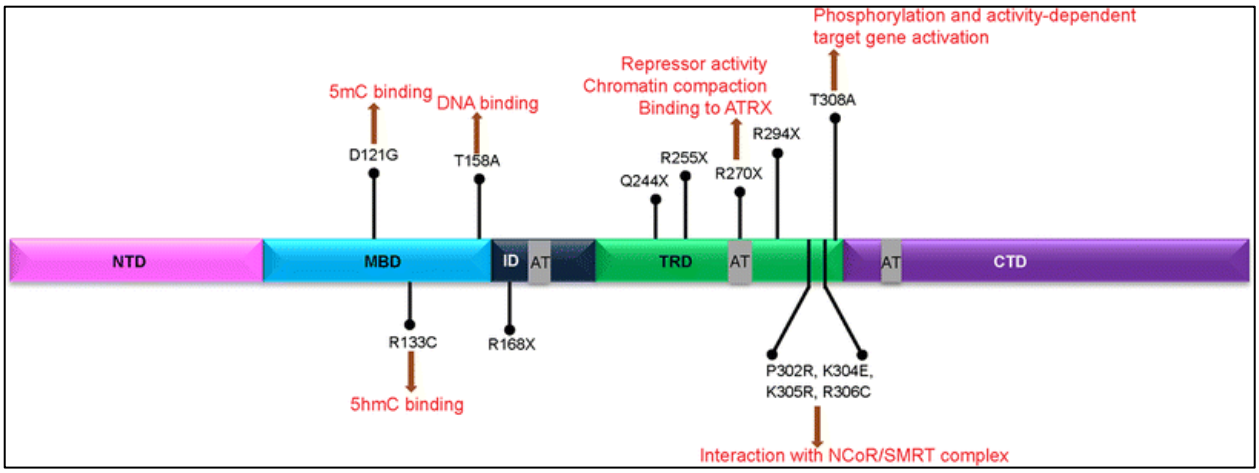

Fig 1.3 Distribution of known MeCP2 mutations and affected interactions/functions

The most common mutations identified in RTT patients and the abolished interactions and functions of MeCP2 due to MeCP2 mutation. The amino acid numbers are according to the location on MeCP2E2 isoform.

Permission to reuse figure from Liyanage & Rastegar 2014

RTT Mouse Models

Various different animal models have been established and thoroughly analyzed to study the role of MeCP2 in brain function as well as to understand the molecular and cellular bases of RTT pathogenesis. The most frequently characterized MeCP2-RTT mice models include constitutive *Mecp2* null knockout (*Mecp2*$^{tm1.1Bird}$; Bird strain), MeCP2 mutant mice expressing a truncated protein (Mecp2^{Jae}; Jaenisch strain), mice carrying well-known RTT associated *MECP2* mutations (Mecp2^{T308X}, Mecp2^{T158A}, Mecp2^{A140V}, Mecp2^{R168X}, Mecp2^{R270X} and Mecp2^{R273X}), mice overexpressing wild-type full-length human MeCP2 (MeCP2^{Tg1}), and region- or cell-type-specific *Mecp2* deletion/mutation using CRE-LOXP recombination system (Calfa et al 2011b, Chao et al 2010, Chen et al 2001, Collins et al 2004, Guy et al 2011, Guy et al 2001, Moretti et al 2006, Samaco et al 2009, Shahbazian et al 2002a).

Bird strain (*Mecp2*$^{tm1.1Bird}$) mice carry deletions spanning *Mecp2* exon 3 and 4 since early embryonic development. These mice are referred to "null MeCP2" mouse model as MeCP2 expression is not detectable using antibodies against either N- or C-termini of the protein. *Mecp2*^{Jae} (Jaenisch strain) mice constitutively express a truncated MeCP2 protein with an intact C-terminus lacking the MBD due to exon 3 deletions. These mice usually are considered mutant mice rather than "knockout" or "null" mice. Although these mutant mice cannot model all aspects of the human disease, they produce and recapitulate many characteristic features of RTT (**Table 1.1**). In both MeCP2 Bird and Jaenisch models, male and female mice appear normal without obvious deficits during their early postnatal stage and then undergo a progressive deterioration after the onset of symptoms until the premature death (Ricceri et al 2008). Specifically, hemizygous Jaenisch male mice started to exhibit unusual gait as early as 4-5 weeks of age. Their symptoms including shaking paws, hindlimb clasping, hypoactivity, body tremor,

episodes of seizures, significant loss of body weight and breathing abnormalities became evident after age of 5-6 weeks and continued to progress resulting in a short lifespan of 8-12 weeks. Behavioral and anatomical studies using the same mutant (Stearns et al 2007) revealed their abnormalities in locomotion, stereotypies, and anxiety, which were reminiscent of the clinical RTT phenotypes. These mutant male mice also exhibited cognitive deficits in fear conditioning and object recognition tasks with a 25% reduction in whole brain volume. Heterozygous mutant female mice seemed normal for the first 4 months and began to show symptoms at the adult stage. It took 6 month or longer time for female mutant mice to develop typical symptoms and they usually survived beyond 1 year of age. MeCP2 female heterozygous mice (*Mecp2*$^{-/+}$) expressed a mosaic pattern of wild-type and mutant cells due to XCI. Therefore, this combination of mosaic mutant MeCP2 expression, skewed XCI pattern and reduced MeCP2 levels in the wild-type cells led to delayed symptoms and behavioral phenotypes variability in the *Mecp2*$^{-/+}$ heterozygous mice (Braunschweig et al 2004).

In addition to Bird *Mecp2* knockout and Jaenisch *Mecp2* mutant models, *Mecp2*$^{308/Y}$ is the third common mouse model for RTT (**Table 1.1**). These *Mecp2*$^{308/Y}$ mice express a truncated protein from an introduction of a premature STOP codon in the mouse *Mecp2* allele after amino acid 308. This truncated protein retains the MBD, TRD and nuclear localization signal and still maintain residual protein function. *Mecp2*$^{308/Y}$ mice appeared normal and exhibited normal motor function until at the 6 weeks of age. Then they developed progressive neurological diseases representing many features of RTT including tremors, motor impairments, hypoactivity, increased anxiety-related behavior, seizures, kyphosis, and stereotypic forelimb motions. *Mecp2*$^{308/Y}$ mice exhibit much milder phenotypes and 90% of mutant males could survive for at least 1 year (Shahbazian et al 2002a).

	Mecp2$^{-/Y}$	*Mecp2*$^{308/Y}$	*Mecp2*^{Tg}
MeCP2 aberration	deletion of exon 3; exons 3 and 4	truncation at amino acid 308	overexpression of *MECP2*
Neurological phenotype	severe	progressive	progressive
LTP	reduced	reduced	enhanced
Hypoactivity	✓	✓	✓
Stereotypies		forepaw rubbing	forepaw clasping
Kyphosis		✓	✓
Spasticity	hindlimb clasping	hindlimb clasping	hindlimb clasping
Tremors	✓	✓	
Seizures	✓	✓	✓
Motor dysfunction	✓	✓	✓
Breathing abnormalities	✓		?
Anxiety	decreased	increased	increased
Learning and memory deficits	✓	✓	
Social behavior abnormalities		✓	
Ataxia	✓	✓	✓
Age of death	8–10 weeks	15 months	7–12 months
References	Chen et al., Guy et al.,	Shahbazian et al.	Collins et al.

Table 1.1 Common *Mecp2* Mouse Models

The phenotypes described for *Mecp2* null mice and *Mecp2*^{308} mice are based on characterization of male mice. Female mice heterozygous for each of the mutations manifest symptoms at a later age, typically have a milder disease course due to mosaicism, and often have favorable XCI. *Mecp2*^{Tg} mice show phenotypes in both males and females because the extra copy is on an autosome.

It might be argued that *Mecp2*$^{+/-}$ female heterozygous should be the best experimental model for RTT research, however most studies used hemizygous males. Male mutant mice consistently develop severe and characteristic behavioral phenotypes much earlier than female heterozygous mice. Male mutant mice also provide homogenous cell population without XCI, which would be more valuable for experimental work in the laboratory (Calfa et al 2011b). In contrast, MeCP2 female heterozygous mutant mice develop and exhibit RTT-related phenotypes at a later time, which does not truly recapitulate onset and progression of symptoms associated with RTT. Therefore, *Mecp2*^{Jae} (Jaenisch strain) mice expressing a truncated MeCP2 protein lacking the MBD due to exon 3 deletions were used in the current dissertation studies.

Additionally, CRE-LoxP system was applied to successfully generate conditional knockout mouse models to examine the function of MeCP2 in specific cell type and brain regions. Specific regions and cells targeted included forebrain neurons, neurons in hypothalamus, dopaminergic and noradrenergic neurons, serotonergic neurons and GABAergic neurons et al (Guy et al 2011). Interestingly, MeCP2 deficiency in GABAergic neurons almost recapitulated most of the phenotypes displayed in *Mecp2*-null mice including altered synaptic activity and plasticity (Chao et al 2010). MeCP2 deficiency might directly lead to a change in GABAergic neurotransmission that causes a shift in the excitation/inhibition (E/I) balance and thereby RTT symptoms. Although GABAergic neurotransmission seems to be involved in RTT pathogenesis, neither cell type or brain region is confirmed to be critical in RTT pathogenesis. The question whether RTT is caused specifically by certain subtype neurons dysfunction or only by a common dysfunction across the whole brain remains open.

1.4 MeCP2 function

So far only a few of the validated target genes and almost no specific molecular pathways have been identified to be associated with MeCP2 deficiency yet. Recent data suggest that MeCP2 functions have been expanded beyond gene silencing and chromatin architecture to include transcriptional activation, mRNA splicing regulation and protein synthesis modulation **(Fig 1.4)**. Currently, it remains a mystery how a single protein like MeCP2 can modulate a variety of opposing functions.

Intrinsically disordered protein

Bioinformatics analysis and theoretical prediction suggests that MeCP2 has very low levels of secondary structure organization and its structure information is available only for the MBD. Therefore MeCP2 is recognized as an "intrinsically disordered protein" (Adams et al 2007). The function of intrinsically disordered proteins is generally coupled to the adoption of secondary structure upon binding to other proteins or nucleic acids. Except for MBD, the rest of MeCP2 protein domains are highly unstructured so that the protein is allowed to interact with a large variety of macromolecular partners and undergo coil-to helix transitions that might explain the multiple capability of MeCP2 to interact with many different partners. Studies already demonstrated that MeCP2 interacted with the following molecules: heterochromatin protein 1 (HP1); transcriptional corepressors including nuclear receptor corepressor 1 (N-CoR), Switch-independent 3A (Sin3A) and histone deacetylases (HDACs); transcriptional coactivators such as cAMP response element binding protein (CREB); Y box-binding protein (YB1) which is a principle component of messenger ribonucleoprotein particles controlling multiple steps of mRNA processing; TAR DNA-binding protein 43 (TDP-43); as well as DNA

(cytosine-5)-methyltransferase 1 (Dnmt1) (Guy et al 2011). Since MeCP2 is involved in many important regulatory functions and signaling pathways, single amino acid mutations throughout the whole protein could lead to structural and functional alterations associated with RTT-related symptoms.

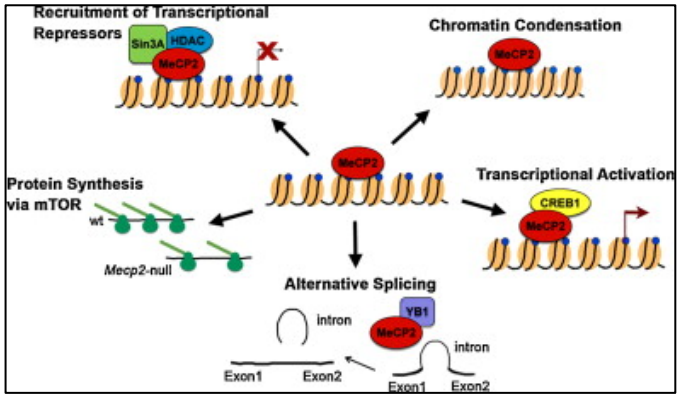

Fig. 1.4 MeCP2 is a multifunctional protein.

MeCP2 can function as a transcriptional repressor that recruits co-repressors to silence methylated genes; it can mediate the formation of a highly compacted chromatin structure in a methylation independent way; it may play a role in transcriptional activation mainly through its interaction with CREB1; it can be involved in mRNA alternative splicing for example through its interactions with YB1; and eventually it can influence protein synthesis through modulation of the mTOR pathway.

Permission to reuse figure from Bedogni et al 2014

Transcriptional Repressor

The first and most characterized function of MeCP2 is a transcriptional repressor (Nan et al 1997, Nan et al 1998). MeCP2 binds to methylated CpG sequence at the upstream of the transcriptional starting site (TSS) of target genes and then recruits transcriptional co-repressor complexes such as: Sin3a/HDAC1 and Ski/NcoR/HDACII resulting in a compact chromatin

structure that represses local gene transcription. Earlier transcriptional profiling studies using either human postmortem tissue or whole brain of *Mecp2* mutant mice identified only a few modest gene expression alterations and these data were not sufficient to support a role for MeCP2 in genome-wide transcriptional repression (Samaco & Neul 2011). In addition, findings from transcriptional profiling studies revealed a consistent downregulation of target genes due to loss of MeCP2 that has argued against a single role of MeCP2 in transcriptional regulation.

Transcriptional Activator

Through transcriptional profiling studies within hypothalamus from both loss- and gain-of-function of MeCP2 mouse models (Mecp2 Bird strain and MECP2-TG), about 400 genes were identified as repressed targets, which were downregulated in the MeCP2 overexpression and upregulated in the absence of MeCP2. In the contrary, the majority about 2000 genes were found activated targets, which were upregulated in the overexpression of MeCP2 and downregulated in the absence of MeCP2 (Chahrour et al 2008). Among these activated target genes, the transcriptional activator, cAMP response element-binding protein (CREB) was identified to bind with MeCP2 and mediate activity-dependent transcriptional activation. Further study through *in vivo* quantitative, genome-wide analysis demonstrated MeCP2 as a major 5-hydroxymethylcytosine (5hmc)-binding protein in the brain. As 5hmC is enriched in active genes in neurons, MeCP2 by binding to 5hmC facilitates transcription in specific neuronal cell type. In addition, a recent study also suggested that AKT/mTOR signaling pathway was attenuated in both MeCP2-null mice and heterozygous female mice that could lead to an impaired protein synthesis caused by MeCP2 dysfunction (Ricciardi et al 2011).

Finally, it should be mentioned that *in vitro* functional and structural studies of isolated domains has revealed that the protein contains no specific binding sties for unmethylated DNA. Findings from *in vivo* works appear to be contradictory regarding the function of MeCP2 in binding unmethylated DNA.

Global Chromatin Regulator

A recent work demonstrates that abundant MeCP2 expression in mature neurons might imply its function as an alternative linker histone competing with histone H1 (Skene et al 2010). Interestingly, MeCP2 expression in glia is about 10–30 times less abundant compared to neurons and neurons have about half amount of histone H1 compared to glia cells. Accordingly, a model has been proposed in mature neurons, characterized by 1.6×10^7 molecules of MeCP2 per nucleus corresponding roughly to one molecule every two nucleosomes. MeCP2 is bound genome-widely, tracks methylated DNA and organizes a compacted chromatin structure thus dampening overall transcriptional activity. The absence of MeCP2 only in neurons, not in glia would lead to a selective increase in histone H1 expression and histone acetylation (Cartron et al 2013). A recent study involving chromatin immunoprecipitation followed by sequencing (ChIP-seq) to search for genome-wide DNA protein binding affinity and subsequent ChIP-qPCR to define specific MeCP2 binding ability showed that MeCP2 bound extensively to the whole genome in cultured cortical neurons and its interaction with specific target genes was not altered upon neuronal stimulation. These studies suggesting MeCP2 broadly binds throughout the genome further support MeCP2 functions more as a global regulator of transcription and chromatin remodeling rather than a sequence-specific transcription factor (Cohen et al 2011, Skene et al 2010).

In the brain, the majority of methylated CpG islands are present in intragenic and intergenic regions, whereas only a very small amount of methylation (less than 3% of CpG islands) is found at 5' promoters. Moreover, gene bodies and transcriptionally active genes in neurons are enriched in 5'-hydroxymethylated CpG (5hmC), which binds MeCP2 and exhibits nuclease hypersensitivity (Mellen et al 2012). All of this evidence provides a new perspective to the MeCP2-mediated chromatin organization in the brain. Additional research works also imply the relevance of MeCP2 activity on chromatin structure (Baker et al 2013, Lyst et al 2013). Lacking this AT-hook domain in MeCP2 appears to impair its DNA binding and chromatin compaction capabilities. The lack of functional MeCP2 in mature neurons will probably lead to a disorganized chromatin structure that prevents neurons from properly responding to stimuli, thus impairing synaptic plasticity.

RNA Splicing and MicroRNA Regulation

MeCP2 plays a role in RNA splicing by regulating the coding genes and microRNAs expression. It was reported that MeCP2 interacted with YB1, a regulator of alternative splicing (Young et al 2005) and directly interacted with RNA as well. In addition, MeCP2 was shown to regulate miRNA expression and quite a few of miRNA targets were identified through *in vitro* and *in vivo* studies. The role of MeCP2 in regulating miRNA contributing to RTT pathology was also demonstrated in MeCP2 mouse models. Studies showed that the loss of MeCP2 in the cerebellum of a RTT mouse model resulted in altered expression of miRNAs (Wu et al 2010). Interestingly, a recent work that identified MeCP2 as a direct target of miRNA-132 to regulate circadian clock gene expression already implied an urge to understand mechanisms underlying sleeping disturbances observed in RTT patients (Alvarez-Saavedra et al 2011). Their work

formed the basis of parts of my dissertation studies, circadian dysfunction in a mouse model of Rett Syndrome in **Chapter 2**.

Post-translational Modification (PTM) of MeCP2

MeCP2 is a multi-functional protein, whose activities might still have to be completely unraveled. MeCP2 has a highly disorganized structure and undergoes post-translational modifications that enable its functional versatility. Posttranslational modification of MeCP2 plays a critical role in interaction with their macromolecular partners. Specifically, MeCP2 was found to undergo many PTMs including acetylation, phosphorylation, ubiquitination, and sumoylation. Several recent reports demonstrated that differential phosphorylation of MeCP2 in response to neuronal activity was a crucial mechanism through which the methyl-binding protein modulated gene expression. All these data together suggest that a complex pattern of PTMs transforms the protein into a regulatory platform responding to various signaling pathways. Thus, the ability of the protein to associate with many different partners in such a PTM dependent manner could potentially account for apparent functional disparity (Bedogni et al 2014).

1.5 MeCP2 in Neuronal Morphology, Synaptic Signaling and Plasticity

Dendritic Morphology

MeCP2 greatly impacts dendritic morphology. As dendritic spines are small protrusions from the dendrites that correlate with the number of synapses serving as postsynaptic targets for synaptic transmission in the brain. Thus, abnormal structural properties of dendritic spines may lead to defects in synaptic connectivity. Studies showed that RTT patients

exhibited a reduction in the number of axonal and dendritic processes and a decrease in the expression of microtubule associated protein 2 (MAP2), a protein important for dendritic cytoskeleton (Armstrong et al 1998). Moreover, RTT neurons showed reduced density in dendritic spines (Chapleau et al 2009). A similar observation was reported in studies with MeCP2 mouse models. Pyramidal neurons in the cortex of MeCP2 null mice showed a reduction in soma size and dendritic arborization. Alterations in dendritic morphology and decreased cortical thickness were observed at early presymptomatic stage in both somatosensory and motor cortex. MeCP2-deficeint neurons also showed a decreased number in dendritic spines and reduced arborization (Zhou et al 2006). Moreover, spine density in the apical tuft dendrites of layer V pyramidal neurons was significantly reduced in the male MeCP2 null mice as early as 4 weeks of age (Landi et al 2011). Electron microscopy studies revealed an increase in premature postsynaptic densities and a reduction in postsynaptic density cross-sectional length in the synapses of hippocampus CA1 region of MeCP2 mutant mice (Moretti et al 2006). Reactivation of MeCP2 expression in MeCP2 null mice resulted in amelioration of behavioral phenotypes and reversal of dendritic structural abnormalities (Robinson et al 2012). The dendritic spines dynamics study using multi-photon microscopy to examine the dendritic spines of layer V apical tufts in the somatosensory cortex. It was found that the formation and motility of filopodia, defined as long spines without heads, were reduced and impaired in MeCP2 mutants (Landi et al 2011). Interestingly, a recent research using *in vivo* tow-photon imaging with Tg1 mouse model of *MECP2* duplication syndrome revealed that MeCP2 overexpression caused excessive dendritic arborization and dendritic spine formation in terminal branches of L5 pyramidal neurons in barrel cortex during early postnatal development, indicating that that MeCP2 overexpression induces dendritic overgrowth. Then a subsequent period of elevated

spine turnover and synapse loss led to decreased spine density after postnatal week 12 in MeCP2 overexpression model. These abnormalities of dendritic and synaptic homeostasis correlated with the onset of behavioral symptoms (Jiang et al 2013). Together, these studies stongly imply that maintenance of MeCP2 in certain defined concentration seems to be crucial for their proper dendritic morphlogy in CNS (Chao & Zoghbi 2012).

Synaptic Signaling

Substantial abnormalities in synaptic signaling were discovered in MeCP2 mouse models. MeCP2 deficient neurons exhibited decreased excitatory postsynaptic currents (EPSCS) in hippocampal glutamatergic neuronal cultures (Chao et al 2007, Collins et al 2004). Whole cell patch recordings revealed a reduction in both spontaneous action potential (AP) firing rate and spontaneous EPSCs in the layer V pyramidal neurons in the primary somatosensory cortex in MeCP2 male mutant mice (Chang et al 2006, Dani et al 2005). These data indicated a reduction in excitatory synaptic transmission and an increase in inhibitory synaptic signaling due to MeCP2 deficiency. Thus, MeCP2 dysfunction induced a shift of the homeostatic balance between excitation and inhibition (E/I),. The shift in E/I balance in MeCP2 mutants was brain-microcircuit specific as the excitation and inhibition imbalance was not the same in all brain regions (Shepherd & Katz 2011). In the cortex, MeCP2 deficiency led to a change in E/I ratio favoring inhibition (Dani et al 2005, Wood et al 2009). In contrast, an E/I ratio shift towards favoring excitation was reported in both hippocampus (Calfa et al 2011a, Fischer et al 2009, Moretti et al 2006) and brainstem circuitry responsible for generating respiratory patterns (Kline et al 2010, Kron et al 2011, Taneja et al 2009). In contrast to cortex, loss of Mecp2 resulted in enhanced excitation in many brainstem neuronal groups, including the medullary

nucleus tractus solitarius (nTS) and the ventrolateral medulla (VLM). In the absence of MeCP2, these nTS neurons exhibited an increase in the amplitude of spontaneous and evoked EPSCs, and in the probability of action potential firing pattern without any change in inhibitory transmission or intrinsic neuronal excitability (Kline et al 2010). Synaptic hyperexcitability in VLM were also reported in MeCP2-null mice, in parallel with defects in GABAergic inhibitory signaling. Recent study mapping expression of activity-dependent, immediate-early gene product Fos in MeCP2 null mice brain revealed a significant reduction in Fos labeling in limbic cortices and subcortical structures, and an enhancement expression in the hindbrain (Kron et al 2012). This study further supports the differential effects of MeCP2 across different brain regions and microcircuits.

Synaptic Plasticity

Electrophysiology studies of RTT mouse models indicated impairments in long-term plasticity including long-term potentiation (LTP) and long-term depression (LTD). LTP and LTD is widely believed as the representing forms of synaptic plasticity underlying experience dependent modifications of brain function including learning and memory. Studies indicated that LTP was reduced in CA1 region of the hippocampal slices in MeCP2-deficienct mice (Weng et al 2011b). Impairments in synaptic plasticity were also reported in layer II/III from primary motor or sensory cortex slices from both $Mecp2^{308/y}$ and MeCP2 mutant mice, suggesting that abnormalities of synaptic plasticity extended beyond the hippocampus region and involved additional brain regions (Lonetti et al 2010). These data together with morphological studies imply the loss of MeCP2 create malfunction of numerous synapses across the forebrain, midbrain and hindbrain leading to impairment in neuronal networks and RTT-like phenotypes.

1.6 MeCP2 and BDNF

Neurotrophin family of growth factors consists of nerve growth factor (NGF), brain-derived neurotrophic factor (BDNF), neurotrophin-3 (NT-3) and neurotrophin-4/5 (NT-4/5). BDNF is the best characterized for its gene structure and modulation, secretion processing and signaling cascades (Greenberg et al 2009). BDNF is initially synthesized in the endoplasmic reticulum (ER) as a precursor protein proBDNF. Following the cleavage of the signal peptide, proBDNF is transported to the Golgi apparatus and converted into mature BDNF (mBDNF) intracellularly. Mature BDNF binds tropomyosine-related kinase B (TrkB) receptors and promotes neuronal survival and long-term potentiation through activation of three major downstream signaling transduction pathways following TrkB receptor activation: the mitogen-activated protein kinase (MAPK) pathway, the phosphatidyl-inositol 3-kinase (PI3K) pathway, and the phospholipase C (PLC) pathway (Cohen & Greenberg 2008). BDNF has been extensively studied for its essential role in cell differentiation, neuronal survival, migration, dendritic arborization, synaptogenesis, and activity-dependent forms of synaptic plasticity (Li & Pozzo-Miller 2014).

Interaction between MeCP2 and BDNF

Several studies using applied candidate gene approaches with samples from both RTT patient and mouse tissues identified putative MeCP2 targets that might be contributing to RTT pathogenesis. Mouse cortical culture studies suggested the brain-derived neurotrophic factor, *Bdnf* as one of MeCP2 targets (Chen et al 2003, Martinowich et al 2003). *Bdnf* is considered a key signaling molecule in brain development and neuroplasticity (Greenberg et al 2009). These *in vitro* studies indicated that MeCP2 bound to the promoter III of the *Bdnf* gene and repressed

its gene transcription in the absence of neuronal activity. Membrane depolarization triggered the phosphorylation of MeCP2 through a CaMKII-dependent mechanism and mediated the transcription de-repression due to its release from the *Bdnf* promoter binding (Chen et al 2003). Another study reported that depolarization-induced increase in BDNF expression was parallel with a decrease in CpG methylation level in the *Bdnf* promoter IV region. Furthermore, the increase in *Bdnf* transcription was mediated by the dissociation of MeCP2 and its interacting repressor complex from the same *Bdnf* promoter region (Martinowich et al 2003). These i*n vitro* culture studies provided evidence that MeCP2 interacted the *Bdnf* promoter and repressed its transcription in an activity-dependent manner. Subsequently, study demonstrated that MeCP2 was phosphorylated at serine 421 in suprachiasmatic nucleus (SCN) in mice hypothalamus under constant darkness condition in response to a brief light exposure. This phosphorylation resulted in a dissociation of MeCP2 from the *Bdnf* promoter that led to an activity-dependent increase in BDNF expression in cultured hippocampal neurons. These findings further supported the function of MeCP2 in activity-dependent regulation of *Bdnf* transcription (Zhou et al 2006).

However, *in vivo* studies demonstrated an interaction between Mecp2 and *Bdnf,* and a correlation between altered BDNF levels and neurologic symptoms in the mouse models. An i*n vivo* study reported that BDNF protein levels were significantly decreased throughout the entire brain during late symptomatic stage due to the absence of MeCP2 (Kline et al 2010). Moreover, conditional removal of *Bdnf* in postmitotic neurons led to some of the phenotypes similar to MeCP2 mutant mice, while overexpression of BDNF specifically in forebrain region improved impaired locomotor function, increased the firing rate of layer V cortical pyramidal neurons and extended lifespan in MeCP2 mutant mouse model (Chang et al 2006). One possible

explanation for the discrepancy between these i*n vivo* and *in vitro* data is that MeCP2 deficiency or dysfunction reduces cortical neuronal activity and subsequently diminishes neuronal activity in overall leads to a decrease in BDNF expression levels as *Bdnf* is known to be highly upregulated in response to both membrane depolarization and synaptic activation. In support of this hypothesis, it was reported that global overexpression of MeCP2 in mice was associated with increased expression of BDNF mRNA in the hypothalamus, whereas MeCP2 downregulation in the hypothalamus correlates with decreased BDNF levels (Chahrour et al 2008).

Therapeutic effects of BDNF in RTT

BDNF could be a potential therapeutic target for RTT treatment. Studies indicated that conditional overexpression of BDNF in MeCP2 mutant mouse forebrain rescued numerous deleterious effects caused by MeCP2 dysfunction including motor hypoactivity, reduced cortical neuronal activity, low brain weight, dampened spontaneous firing of cortical pyramidal neurons and premature death (Chang et al 2006). In addition, exogenous application of BDNF into brainstem slices significantly reversed synaptic dysfunction in MeCP2 null mice (Kline et al 2010). However, there are still obstacles to use BDNF as a clinical approach for RTT as BDNF has a short half-life and inability to cross the blood-brain barrier (BBB). Pharmocological manipulations including administration of the recombinant mature BDNF, enhancing endogenous BDNF expression and its downstream TrkB signaling pathways are considered as practical alternatives for RTT treatments. AMPAkines, a family of non-trophic agents that increase BDNF expression represent promising alternatives to increased BDNF signaling. Another compound is the BDNF mimetic LM22A-4 that selective activates TrkB but not other

Trk family members. Both AMPAkines and LM22A-4 were proved effectively in reversal of cardiorespiratory irregularities in *Mecp2* knockout mice (Ogier et al 2007, Schmid et al 2012). Other BDNF-related compounds were examined for the amelioration of RTT-related neurological symptoms. For example, a small molecule TrkB agonist, 7,8-dehydroxyflavone (7,8-DHF) was reported to extend the lifespan, improve locomotor activity and breathing pattern deficits in *Mecp2* knockout mice (Jang et al 2010, Johnson et al 2012) (Also see **Chapter 3**). The insulin-like growth factor-1 (IGF-1) is currently in Phase II clinical trial in order to validate its beneficial effects in treating RTT individuals after a successful completion of Phase I clincal trial that originated from positive findings with *Mecp2* knockout mouse models (Khwaja et al 2014, Tropea et al 2009).

1.7 Therapeutic approaches and clinical management for RTT

Clinical Management

Some of RTT female patients can live into middle age and they may survival longer if under proper care indicating the need for careful planning and long-term clinical management for these individuals. However, so far no cure for RTT has been identified. Current treatment for RTT is based entirely on control symptoms and RTT patients only receive supportive and symptomatic treatments. MeCP2 is a multifunction protein and very abundant in CNS, and affects numerous target genes. So far only few validated target genes have been identified for its specific function and molecular pathways yet. Additional basic and clinical research works are certainly needed to determine the downstream MeCP2 target genes that may contribute to a specific symptom or a combination of clinical features. The general goals of clinical management include limiting the severity of RTT symptoms, extending and improving the life

quality of RTT individuals through careful planning of long-term care.

In additional to RTT classical neurological features, symptoms from other systems are common among RTT individuals. Sleep disturbances are often seen in RTT patients. Thus proper sleep management through medication treatment is essential for maintaining general health in RTT patients. Moreover, irregular breathing is one of the most typical features in RTT. RTT breathing irregularities vary from hyperventilation, apnea, breath holding and air swallowing that usually occur during both wakefulness and sleep. Cardiac dysfunction from RTT patients usually leads to a higher percentage rate in sudden death incidences among the patients. Another prominent feature of RTT heart dysfunction is indicated by a prolonged QT interval measured with electrocardiogram (EKG). Another possibility leading to cardiac dysfunction may arise from failure of respiratory system. A majority of RTT individuals have some types of seizure activities. The missense MECP2 mutations mentioned previously such as T158M and R106W are the most frequently mutations to be associated with epilepsy disorders through genotype-phenotype analysis (Glaze et al 2010). Additional RTT clinical phenotypes also include osteopenia causing bone mass loss and fracture, growth failure, movement abnormalities, anxiety and mood disorders, and gastrointestinal dysfunction implying a requirement of nutrition and general support for RTT patients. In summary, regarding RTT patient care, those above-mentioned symptoms from different systems need to carefully considered and controlled to limit disease progression and improve life quality of RTT individuals.

Therapeutic Alternatives

Very few clinical trials have been conducted in the RTT populations due to variable phenotypic severity and disease complexity. The insulin-like growth factor-1 (IGF-1) is believed a promising therapeutic treatment for RTT individuals. IGF-1 usually binds to the IGF-1 receptors then activate a receptor tyrosine kinase and downstream signaling cascades that are similar to the BDNF/TrkB signaling pathways. The advantages of IGF-1 include the ability to cross the blood brain barrier and then stimulate proliferation of neural progenitors, neuronal survival, neurite outgrowth, and synaptic formation. Previous study with MeCP2 mutant mouse model indicated that systemic administration of either full length 1GF-1 or its active tri-peptide fragment reversed at least partially, many RTT-relevant features such as locomotor function impairment, breathing abnormalities, and cardiac irregularities and dendritic spine density defects in the cortex (Tropea et al 2009). These results suggest that IGF-1 is a promising therapeutic option for RTT individuals. IGF-1 is currently in phase II clinical trial to examine the effects of mecasermin, a recombined human IGF-1 on RTT individuals while the phase I study has already proved the safety and tolerance in RTT girls (Khwaja et al 2014).

In addition, a number of approaches targeted to activate and mimic BDNF pathways have proved promising for RTT preclinical studies. Molecules that mimic BDNF/TrkB signaling pathway, called "BDNF mimetics" that have the capability to pass through the BBB and bind to the TrkB receptor to activate intracellular pathways are discovered as potential therapeutic targets for RTT individuals. For example, the small molecular selective TrkB agonists, such as LM22A-4 and 7,8-dihydroxyflavone (7,8-DHF) were already reported to ameliorate many RTT-like phenotypes in *Mecp2* mouse models (Johnson et al 2012, Schmid et al 2012).

More recently, induced pluripotent stem cells (iPSCs) reprogrammed from skin fibroblasts of RTT individuals were successfully established and differentiated into neurons that potentially can be used for *in vitro* disease modeling and drug screening. Thus iPSCs reprogramming is believed to be a novel research tool to facilitate a better understanding of RTT pathogenesis. Reprogramming is a procedure to convert differentiated somatic cells to a pluripotent state Usually four transcription factors (Oct4, Sox2, Klf4, and Myc) are transfected together to generate iPSCs (Takahashi & Yamanaka 2006). Recent studies indicated that iPSCs technology was applied successfully to model RTT. The general procedures of IPSCs include the following steps: iPSCs clones expressing either wild type or mutant MeCP2 are produced from RTT patients; mutant RTT iPSCs are differentiated into relevant cell types and used for *in vitro* disease model; wild type iPSCs can be used in cell replacement therapy (Cheung et al 2011, Dajani et al 2013, Marchetto et al 2010). This gained knowledge will aid the development of standard diagnostics as well as personalized medicine to improve efficacies and to identify potential new therapeutics for RTT individuals.

References

Adams VH, McBryant SJ, Wade PA, Woodcock CL, Hansen JC. 2007. Intrinsic disorder and autonomous domain function in the multifunctional nuclear protein, MeCP2. *J Biol Chem* 282: 15057-64

Adkins NL, Georgel PT. 2011. MeCP2: structure and function. *Biochem Cell Biol* 89: 1-11

Adler DA, Quaderi NA, Brown SD, Chapman VM, Moore J, et al. 1995. The X-linked methylated DNA binding protein, Mecp2, is subject to X inactivation in the mouse. *Mamm Genome* 6: 491-2

Alvarez-Saavedra M, Antoun G, Yanagiya A, Oliva-Hernandez R, Cornejo-Palma D, et al. 2011. miRNA-132 orchestrates chromatin remodeling and translational control of the circadian clock. *Hum Mol Genet* 20: 731-51

Amir RE, Van den Veyver IB, Wan M, Tran CQ, Francke U, Zoghbi HY. 1999. Rett syndrome is caused by mutations in X-linked MECP2, encoding methyl-CpG-binding protein 2. *Nat Genet* 23: 185-8

Armstrong DD. 2001. Rett syndrome neuropathology review 2000. *Brain Dev* 23 Suppl 1: S72-6

Armstrong DD. 2005. Neuropathology of Rett syndrome. *J Child Neurol* 20: 747-53

Armstrong DD, Dunn K, Antalffy B. 1998. Decreased dendritic branching in frontal, motor and limbic cortex in Rett syndrome compared with trisomy 21. *J Neuropathol Exp Neurol* 57: 1013-7

Baker SA, Chen L, Wilkins AD, Yu P, Lichtarge O, Zoghbi HY. 2013. An AT-hook domain in MeCP2 determines the clinical course of Rett syndrome and related disorders. *Cell* 152: 984-96

Ballas N, Lioy DT, Grunseich C, Mandel G. 2009. Non-cell autonomous influence of MeCP2-deficient glia on neuronal dendritic morphology. *Nat Neurosci* 12: 311-7

Bedogni F, Rossi RL, Galli F, Cobolli Gigli C, Gandaglia A, et al. 2014. Rett syndrome and the urge of novel approaches to study MeCP2 functions and mechanisms of action. *Neurosci Biobehav Rev*

Braunschweig D, Simcox T, Samaco RC, LaSalle JM. 2004. X-Chromosome inactivation ratios affect wild-type MeCP2 expression within mosaic Rett syndrome and Mecp2-/+ mouse brain. *Hum Mol Genet* 13: 1275-86

Calfa G, Hablitz JJ, Pozzo-Miller L. 2011a. Network hyperexcitability in hippocampal slices from Mecp2 mutant mice revealed by voltage-sensitive dye imaging. *J Neurophysiol* 105: 1768-84

Calfa G, Percy AK, Pozzo-Miller L. 2011b. Experimental models of Rett syndrome based on Mecp2 dysfunction. *Exp Biol Med (Maywood)* 236: 3-19

Carotenuto M, Esposito M, D'Aniello A, Rippa CD, Precenzano F, et al. 2013. Polysomnographic findings in Rett syndrome: a case-control study. *Sleep Breath* 17: 93-8

Cartron PF, Nadaradjane A, Lepape F, Lalier L, Gardie B, Vallette FM. 2013. Identification of TET1 Partners That Control Its DNA-Demethylating Function. *Genes Cancer* 4: 235-41

Chahrour M, Jung SY, Shaw C, Zhou X, Wong ST, et al. 2008. MeCP2, a key contributor to neurological disease, activates and represses transcription. *Science* 320: 1224-9

Chahrour M, Zoghbi HY. 2007. The story of Rett syndrome: from clinic to neurobiology. *Neuron* 56: 422-37

Chang Q, Khare G, Dani V, Nelson S, Jaenisch R. 2006. The disease progression of Mecp2 mutant mice is affected by the level of BDNF expression. *Neuron* 49: 341-8

Chao HT, Chen H, Samaco RC, Xue M, Chahrour M, et al. 2010. Dysfunction in GABA signalling mediates autism-like stereotypies and Rett syndrome phenotypes. *Nature* 468: 263-9

Chao HT, Zoghbi HY. 2012. MeCP2: only 100% will do. *Nat Neurosci* 15: 176-7

Chao HT, Zoghbi HY, Rosenmund C. 2007. MeCP2 controls excitatory synaptic strength by regulating glutamatergic synapse number. *Neuron* 56: 58-65

Chapleau CA, Calfa GD, Lane MC, Albertson AJ, Larimore JL, et al. 2009. Dendritic spine pathologies in hippocampal pyramidal neurons from Rett syndrome brain and after expression of Rett-associated MECP2 mutations. *Neurobiol Dis* 35: 219-33

Chen RZ, Akbarian S, Tudor M, Jaenisch R. 2001. Deficiency of methyl-CpG binding protein-2 in CNS neurons results in a Rett-like phenotype in mice. *Nat Genet* 27: 327-31

Chen WG, Chang Q, Lin Y, Meissner A, West AE, et al. 2003. Derepression of BDNF transcription involves calcium-dependent phosphorylation of MeCP2. *Science* 302: 885-9

Cheung AY, Horvath LM, Grafodatskaya D, Pasceri P, Weksberg R, et al. 2011. Isolation of MECP2-null Rett Syndrome patient hiPS cells and isogenic controls through X-chromosome inactivation. *Hum Mol Genet* 20: 2103-15

Cheval H, Guy J, Merusi C, De Sousa D, Selfridge J, Bird A. 2012. Postnatal inactivation reveals enhanced requirement for MeCP2 at distinct age windows. *Hum Mol Genet* 21: 3806-14

Cohen S, Greenberg ME. 2008. Communication between the synapse and the nucleus in neuronal development, plasticity, and disease. *Annu Rev Cell Dev Biol* 24: 183-209

Collins AL, Levenson JM, Vilaythong AP, Richman R, Armstrong DL, et al. 2004. Mild overexpression of MeCP2 causes a progressive neurological disorder in mice. *Hum Mol Genet* 13: 2679-89

Dajani R, Koo SE, Sullivan GJ, Park IH. 2013. Investigation of Rett syndrome using pluripotent stem cells. *J Cell Biochem* 114: 2446-53

Dani VS, Chang Q, Maffei A, Turrigiano GG, Jaenisch R, Nelson SB. 2005. Reduced cortical activity due to a shift in the balance between excitation and inhibition in a mouse model of Rett syndrome. *Proceedings of the National Academy of Sciences of the United States of America* 102: 12560-5

Derecki NC, Cronk JC, Kipnis J. 2013. The role of microglia in brain maintenance: implications for Rett syndrome. *Trends Immunol* 34: 144-50

Derecki NC, Cronk JC, Lu Z, Xu E, Abbott SB, et al. 2012. Wild-type microglia arrest pathology in a mouse model of Rett syndrome. *Nature* 484: 105-9

Dragich JM, Kim YH, Arnold AP, Schanen NC. 2007. Differential distribution of the MeCP2 splice variants in the postnatal mouse brain. *J Comp Neurol* 501: 526-42

Fischer M, Reuter J, Gerich FJ, Hildebrandt B, Hagele S, et al. 2009. Enhanced hypoxia susceptibility in hippocampal slices from a mouse model of rett syndrome. *J Neurophysiol* 101: 1016-32

Glaze DG, Percy AK, Skinner S, Motil KJ, Neul JL, et al. 2010. Epilepsy and the natural history of Rett syndrome. *Neurology* 74: 909-12

Greenberg ME, Xu B, Lu B, Hempstead BL. 2009. New insights in the biology of BDNF synthesis and release: implications in CNS function. *The Journal of neuroscience : the official journal of the Society for Neuroscience* 29: 12764-7

Guideri F, Acampa M. 2005. Sudden death and cardiac arrhythmias in Rett syndrome. *Pediatr Cardiol* 26: 111

Guy J, Cheval H, Selfridge J, Bird A. 2011. The role of MeCP2 in the brain. *Annu Rev Cell Dev Biol* 27: 631-52

Guy J, Gan J, Selfridge J, Cobb S, Bird A. 2007. Reversal of neurological defects in a mouse model of Rett syndrome. *Science* 315: 1143-7

Guy J, Hendrich B, Holmes M, Martin JE, Bird A. 2001. A mouse Mecp2-null mutation causes neurological symptoms that mimic Rett syndrome. *Nat Genet* 27: 322-6

Hagberg B, Goutieres F, Hanefeld F, Rett A, Wilson J. 1985. Rett syndrome: criteria for inclusion and exclusion. *Brain Dev* 7: 372-3

Itoh M, Tahimic CG, Ide S, Otsuki A, Sasaoka T, et al. 2012. Methyl CpG-binding protein isoform MeCP2_e2 is dispensable for Rett syndrome phenotypes but essential for embryo viability and placenta development. *J Biol Chem* 287: 13859-67

Jiang M, Ash RT, Baker SA, Suter B, Ferguson A, et al. 2013. Dendritic arborization and spine dynamics are abnormal in the mouse model of MECP2 duplication syndrome. *The Journal of neuroscience : the official journal of the Society for Neuroscience* 33: 19518-33

Johnson RA, Lam M, Punzo AM, Li H, Lin BR, et al. 2012. 7,8-dihydroxyflavone exhibits therapeutic efficacy in a mouse model of Rett syndrome. *J Appl Physiol (1985)* 112: 704-10

Jugloff DG, Vandamme K, Logan R, Visanji NP, Brotchie JM, Eubanks JH. 2008. Targeted delivery of an Mecp2 transgene to forebrain neurons improves the behavior of female Mecp2-deficient mice. *Hum Mol Genet* 17: 1386-96

Khwaja OS, Ho E, Barnes KV, O'Leary HM, Pereira LM, et al. 2014. Safety, pharmacokinetics, and preliminary assessment of efficacy of mecasermin (recombinant human IGF-1) for the treatment of Rett syndrome. *Proceedings of the National Academy of Sciences of the United States of America* 111: 4596-601

Kishi N, Macklis JD. 2004. MECP2 is progressively expressed in post-migratory neurons and is involved in neuronal maturation rather than cell fate decisions. *Mol Cell Neurosci* 27: 306-21

Kline DD, Ogier M, Kunze DL, Katz DM. 2010. Exogenous brain-derived neurotrophic factor rescues synaptic dysfunction in Mecp2-null mice. *The Journal of neuroscience : the official journal of the Society for Neuroscience* 30: 5303-10

Kriaucionis S, Bird A. 2004. The major form of MeCP2 has a novel N-terminus generated by alternative splicing. *Nucleic Acids Res* 32: 1818-23

Kron M, Howell CJ, Adams IT, Ransbottom M, Christian D, et al. 2012. Brain activity mapping in Mecp2 mutant mice reveals functional deficits in forebrain circuits, including key nodes in the default mode network, that are reversed with ketamine treatment. *The Journal of neuroscience : the official journal of the Society for Neuroscience* 32: 13860-72

Kron M, Zimmermann JL, Dutschmann M, Funke F, Muller M. 2011. Altered responses of MeCP2-deficient mouse brain stem to severe hypoxia. *J Neurophysiol* 105: 3067-79

Landi S, Putignano E, Boggio EM, Giustetto M, Pizzorusso T, Ratto GM. 2011. The short-time structural plasticity of dendritic spines is altered in a model of Rett syndrome. *Sci Rep* 1: 45

Lee JY, Leonard H, Piek JP, Downs J. 2013. Early development and regression in Rett syndrome. *Clin Genet* 84: 572-6

Lewis JD, Meehan RR, Henzel WJ, Maurer-Fogy I, Jeppesen P, et al. 1992. Purification, sequence, and cellular localization of a novel chromosomal protein that binds to methylated DNA. *Cell* 69: 905-14

Li W, Pozzo-Miller L. 2014. BDNF deregulation in Rett syndrome. *Neuropharmacology* 76 Pt C: 737-46

Liyanage VR, Rastegar M. 2014. Rett Syndrome and MeCP2. *Neuromolecular Med* 16: 231-64

Lonetti G, Angelucci A, Morando L, Boggio EM, Giustetto M, Pizzorusso T. 2010. Early environmental enrichment moderates the behavioral and synaptic phenotype of MeCP2 null mice. *Biol Psychiatry* 67: 657-65

Lyst MJ, Ekiert R, Ebert DH, Merusi C, Nowak J, et al. 2013. Rett syndrome mutations abolish the interaction of MeCP2 with the NCoR/SMRT co-repressor. *Nat Neurosci* 16: 898-902

Maezawa I, Jin LW. 2010. Rett syndrome microglia damage dendrites and synapses by the elevated release of glutamate. *The Journal of neuroscience : the official journal of the Society for Neuroscience* 30: 5346-56

Marchetto MC, Carromeu C, Acab A, Yu D, Yeo GW, et al. 2010. A model for neural development and treatment of Rett syndrome using human induced pluripotent stem cells. *Cell* 143: 527-39

Martinowich K, Hattori D, Wu H, Fouse S, He F, et al. 2003. DNA methylation-related chromatin remodeling in activity-dependent BDNF gene regulation. *Science* 302: 890-3

McGraw CM, Samaco RC, Zoghbi HY. 2011. Adult neural function requires MeCP2. *Science* 333: 186

Mellen M, Ayata P, Dewell S, Kriaucionis S, Heintz N. 2012. MeCP2 binds to 5hmC enriched within active genes and accessible chromatin in the nervous system. *Cell* 151: 1417-30

Moog U, Smeets EE, van Roozendaal KE, Schoenmakers S, Herbergs J, et al. 2003. Neurodevelopmental disorders in males related to the gene causing Rett syndrome in females (MECP2). *Eur J Paediatr Neurol* 7: 5-12

Moretti P, Levenson JM, Battaglia F, Atkinson R, Teague R, et al. 2006. Learning and memory and synaptic plasticity are impaired in a mouse model of Rett syndrome. *The Journal of neuroscience : the official journal of the Society for Neuroscience* 26: 319-27

Motil KJ, Caeg E, Barrish JO, Geerts S, Lane JB, et al. 2012. Gastrointestinal and nutritional problems occur frequently throughout life in girls and women with Rett syndrome. *J Pediatr Gastroenterol Nutr* 55: 292-8

Na ES, Nelson ED, Adachi M, Autry AE, Mahgoub MA, et al. 2012. A mouse model for MeCP2 duplication syndrome: MeCP2 overexpression impairs learning and memory and synaptic transmission. *The Journal of neuroscience : the official journal of the Society for*

Neuroscience 32: 3109-17

Na ES, Nelson ED, Kavalali ET, Monteggia LM. 2013. The impact of MeCP2 loss- or gain-of-function on synaptic plasticity. *Neuropsychopharmacology : official publication of the American College of Neuropsychopharmacology* 38: 212-9

Nan X, Campoy FJ, Bird A. 1997. MeCP2 is a transcriptional repressor with abundant binding sites in genomic chromatin. *Cell* 88: 471-81

Nan X, Ng HH, Johnson CA, Laherty CD, Turner BM, et al. 1998. Transcriptional repression by the methyl-CpG-binding protein MeCP2 involves a histone deacetylase complex. *Nature* 393: 386-9

Neul JL, Kaufmann WE, Glaze DG, Christodoulou J, Clarke AJ, et al. 2010. Rett syndrome: revised diagnostic criteria and nomenclature. *Ann Neurol* 68: 944-50

Nguyen MV, Du F, Felice CA, Shan X, Nigam A, et al. 2012. MeCP2 is critical for maintaining mature neuronal networks and global brain anatomy during late stages of postnatal brain development and in the mature adult brain. *The Journal of neuroscience : the official journal of the Society for Neuroscience* 32: 10021-34

Nomura Y. 2005. Early behavior characteristics and sleep disturbance in Rett syndrome. *Brain Dev* 27 Suppl 1: S35-S42

Ogier M, Katz DM. 2008. Breathing dysfunction in Rett syndrome: understanding epigenetic regulation of the respiratory network. *Respir Physiol Neurobiol* 164: 55-63

Ogier M, Wang H, Hong E, Wang Q, Greenberg ME, Katz DM. 2007. Brain-derived neurotrophic factor expression and respiratory function improve after ampakine treatment in a mouse model of Rett syndrome. *The Journal of neuroscience : the official journal of the Society for Neuroscience* 27: 10912-7

Olson CO, Zachariah RM, Ezeonwuka CD, Liyanage VR, Rastegar M. 2014. Brain region-specific expression of MeCP2 isoforms correlates with DNA methylation within Mecp2 regulatory elements. *PLoS One* 9: e90645

Percy AK, Lane JB. 2005. Rett syndrome: model of neurodevelopmental disorders. *J Child Neurol* 20: 718-21

Petel-Galil Y, Benteer B, Galil YP, Zeev BB, Greenbaum I, et al. 2006. Comprehensive diagnosis of Rett's syndrome relying on genetic, epigenetic and expression evidence of deficiency of the methyl-CpG-binding protein 2 gene: study of a cohort of Israeli patients. *J Med Genet* 43: e56

Ramirez JM, Ward CS, Neul JL. 2013. Breathing challenges in Rett syndrome: lessons learned from humans and animal models. *Respir Physiol Neurobiol* 189: 280-7

Ramocki MB, Tavyev YJ, Peters SU. 2010. The MECP2 duplication syndrome. *Am J Med Genet A* 152A: 1079-88

Reiss AL, Faruque F, Naidu S, Abrams M, Beaty T, et al. 1993. Neuroanatomy of Rett syndrome: a volumetric imaging study. *Ann Neurol* 34: 227-34

Rett A. 1966. [On a unusual brain atrophy syndrome in hyperammonemia in childhood]. *Wien Med Wochenschr* 116: 723-6

Ricceri L, De Filippis B, Laviola G. 2008. Mouse models of Rett syndrome: from behavioural phenotyping to preclinical evaluation of new therapeutic approaches. *Behav Pharmacol* 19: 501-17

Ricciardi S, Boggio EM, Grosso S, Lonetti G, Forlani G, et al. 2011. Reduced AKT/mTOR signaling and protein synthesis dysregulation in a Rett syndrome animal model. *Hum Mol Genet* 20: 1182-96

Robinson L, Guy J, McKay L, Brockett E, Spike RC, et al. 2012. Morphological and functional reversal of phenotypes in a mouse model of Rett syndrome. *Brain* 135: 2699-710

Ronnett GV, Leopold D, Cai X, Hoffbuhr KC, Moses L, et al. 2003. Olfactory biopsies demonstrate a defect in neuronal development in Rett's syndrome. *Ann Neurol* 54: 206-18

Roze E, Cochen V, Sangla S, Bienvenu T, Roubergue A, et al. 2007. Rett syndrome: an overlooked diagnosis in women with stereotypic hand movements, psychomotor retardation, Parkinsonism, and dystonia? *Mov Disord* 22: 387-9

Samaco RC, Mandel-Brehm C, Chao HT, Ward CS, Fyffe-Maricich SL, et al. 2009. Loss of MeCP2 in aminergic neurons causes cell-autonomous defects in neurotransmitter synthesis and specific behavioral abnormalities. *Proceedings of the National Academy of Sciences of the United States of America* 106: 21966-71

Samaco RC, Neul JL. 2011. Complexities of Rett syndrome and MeCP2. *The Journal of neuroscience : the official journal of the Society for Neuroscience* 31: 7951-9

Saywell V, Viola A, Confort-Gouny S, Le Fur Y, Villard L, Cozzone PJ. 2006. Brain magnetic resonance study of Mecp2 deletion effects on anatomy and metabolism. *Biochem Biophys Res Commun* 340: 776-83

Schmid DA, Yang T, Ogier M, Adams I, Mirakhur Y, et al. 2012. A TrkB small molecule partial agonist rescues TrkB phosphorylation deficits and improves respiratory function in a mouse model of Rett syndrome. *The Journal of neuroscience : the official journal of the Society for Neuroscience* 32: 1803-10

Schule B, Armstrong DD, Vogel H, Oviedo A, Francke U. 2008. Severe congenital encephalopathy caused by MECP2 null mutations in males: central hypoxia and reduced neuronal dendritic structure. *Clin Genet* 74: 116-26

Shahbazian M, Young J, Yuva-Paylor L, Spencer C, Antalffy B, et al. 2002a. Mice with truncated MeCP2 recapitulate many Rett syndrome features and display hyperacetylation of histone H3. *Neuron* 35: 243-54

Shahbazian MD, Antalffy B, Armstrong DL, Zoghbi HY. 2002b. Insight into Rett syndrome: MeCP2 levels display tissue- and cell-specific differences and correlate with neuronal maturation. *Hum Mol Genet* 11: 115-24

Shepherd GM, Katz DM. 2011. Synaptic microcircuit dysfunction in genetic models of neurodevelopmental disorders: focus on Mecp2 and Met. *Curr Opin Neurobiol* 21: 827-33

Skene PJ, Illingworth RS, Webb S, Kerr AR, James KD, et al. 2010. Neuronal MeCP2 is expressed at near histone-octamer levels and globally alters the chromatin state. *Mol Cell* 37: 457-68

Stearns NA, Schaevitz LR, Bowling H, Nag N, Berger UV, Berger-Sweeney J. 2007. Behavioral and anatomical abnormalities in Mecp2 mutant mice: a model for Rett syndrome. *Neuroscience* 146: 907-21

Takahashi K, Yamanaka S. 2006. Induction of pluripotent stem cells from mouse embryonic and adult fibroblast cultures by defined factors. *Cell* 126: 663-76

Taneja P, Ogier M, Brooks-Harris G, Schmid DA, Katz DM, Nelson SB. 2009. Pathophysiology of locus ceruleus neurons in a mouse model of Rett syndrome. *The Journal of neuroscience : the official journal of the Society for Neuroscience* 29: 12187-95

Tropea D, Giacometti E, Wilson NR, Beard C, McCurry C, et al. 2009. Partial reversal of Rett Syndrome-like symptoms in MeCP2 mutant mice. *Proceedings of the National Academy of Sciences of the United States of America* 106: 2029-34

Weng SM, Bailey ME, Cobb SR. 2011a. Rett syndrome: from bed to bench. *Pediatr Neonatol* 52: 309-16

Weng SM, McLeod F, Bailey ME, Cobb SR. 2011b. Synaptic plasticity deficits in an experimental model of rett syndrome: long-term potentiation saturation and its pharmacological reversal. *Neuroscience* 180: 314-21

Wood L, Gray NW, Zhou Z, Greenberg ME, Shepherd GM. 2009. Synaptic circuit abnormalities of motor-frontal layer 2/3 pyramidal neurons in an RNA interference model of methyl-CpG-binding protein 2 deficiency. *The Journal of neuroscience : the official journal of the Society for Neuroscience* 29: 12440-8

Wu H, Tao J, Chen PJ, Shahab A, Ge W, et al. 2010. Genome-wide analysis reveals methyl-CpG-binding protein 2-dependent regulation of microRNAs in a mouse model of Rett syndrome. *Proceedings of the National Academy of Sciences of the United States of America* 107: 18161-6

Young JI, Hong EP, Castle JC, Crespo-Barreto J, Bowman AB, et al. 2005. Regulation of RNA splicing by the methylation-dependent transcriptional repressor methyl-CpG binding protein 2. *Proceedings of the National Academy of Sciences of the United States of America* 102: 17551-8

Zachariah RM, Olson CO, Ezeonwuka C, Rastegar M. 2012. Novel MeCP2 isoform-specific antibody reveals the endogenous MeCP2E1 expression in murine brain, primary neurons and astrocytes. *PLoS One* 7: e49763

Zhou Z, Hong EJ, Cohen S, Zhao WN, Ho HY, et al. 2006. Brain-specific phosphorylation of MeCP2 regulates activity-dependent Bdnf transcription, dendritic growth, and spine maturation. *Neuron* 52: 255-69

CHAPTER 2

Circadian Dysfunction in a Mouse Model of Rett Syndrome

Abstract

Rett Syndrome (RTT) is a severe X-chromosome-linked monogenic disorder and the majority of RTT cases are caused by the mutations in *MECP2* gene encoding methyl-CpG-binding protein 2 (MeCP2). Sleep disturbances with abnormal sleep/wake cycles are prevalent in RTT patients indicating a deficit in their circadian timing system. Previous studies already revealed that MeCP2 mRNA was intensively expressed in the central pacemaker, the suprachiasmatic nucleus (SCN) of circadian system and MeCP2 directly interacted with core clock genes functioning as a transcriptional activator. In the present study, hemizygous *Mecp2*$^{-/y}$ mice were examined to determine the disruption of circadian system and the potential underlying mechanisms caused by MeCP2 dysfunction. *Mecp2*$^{-/y}$ mice exhibited severe deficits in circadian rhythms of locomotor activity and temporal pattern of daily activity combined with extremely fragmented sleep. In addition, spontaneous electrical activity and molecular core clock component were significantly attenuated in the SCN neurons indicating a weakened and disrupted central clock. Moreover, disrupted core clock expression found in peripheral organs suggested disorganized peripheral oscillators. *Mecp2*$^{-/y}$ MEFs demonstrated reduced core clock gene expression combined with a loss of cyclic binding pattern of histone markers at the promoter regions. At last, RTT Fibroblasts exhibited dysregulated molecular clock expression and *Mecp2*$^{-/y}$ mice were vulnerable to destabilized circadian system as chronic jet lag significantly accelerated the mortality of mutant mice. These data strongly indicate an essential role of MeCP2 in circadian timing system and may have an implication on the long-term health care of RTT patients in regard to stabilization of their circadian system and sleep wake cycles.

Introduction

Circadian system

Almost all the organisms display behavioral and biochemical rhythmic oscillations over a 24 hour period from archaebacteria to humans. These circadian (Latin; *circa*-, ”approximately”, -*diem*, “day”) rhythms are evolutionarily conserved and driven by the central pacemaker to synchronize biological activity to the cycle of light and darkness so that they enable the physiology and behavior of the organism to anticipate, and thereby adapt to the solar day and night. There are at least three fundamental properties of biological circadian rhythms: 1) self-sustaining: they are not merely stimulus-evoked responses since they persist in the absence of external cues; 2) entrainment:, they can adjust to external cues and attains a period that equals that of environmental light-dark cycle; 3) temperature compensation:; the period and amplitude of rhythms are not affected by different temperature. In mammals the circadian system is arranged in a hierarchical structure and can be divided into two major components: the central clock, located in the suprachiasmatic nucleus (SCN) of hypothalamus containing the master oscillatory network that is necessary for maintaining the daily rhythms in accordance with the external environment; and the peripheral clocks that are present in nearly every tissue and organ system (Albrecht & Eichele 2003). While the SCN ensures that peripheral clocks are appropriately synchronized, peripheral tissues oscillators can be entrained independently of the central clocks. It is believed that the SCN functions as a conductor of an orchestra of clocks that synchronizes all peripheral clocks and integrates input pathways to generate coherent systemic rhythms in the organism (Davidson et al 2003, Dibner et al 2010).

The suprachiasmatic nucleus (SCN)

SCN, the master pacemaker is a bilaterally paired nucleus made up of tightly compacted, small –diameter neurons that are located just lateral to the third ventricle, atop the optic chiasm. SCN is anatomically divided into two subdivisions: a ventral core region and a dorsal shell region (Golombek & Rosenstein 2010). As indicated in **Fig 2.1**, the core neurons act as an integrator of external inputs and receive information from the retina, This input is relayed along the retinohypothalamic tract (RHT), the second projection of the geniculohypothalamic tract (GHT) via intergeniculate leaflet (IGL) of the thalamus and a further afferent projection originating from the raphe nucleus. Light stimulation is perceived primarily by intrinsically photosensitive retinal ganglion cells (ipRGCs) in the retina that express the photopigment melanopsin and propagate photic information to the SCN via the RHT via releasing glutamate and pituitary adenylyl cyclase-activating peptide (PACAP) as neurotransmitters at RHT terminal synapses. Non-photic cues such as physical activity, social interactions and feeding routines are relayed via the GHT from IGL and Raphe nuclei by incorporating neuropeptide Y (NPY), 5-hydroxytryptamine (5-HT) and gamma aminobutyric acid (GABA) as neuronal mediators (Albrecht 2012). These sensory processing ventral cells expressing the neuropeptides vasoactive intestinal peptide (VIP) and gastrin-releasing peptide (GRP) as well as neurotransmitter GABA exhibit relatively low amplitude rhythms in clock gene expression so that it may be easier to reset to environmental cues. In contrast, neurons in the dorsal shell releasing different types of neuropeptides GABA and arginine vasopressin (AVP) as well as prokineticin 2 (PK2) likely generate robust circadian oscillations at the level of gene expression.

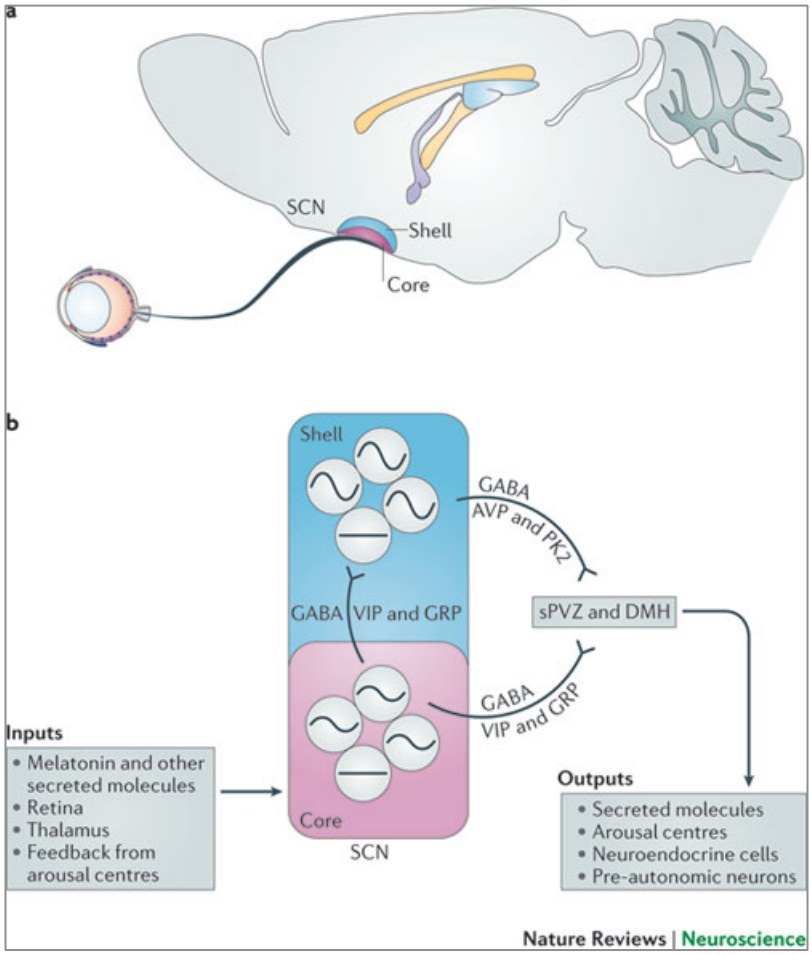

Fig 2.1 The suprachiasmatic nucleus circuit

A. The suprachiasmatic nucleus (SCN) is located in the hypothalamus compromising of a ventrolateral core and a dorsomedial shell.

B. SCN core neurons integrate external information including light and non-photic cues from the retinohypothalamic tract (RHT), the thalamus and midbrain structures. Core neurons relay this information to the rest of the SCN using GABA, VIP and GRP. Shell neurons use GABA and AVP or PK2 to communicate with other cell populations. The amplitudes of the rhythms in gene expression and neural activity in core and shell neurons are relatively low and high, respectively. The outputs of SCN neurons travel mainly to other hypothalamic regions, including sPVZ and DMH, and these hypothalamic relay nuclei send projections throughout the CNS and endocrine system.

Permission to reuse figure from Colwell CS 2011

Regardless of whether an animal is diurnal or nocturnal, neurons in SCN are electrically active and display high spontaneous firing rate with peaks of around 6-10 Hz during the middle of the day. During the night, SCN neuron populations are electrically inactive with a firing rate about 3-4 Hz and are mostly responsive to excitatory or depolarizing stimulation (Colwell 2011).

The SCN is not the only structure in the brain that displays daily oscillation. Nuclei in the thalamus and hypothalamus, amygdala, hippocampus, habenula, and the olfactory bulbs show such similar oscillations. The most robust rhythms, beyond those observed in the SCN, are found in the olfactory bulbs and tissues that have neuroendocrine functions. These brain areas include the arcuate nucleus (ARC), the paraventricular nucleus (PVN), and the pituitary gland. The SCN outputs from both core and shell subpopulations travel mainly to other hypothalamic nuclei and drive circadian rhythms by either direct outputs to paraventricular nucleus (PV) or relays through subparaventricular zones (SPVZ), sending projections throughout the nervous and endocrine system and regulate multiple rhythmic behavior and physiological processes. For example, the ventral SPZ (vSPZ) drives the dorsomedical nucleus of the hypothalamus (DMH) to control the circadian rhythms of wake-sleep, locomotion, feeding, stress hormone release as well as body temperature cycle (Albrecht 2012, Dibner et al 2010, Mohawk et al 2012).

Molecular clock

Key components of the molecular clock that drive rhythmic behavior have been extensively

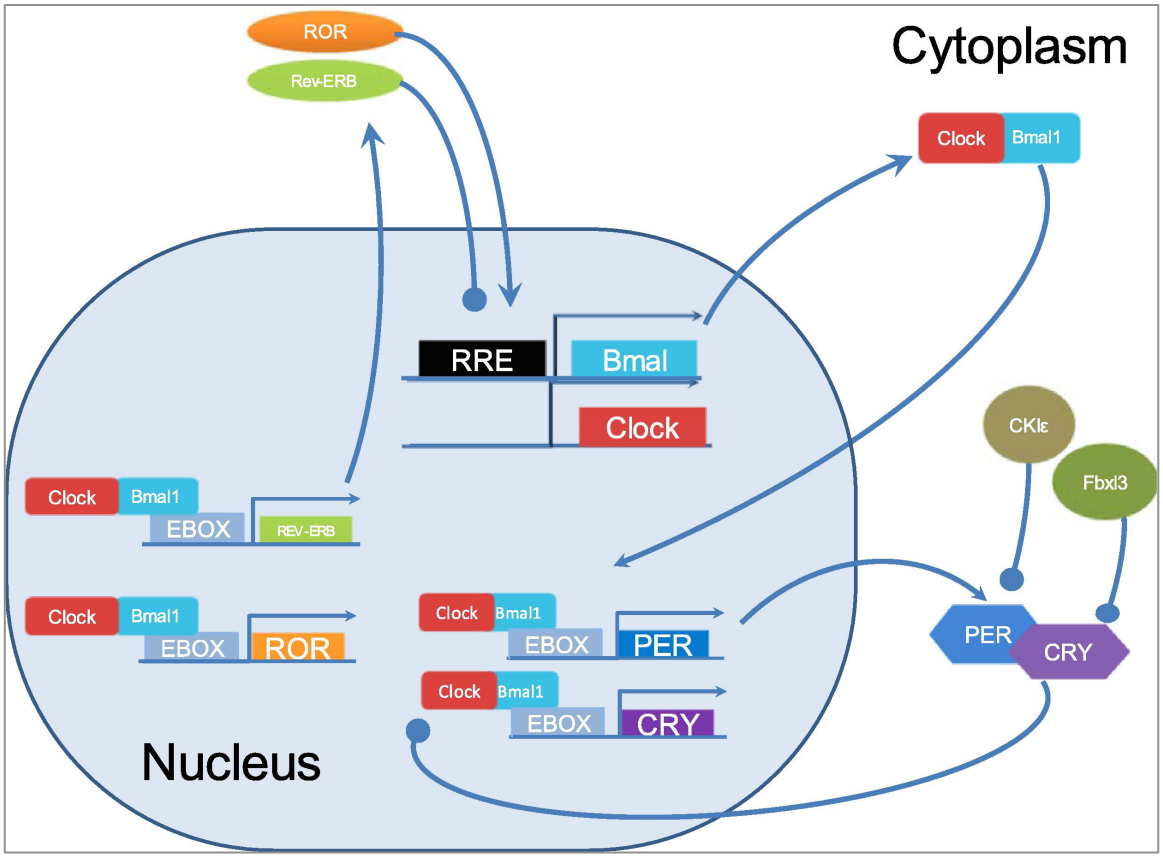

Fig 2.2 Schematic representation of the TTFL core circadian clock

BMALl and CLOCK transcription products translocate to the cytoplasm and dimerize. They then translocate back to the nucleus binding to E-box elements and promoting PER, CRY, REV-ERB and ROR transcription. Upon translation, PER and CRY proteins accumulate in the cytoplasm, dimerize and return to the nucleus where they suppress their own transcription through directly inhibition of the binding of the CLOCK/BMAL1 complex. PER and CRY are subsequently degraded through ubiquitylation following casein kinae- and Fbx13-dependent phosphorylation, respectively. A second feedback loop includes ReV-ERB and RORs, which repress and activate the transcription of BMAL1 respectively.

Permission to reuse figure from Robinson & Reddy 2014

studied and characterized in numerous species including flies, mollusks, fish and mammals. The mammalian circadian clock consists of a cell-autonomous and auto-regulatory transcription translational feedback loop (TTFL, **Fig 2.2**) (Frank et al 2013, Robinson & Reddy 2014)**.** The core component of TTFL, circadian locomotor output cycles kaput (CLOCK) forms basic helix-loop-helix transcription factors complex with brain and muscle ARNT-like protein 1 (BMAL1) and interacts with enhancer box (E-box) regulatory elements in the *Period (Per)* and *Cryptochrome* (*Cry*) genes to activate their transcription of a family of genes including *Per1, Per2, Per3, Cry1* and *Cry2* genes. The level of the transcripts for *Per* and *Cry* genes reaches their peak during the middle and late period of the day, whereas the PER and CRY proteins accumulate upon translation, dimerize, and translocate back to the nucleus in the early evening. The PERs, CRYs and other proteins form complexes and turn off their own transcriptional activity through direct interaction with CLOCK-BMAL1. As the negative elements are degraded by ubiquitylation, repression of CLOCK and BMAL1 is removed allowing the new cycle of transcription to begin at the following morning. The whole process takes approximately 24 hours to complete. In addition to this core feedback loop, a second important feedback loop involves the nuclear receptors REV-ERBs and retinoic acid-related orphan receptors (RORs), which are also driven by CLOCK/BMAL1. Their protein products in turn activate and repress the transcription of BMAL1 in an anti-phase transcriptional cycle. Another group of clock-regulated genes carrying their D-box regulatory elements are downstream of the core oscillator and are ultimately responsible for generating the circadian cycles of cellular activity underlying circadian behavior and physiology. In the SCN, this output includes genes

and proteins involved in synaptic transmission, metabolism, and electrophysiological activity of ion channels and receptors.

Sleep-wake cycle

The sleep/wake cycle is one of the most studied circadian cycles. Circadian disruption can profoundly impact sleep and sleep disruption has been found tightly associated with a wide range of neuropsychiatric diseases including emotional, cognitive and neurodegenerative diseases. Sleep is proposed to be a two-process model for its regulation: homeostatic component and circadian drives for sleep (Borbely 1982, Saper & Sehgal 2013). Recent studies have clarified the relationship between the SCN and the sleep-wake cycle. Projections originating from the SCN are relayed through sPVZ and DMH into the nuclei that promote states of sleep such as ventro-lateral pre-optic area (VLPO) and wakefulness involving tubero-mammillary nucleus, TMN and locus coeruleus. The homeostatic component seems to respond to prior sleep-wake history by increasing sleepiness with time spent awake and decreasing these variables with time spent asleep. However, the underlying physiological mechanisms are not well understood (Schwartz & Roth 2008). Together, sleep homeostatic mechanism tracks sleep need, whereas the circadian clock drives sleep to occur at a particular time of the light/dark cycle. The combination of circadian and homeostatic sleep drive determines the length of sleep.

Circadian disruption related disorders

It is clear that being synchronous with the environment confers many biological advantages,

while being out of synchrony could be detrimental. For example, jet lag due to shifting the light-dark cycle occurs when flying across different time zones and results in the progressive resynchronization of the circadian system to the new environment time. In addition, this temporarily disrupts the rhythmic expression of circadian-related genes within the SCN and decouples the SCN from peripheral oscillators. The consequential clock misalignment due to repeated phase shifting of light/dark cycle leads to various aspects of tiredness, mental confusion, cognitive deficits, even increased risks of cancer, cardiovascular disease and obesity as well as diabetes (Hastings et al 2014). Furthermore, many studies already demonstrate that sleep and circadian rhythm disruption is a common feature and diagnostic criteria for neuropsychiatric diseases, especially in schizophrenia, bipolar disorder and major depression (Jagannath et al 2013). Finally, it is well established that neurodegenerative diseases including Alzheimer's disease, Huntington's disease and Parkinson's disease compromise sleep and circadian clock functions. Although clock disturbance might not be the primary cause of neurodegeneration, it is evident that as the disease progresses and impairs clock and sleep functions, this will enhance the brain's susceptibility to the pathology and aggravate its progression. So defects in circadian controlled sleep–wake cycle may contribute to the pathogenesis of neurodegenerative diseases (Hastings & Goedert 2013).

Sleep disturbances in Rett Syndrome (RTT)

Rett syndrome is the leading cause of severe intellectual disability in females and caused by mutations in the X chromosome-linked gene encoding methyl-CpG-binding protein 2 (MECP2).

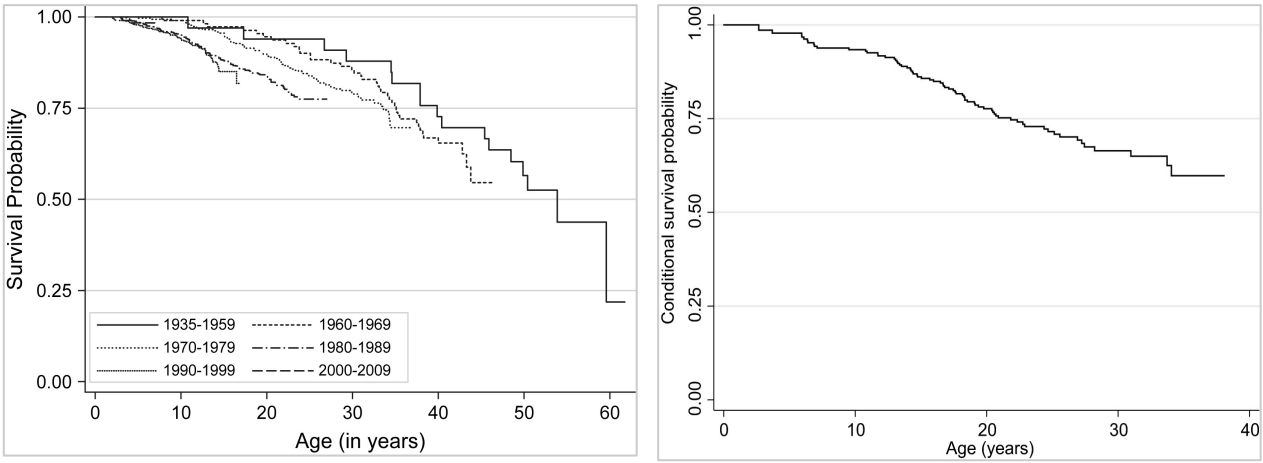

Fig 2.3 Kaplan Meier survival Curve for RTT female patients demonstrating the potential survival into middle age

Left panel: Kaplan Meier Survival patterns for 1928 RTT female participants by decade of birth registered from the North American Rett syndrome Database (NARD).

Right Panel: Kaplan Meier Survival Curve for 396 girls and women with RTT registered with the Australian Rett Syndrome Database (ARSD) (Median age 18.3)

Permission to reuse figure from Kirby RS et al 2010; Anderson A et al 2014

For general review of RTT and MeCP2 function please see **Chapter 1**. Sleep disturbances are very common in RTT patients and have already become standard criteria for RTT diagnosis (Chapleau et al 2013). Previous clinical studies with RTT patients clearly indicate that sleep problems are reported in more than 80% cases that include irregular sleep/wake patterns with increased sleep latencies or delayed/advanced sleep onset, excessive daytime sleep and night-time behavior such as screaming, crying and laughing (Anderson et al 2014, d'Orsi et al 2009, Ellaway et al 2001, Hagebeuk et al 2013, Nomura 2005, Young et al 2007). In addition, studies showed that frequent arousals not caused by apneas or seizures, and low sleep efficiencies were present in RTT cases (Carotenuto et al 2013). Especially, sleep disturbances

usually appear in the latest phase (IV) and are highly prevalent in older women, whereas sleep problems in autism generally begin during early childhood (Roane et al 2001). Thus, RTT is considered to be distinguishable from autism spectrum conditions, at least in terms of sleep disturbances studies (Guenole & Baleyte 2011). These sleep problems in RTT indicate deficits in circadian timing system, however the circadian control of sleep in RTT patients and it underlying mechanism still remains poorly understood.

Implication of current study

It is believed that approximately 10-15% of all the transcripts in any given cell are expressed in a cyclic manner under the circadian control. Epigenetic mechanism such as cyclic chromatin remodeling seems to play a pivotal role in the transcriptional oscillation of clock controlled gene transcription (Aguilar-Arnal & Sassone-Corsi 2013, Masri & Sassone-Corsi 2013). MeCP2 is a brain abundant multifunctional protein involved in transcriptional regulation and chromatin modulation (see **Chapter 1**). Previous studies using *in situ* hybridization demonstrated an intensive MeCP2 mRNA expression within the SCN−the central circadian clock−in the adult mouse (Dragich et al 2007). In addition, MeCP2 directly interacted within promoter regions of *mPer1* and *mPer2* revealed by ChIP-qPCRs and overexpression of MeCP2 activated mPer1 and mPer2 expression in cultured cells (Alvarez-Saavedra et al 2011).

MeCP2$^{-/y}$ mutant male mice were examined in my dissertation studies. It could be argued that female heterozygous mice should be the best experimental models for RTT research as majority RTT patients are females. However, male mutant mice consistently develop severe

and characteristic behavioral phenotypes that recapitulate many of RTT phenotypes. In addition, these mutant male mice provide homogenous cell population without the effects of XCI so that they would be more valuable models for experimental research in the laboratory. In contrast, MeCP2 female heterozygous mice develop and exhibit RTT-related phenotypes at a later stage, which does not truly recapitulate the onset and progression of symptoms associated with RTT. Here we used a mouse model of RTT, *Mecp2*$^{-/y}$ hemizygous mice (Jaenisch strain) combined with behavioral analysis, electrophysiology and molecular biology methods in the present study. The significant circadian deficits are discovered in behavioral rhythms, SCN neuronal activities and molecular clock components. The significance of the current study is to examine the need and importance of sleep hygiene in clinical care and disease management of RTT individuals. It has been reported that the likelihood of RTT survival was around 70-80% at 25 years and about 60% at 38 years in a cohort of North American Rett Database (Kirby et al 2010) and Australian Rett Syndrome Database (Anderson et al 2014). These studies aimed for description of overall survival and adult health in RTT patients have clearly indicated that RTT individuals have a great potential for prolonged survival with approximately 60% surviving to early middle age. Thus, it becomes critical to develop and advocate a proper long-term care plans that maintain and improve life quality of RTT individuals. The current study would provide a better understanding of the mechanisms underlying the association between sleep disturbances and disrupted circadian function. The present data strongly suggest that the stabilization of sleep/circadian rhythms might provide a new and powerful therapeutic target for RTT treatment through a combination of behavioral therapy and medicine that regulate sleep.

Materials and Methods

Animals

Animals were housed in the University of California, Los Angeles (UCLA) animal care facility and all the procedures were performed in accordance with guidelines approved by the Animal Research Committee (ARC) at UCLA. All the experiments except for PER2 bioluminescence experiments were conducted with *Mecp2*$^{1lox/y}$ male mice and their C57BL/6 wild-type littermates. Female heterozygous founder mice (Strain name: *B6.Cg-Mecp2*$^{tm1.1Jae}$/Mmucd) were obtained from Mutant Mouse Regional Resource Center (MMRRC) at UC Davis and used to establish a colony of *Mecp2*^{1lox} mutant mice carrying germline-recombined *Mecp2*-mutant allele at UCLA. *Mecp2*$^{tm1.1Jae}$ (Jaenisch strain) mice constitutively express a truncated MeCP2 protein lacking the MBD due to exon 3 deletions but with an intact C-terminus and they usually are considered mutant mice rather than "knockout" or "null" mice. This mutant line was maintained by backcrossing heterozygous *Mecp2*$^{1lox/+}$ females with C57/BL6 wild-type males (Chen et al 2001). For *ex vivo* PER2::LUC driven bioluminescence experiments, *Mecp2*$^{-/+}$ female heterozygous mice were crossed with mice homozygous PER2::LUC knock-in mice (*mPer2*$^{Luc/Luc}$) (Yoo et al 2004) for the luciferase reporter inserted as an in-frame fusion to the endogenous *Period2* gene on a C57BL/6J background (minimum of 12 generations). Hemizygous *Mecp2*$^{-/y}$ mice and their wild-type littermates *Mecp2*$^{+/+}$ with a heterozygous mPer2$^{Luc/+}$ allele were used to monitor real time PER2::LUCIFERACE bioluminescence rhythms. Mutant littermate and WT controls were studied in parallel and inspected daily for signs of ill health and euthanized if necessary.

Wheel running activity

Methods used were similar to those described previously (Kudo et al 2011a, Kudo et al 2011b). Male *Mecp2*$^{-/y}$ mice and wild-type littermates at the age of 4-5 weeks were housed individually for monitoring wheel-running activity. The running wheels and data acquisition system were obtained from Mini Mitter Co. (Bend, OR) and animals' wheel-running activities were recorded as revolutions (rev) per 3 min intervals. Mice were entrained to a 12:12 h light-dark (LD) cycle for a minimum of 1 week prior to a collection of 10 days of data under LD condition (light intensity 300 lux), and subsequently were placed into constant darkness (DD) to assess their free-running activity pattern for 10 days. Wheel revolutions were recorded in 3 min bins for 10 days and data under each condition were averaged for analysis. The locomotor activity rhythms were analyzed by periodogram analysis combined with the $\chi 2$ test with $P = 0.05$ significance levels (El Temps, Barcelona, Spain) on the raw data. The periodogram shows the power of amplitude rhythm (%V) in all the time series interested and the power values were determined by the multiplying Qp values of the periodogram by 100/N (Qp X 100/N: N = total number of data points) with the EI Temps program (Barcelona, Spain). Slopes of an eye-fitted line through the onsets were used to validate periods estimates made with the periodogram analysis. In general, power values over 30% were considered an indication of strong and coherent activity rhythms. Lower power can be a reflection of a decrease in precision, amplitude, or an increase in variability in the behavioral rhythm. The averaged number of wheel revolutions per hour for 10 days represented activity levels (rev/hr). Fragmentation was determined by the averaged number of activity bouts per day (bouts/day) with ClockLab

software (Actimetrics, Wilmette, IL), whereas the bout was defined as 21 consecutive minutes activity (maximum gap: 21 min; threshold: 3 counts/min). Precision was analyzed by calculating the daily variation in onset from a best-fit regression line drawn through 10 days of activity in either LD or DD condition with the Clocklab program. The activity duration was the designated alpha (α) while the remaining duration of non-wheel running activity is rho (ρ). All animals handling was carried out either in the light portion of the LD cycle or in DD with the aid of night vision goggles (FJW Industries, Palantine, IL).

Negative masking

Negative masking behavior in *Mecp2*$^{-/y}$ mice and wild-type littermates were examined during 1 hour of full spectrum white light at 50 lux intensity from ZT 14 to ZT 15 (2 hours after lights off). Before the 1-hour light exposure experiment, animals were first entrained in a 12:12 hour LD cycle for at least a week and the baseline activity was determined as the activity level (wheel revolutions per hour) measured during the same ZT (ZT 14-ZT15) in the night just before 1 hour light treatment. Masking activity was determined as the activity (Rev/hour) measured during 1-hour light pulse and compared to baseline activity measured in the previous night.

Immobility-defined sleep measurement

Mecp2$^{-/y}$ mice and wild-type littermates at the age of 7-8 weeks old were housed individually in the absence of wheels and nesting materials, and entrained in 12:12 LD cycle. Mice were recorded via video surveillance cameras with visible light filters (Gadspot Inc., City

of Industry, CA) connected to the video-capture card (Adlink Technology Inc., Irvine, CA). The AnyMaze software (Stoelting Co., Wood Dale, IL) was applied to track the animal's sleep behavior as described previously that there were 99% correlation between immobility-defined sleep and EEG-defined sleep if an immobility detection threshold was set to a 95% of immobile area in an animal for a minimum of 40 seconds (Fisher et al 2012). Therefore, the sleep behavior was determined as 95% sensitivity of immobility detection for full duration of immobility that last at least 40 seconds, which was approved optimal and applied in previous published study (Loh et al 2013) as well as the present study. Animals were continuously monitored and recorded for consecutive 3 days under a 12:12 h LD cycle and data from day 2 and day 3 were collected for further analysis. Immobility-defined sleep data were calculated on the basis of 1 min bin and total sleep time was analyzed by summation of the duration of each sleep episode during the day (ZT 0-12) and night (ZT 12-24), respectively. A sleep bout was defined as a continuous immobility with at least 40 seconds of sleep per bin. The number of sleep bouts was calculated with Clocklab for continuous immobility data that met the minimum of 40 seconds immobility per 1 min bin. Average bout duration (number of consecutive bins with at least 40 sec of sleep per bin) was calculated during the day and night, respectively for comparison.

Whole cell patch-clamp electrophysiology

Methods used were similar to those described previously (Itri et al 2005, Itri et al 2010). *Mecp2*$^{-/y}$ mutant mice and wild-type littermates were recorded at the age of 5-6 weeks at ZT

(zeitgeber time) 2.5 and ZT 12.5 for day time (ZT 4-6) and night time (ZT 14-16) recordings, respectively. Animals entrained on a 12:12 LD or reverse LD cycle were anesthetized using isoflurane and their brains were dissected and placed in the fresh ice-cold, oxygenated slice solution containing 125 mM NaCl, 26 mM $NaHCO_3$, 3 mM KCl, 5 mM $MgCl_2$, 1.25 NaH_2PO_4, 1 mM $CaCl_2$ and 10 mM glucose (PH 7.2-7.4, osmolarity 290-310 mOsm) for 5 minutes. 300μm coronal slices of mid-SCN were collected in slice solution by a vibratome and then incubated for 30 minutes at 32°C followed by 1hr incubation at room temperature in artificial cerebral spinal fluid (ACSF; 125 mM NaCl, 26 mM $NaHCO_3$, 3 mM KCl, 2 mM $MgCl_2$, 1.25 NaH_2PO_4, 2 mM $CaCl_2$ and 10 mM glucose) while continually being aerated with 95% O2/5% CO2. Slices were placed in a recording chamber (PH-1, Warner Instruments, Hamden, CT) attached to the stage of an upright DIC microscope (OLYMPUS, Tokyo, Japan). SCN slices were incubated continuously (2 ml/min) with ACSF aerated with 95% O2/5% CO2 at room temperature during the whole experiment. The whole cell recording electrodes (3-7MΩ) were pulled from glass capillaries and recording micropipettes were filled with standard internal solution consisting of K-gluconate, 112.5 mM, EGTA 1 mM; MgATP 5 mM, GTP 1 mM, leupeptin 0.1 mM; phosphocreatine 10 mM, NaCl 4 mM; KCl 17.5 mM, $CaCl_2$ 0.5 mM, $MgCl_2$ 1 mM and Hepes 10 mM (PH 7.25-7.3 and osmolarity 290-300 mOsm). Recordings were obtained with the AXOPATCH 200B amplifier (Molecular Devices, Sunnyvale, CA) and monitored on-line with pCLAMP (Ver 10, Molecular Devices). KCl agar-bridge was used in the ground path to minimize any change in offset potentials due to ionic concentration changes. SCN neurons were directly visualized within SCN location according to anatomical structure

under DIC microscopy. Series and input resistance were monitored repeatedly and recordings were discarded if access resistance was greater than 40 MΩ or if values changed more than 20% during the course of the experiment. Spontaneous firing rates (SFR) were recorded with pCLAMP for 1 min using current-clamp in the whole cell patch configuration and no current was injected during recording.

Real-time imaging of PER2::LUC bioluminescence by a photomultiplier tube photodetector (PTP)

Methods used for real-time monitoring of PER2::LUC bioluminescence with *ex vivo* explants were similar to those described previously (Loh et al 2011). *Mecp2*$^{-/y}$ mutant mice and wild-type littermates at age of 5-6 weeks entrained in a stable 12:12 LD cycle were sacrificed between ZT10 and ZT11. SCN, hippocampus, heart, lung, liver, and adrenal explants were prepared with the explants and entered the Lumicycle photometer (Actimetrics, Widlmetter, IL) no later than ZT 12. Dissection and culture guidelines were followed with previous study (Yamazaki & Takahashi 2005). The prepared explants were transferred onto Millicell membranes (0.4 μm, PICMORG50, Millipore, Bedford, MA) resting on 1.2 ml of recording media that contained freshly added 0.1 mM luciferin (sodium salt monohydrate, Biosynth, Staad, Switzerland), and the 35 mm dishes were sealed using autoclaved high-vacuum grease (Dow Corning, Midland, MI). The explants were monitored at 37°C for 7-10 consecutive days, and the raw bioluminescence values were normalized by a series of steps: first subtracting the recorded baseline, then subtracting a running average of 24 hours of this baseline-subtracted

bioluminescence, and finally performing a 2-hour smoothing average. Period was calculated from an average of minimum of 6 peak-to-peak times. Amplitude was calculated by the summation of the peak and subsequent trough values. Rate of amplitude damping was calculated from the slope of at lease 6 consecutive amplitudes using the formula: $y=ae^{bx}$, where x = the number of days to damp for the value of y (amplitude) that is 1/e of the first amplitude, a was the intercept of the exponential regression through amplitude versus time, and b was the x variable coefficient. Together, the value of x meant the number of days to damp as an indicator of damping. Due to using a 24-hour moving average as a normalizing factor, the first actual recorded peak could not be used to determine the phase of the explants. Instead, the first for phase relationships mentioned in the results was referred to the second recorded peak.

Cell culture

Primary mouse embryonic fibroblasts (MEFs) were prepared from E13.5 embryos following a previous described protocol (Takahashi & Yamanaka 2006). *Mecp2*$^{-/y}$ MEFs and wild-type (WT) *Mecp2*$^{+/y}$ MEFs were dissected and collected from individual embryos isolated from E13.5-day-pregant female *Mecp2*$^{-/+}$ (heterozygous) mice in the C57B/L6 background. Following dissection, genotyping was performed to confirm MEFs genotype and only *Mecp2*$^{-/y}$ and *Mecp2*$^{+/y}$ MEFs from the same littermates were used for subsequent RT-qPCR and ChIP-qPCR experiments. MEFs in homogenous population were cultured and expanded with Dulbecco's modified eagle medium (DMEM, Life Technologies) with high glucose (4.5 g/L), 10% Fetal Bovine Serum (FBS), 2 mM L-glutamine, and 1x penicillin/streptomycin. Human

Foreskin Fibroblasts (HFFs) from RTT individuals and control human subject were commercially available (American Type Culture Collection, ATCC) and maintained according to manufacturer's recommended protocol. Three types of HFFs were used for RT-qPCR: GM17880B (RTT T158M), GM11273A (RTT 106W) and a wild-type control line (WT HFF). HFFs were cultured and expanded with 10% FBS MEFs medium. For synchronization protocol, MEFs or HFFs were stimulated with 0.1μM dexamethasone (D2915, Sigma-Aldrich) as described previously (Asher et al 2008, Nagoshi et al 2004). Specifically, cells were incubated with 0.1μM dexamethasone for 2 hours at 37 ^{0}C after cells reached confluence for 3 days. After 2 hours of incubation, medium was changed to 10% normal MEFs medium at time = 0. Then at each indicated time following synchronization, cells were washed with cold PBS and collected for total RNAs and chromatin.

Quantitative real time polymerase chain reaction (PCR)

Total RNAs were extracted from MEFs or HFFs using the Trizol (Invitrogen) protocol provided by the manufacturer. Specifically, cDNA was obtained by reverse transcription (RT) with Superscript III SuperMix Kit (Invitrogen) following manufacturer's protocol and non-RT controls were performed simultaneously to monitor genomic DNA contamination. Quantitative real time PCRs were performed with SYBR Green (Fast SYBR Green Master Mix, Life Technologies) using StepOnePlus system (Applied Biosystems, Life Technology). Oligonucleotide primers sequences were designed to cross intron-exon boundaries and validated for specificity and efficiency. Forward and reverse primers with corresponding transcripts were

listed as follow:

m*Bmal1* (180 bp): Forward: 5'-CCAACCCATACACAGAAGCA-3
Reverse: 5'-AGCTCTGGCCAATAAGGTCA-3'

m*Per2* (100 bp): Forward: 5'-GGGCATTACCTCCGAGTATA-3'
Reverse:5'-GGCCACTTGGTTAGAGATGTA-3'

m*Gapdh* (200 bp): Forward: 5'- AGAGAGGGAGGAGGGGAAATG
Reverse: 5'- AACAGGGAGGAGCAGAGAGCAC

h*Per1* (130 bp): Forward: 5'- CTGAGGAGGCCGAGAGGAAAGAA-3'
Reverse: 5'-AGGAGGAGGAGGCACATTTACGC-3'

h*Per2* (125bp) Forward: 5'- TGGATGAAAGGGCGGTCCCT-3'
Reverse: 5'- ACTGCAGGATCTTTTTGTGGA-3'

h*Gapdh* (200bp) Forward: 5'- CCGCATCTTCTTTTGCGT-3'
Reverse: 5'- TAAAAGCAGCCCTGGTGACC-3'

Reactions were performed with the equivalent of 20ng of starting total RNA in a 20-µl reaction volume comprising of the 2 X SYBR Green Master Mix and 0.5µM each of the forward and reverse primers. Melting curves were calculated at the end of each reaction to check PCR products specificity. The relative levels of clock gene transcripts were determined using the $2^{-\Delta\Delta Ct}$ methods with *Gapdh* as the normalizing reference gene. Studies confirmed that the levels of housekeeping gene transcript *Gapdh* did not fluctuate within all indicated time points.

Chromatin immunoprecipitation (ChIP)

Mecp2$^{-/y}$ MEFs and control *Mecp2*$^{+/y}$ MEFs were first synchronized with 0.1 µM dexamethasone for 2 hours and then collected every 12 h post synchronization: 12, 24, 36, and 48 hrs. For ChIP-qPCR experiments, 10^8 re-suspended MEFs plated on 10cm^2 plate at each

time point were cross-linked by adding 270 µl of 37% formaldehyde per 10 ml at a final concentration of 1% (vol/vol). Cells were cross-linked for 10 min at room temperature on a slowly rotating stage. To avoid over cross-linking, 1 ml of glycine (2.5M, Sigma) was added to MEFs per 10ml solution. MEFs were collected by centrifugation at 1,500 g for 10 minutes at 4°C and pellets were obtained and washed with cold PBS twice. Immediately, MEFs samples were snap frozen with liquid nitrogen and stored at -80°C until ready for ChIP. Nuclei of cross-linked pellets were isolated by stepwise hypotonic process as cell pellets were incubated with different lysis buffers supplemented with protease inhibitor cocktail (Roche). Nuclei pellets were collected by centrifugation and suspended in 0.3ml lysis buffer containing 10 mM Tris-HCl (pH 8.0), 1 mM EDTA (pH 8.0), 100 mM NaCl, 0.5 mM EGTA (pH 8.0), 0.1% Na-DOC (wt/vol, use 5% Na-DOC solution) and 0.5% N-lauryl-sarcosine (wt/vol with a 10% N-lauryl-sarcosine solution). The re-suspended nuclei were sonicated using Bioruptor (Diagenode) for 30 cycles (30 sec ON/30 sec OFF) at high power, resulting in DNA fragments of 400 - 600 base pairs (bp) in length. While preparing the nuclei lysate, 1µg of specific antibodies were coupled with 30 µl of Dynabeads (Dynabeads® M-280 Sheep Anti-Mouse IgG or Dynabeads M-280 Sheep anti-Rabbit IgG, Invitrogen) per ChIP reaction at 4°C on a rotating platform for 6 hrs. The beads were washed three times with blocking buffer after 6hrs rotation. 100µg of sheared chromatin were then added to antibody pre-coupled Dynabeads for overnight immunoprecipitation at 4^{o}C. On thennext day, the Dynabeads were washed with RIPA buffer comprising of 10 mM Tris-HCl (pH 8.0), 1 mM EDTA (pH 8.0), 140 mM NaCl, 1% (vol/vol) Triton X-100, 0.1% SDS (vol/vol, use 20% SDS solution and 0.1% Na-DOC (wt/vol with 5%

Na-DOC solution) 5 times followed by one time wash with TE buffer, then eluted from beads by incubating with elution buffer containing 50mM Tris-HCl, pH8.0, 10mM EDTA, pH 8.0 and 1% SDS at 65°C for 15 minutes with brief mixing on vortex. 2.5µL of Proteinase K was added to the eluted chromatin and WCE (whole cell extracts saved from sheared chromatin). MEFs samples were then reverse-crosslinked at 65°C for at least 6 hrs. After 6 hours of reverse cross-linking, the eluted samples were purified with DNA Clean & Concentrator™-5 kit (Zymo). Purified DNA fragments were subjected to real time qPCRs to analyze the protein to DNA interaction within Per2 promoter regions. Quantitative real time PCRs were performed on a StepOnePlus System (Applied Biosystems, Life Technologies) with SYBR Green regent (Fast SYBR Green Master Mix, Applied Biosystems). Results were often presented as "percent input" values which were calculated by quantifying the abundance of DNA fragments of interest added to the ChIP reaction with respect to the abundance of total input DNA fragments found in the final immunoprecipitate. Primers sequences were already validated and listed as below:

mPer2 (CpG binding site, 178bp): Forward: 5'-ACGTCGTCGCAGGTGATAG-3'
Reverse: 5- CGAGTAGGCTCGTCCACTTC-3'

m*Per2* (Cre1 binding site, 183 bp): Forward: 5'-CCAGGTGGATGAGCTGTGTA-3'
Reverse: 5'-AGCACCTCTGGTTCCTCTGA-3'

m*Per2* (Cre2 binding site, 162 bp): Forward: 5'-GAACCTCTGAGGGAACCACA-3'
Reverse: 5'-GTGCTCCCCATGTCTTGAGT-3'

Circadian destabilization by chronic jet lag

*Mecp*2$^{-/y}$ mice at the age of 5-6 weeks were entrained to a 12:12 h LD cycle. There were two groups of *Mecp*2$^{-/y}$ mice that received either stable LD cycle (control group) or jet lab light

condition (experimental group). *Mecp2*$^{-/y}$ mice in control group continued to be maintained on a previous stable 12:12 LD cycle. *Mecp2*$^{-/y}$ mice in jet lag group were housed under a circadian destabilization condition as a 6-hour phase advance was applied every week to mimic chronic jet lag condition. *Mecp2*$^{-/y}$ mice were examined daily for ill health status and euthanized if necessary until the end of experiments. Lifespan of *Mecp2*$^{-/y}$ mice from control and jet lag group were recorded and analyzed using the Kaplan-Meier survival analysis and statistical differences between these two groups was deemed significant at $P < 0.05$.

Immunohistochemistry (IHC)

Mecp2$^{-/y}$ mice and WT littermates at the age of 8-10 weeks were anaesthetized by isoflurane (Phoenix Pharmaceutical) at ZT 6 and perfused with 4% paraformaldehyde/PBS (Sigma-Aldrich) (pH 7.4). Brains were dissected, post-fixed at 4 °C overnight, and cryoprotected in 30% sucrose/PBS. IHC was performed on the free-floating 50 μm cryostat (Thermo Fisher Scientific) coronal brain sections from the middle of the rostral–caudal axis of SCN. Sections were washed 3 x 5 min with PBS, and then endogenous peroxidase activities were quenched with 3% H_2O_2 and 10% Methanol PBS for 10 min. Following 3 x 5min PBS wash, sections were dipped in 3% normal goat serum in PBS with 0.1% Triton X-100 for 1 h, and then incubated with a rabbit polyclonal VIP antibody (ImmunoStar, catalog # 20077) diluted 1:1,000 in PBS with 3% normal goat serum and 0.1% Triton X-100 at 4 °C for 24 hour. In the next day, sections were washed again with PBS 3 x 5min followed by 2 h incubation with biotinylated goat anti-rabbit secondary antibody (1:2000). Sections were washed 5 x 5 min in PBS and dipped in

Avidin-Biotin (AB) detection Solution (Vector Laboratories) for 1 h. After 3 x 5min PBS wash, SCN sections were placed in Tris-buffered saline (TBS) containing filtered 0.05% 3,3′-diaminobenzidine and 0.001625% H_2O_2. After sufficient color reaction (5–6 min) was observed, sections were washed with TBS and mounted on slides immediately. Then sections were dried overnight, dehydrated with ascending concentrations of ethanol, and cover-slipped. Images were captured with ApoTome structured illumination system with Stereo Investigator software (Carl Zeiss). To determine the number of VIP-positive (VIP+) cells, photographs were taken at 40X magnification and VIP+ cells were counted manually within the SCN using stereological methods. Immune-positive cells located within the grid were included for analysis without considering of staining intensity.

Statistical analysis

All statistical analysis was performed with Prism (ver. 6). Two way ANOVA followed by the post-hoc Holm-Sidak's multiple comparisons tests were used to determine effects of time and genotype on sleep behavior, negative masking, electrophysiology, PER2::LUC rhythms amplitude, clock gene qPCRs and ChIP-qPCRs studies. One factor analysis of variance (ANOVA) and non-parametric tests (Kruskal-Wallis test) were applied to determine the peak/trough values of RTT qPCR data for fold-change histograms. Unpaired t-tests were applied to compare wheel running activity, sleep and phase, periods of PER2::LUC bioluminescence rhythms from wild-type and *Mecp2*$^{-/y}$ mice. Kaplan-Meier survival test were used to compare lifespan of *Mecp2*$^{-/y}$ mice under two different light conditions.

Results

Mecp2$^{-/y}$ mice exhibited severe deficits in circadian rhythms of locomotor activity

We used the wheel-running activity to determine the impact of *Mecp2* mutation on daily and circadian rhythms of behavior (**Fig. 2.4**). Locomotor activity rhythms in wild-type mice were compared to *Mecp2*$^{-/y}$ littermates with the same C57/BL6 background (n=8 for each genotype) at the age of 8-10 weeks under the conditions of normal 12:12 hour light/dark cycle (LD) and constant darkness (DD). Under both LD and DD condition, all of *Mecp2*$^{-/y}$ mice were arrhythmic compared to wild-types as evident from representative double-plotted actograms of the wheel-running activity. Behavioral analysis demonstrated that *Mecp2*$^{-/y}$ mice, a model of RTT, exhibited severely disrupted daily and circadian rhythms in wheel-running activity. Specifically, the strength of free running rhythms (Power, %V) under DD condition was almost diminished in *Mecp2*$^{-/y}$ mice (**Fig 2.4B**). Circadian dysfunction in *Mecp2*$^{-/y}$ mice was also characterized by a significant reduction in both the amount of activity and the precision (onset error) as well as an increased fragmentation under both LD and DD condition (**Fig 2.4 C-F**). Moreover, *Mecp2* mutation also led to severe deterioration revealed by analysis of critical circadian-related parameters (**Table 2.1**). For example: the peak amplitude of the behavioral rhythms, nocturnality (percentage of activity during the night), length of activity period (duration of alpha-phase) and wheel-running coherence measured by fragmentation were dramatically decreased in *Mecp2*$^{-/y}$ mice under both LD and DD condition. There was also a significant difference in the period length of free-running rhythm (tau, τ) between wild-type and *Mecp2*$^{-/y}$

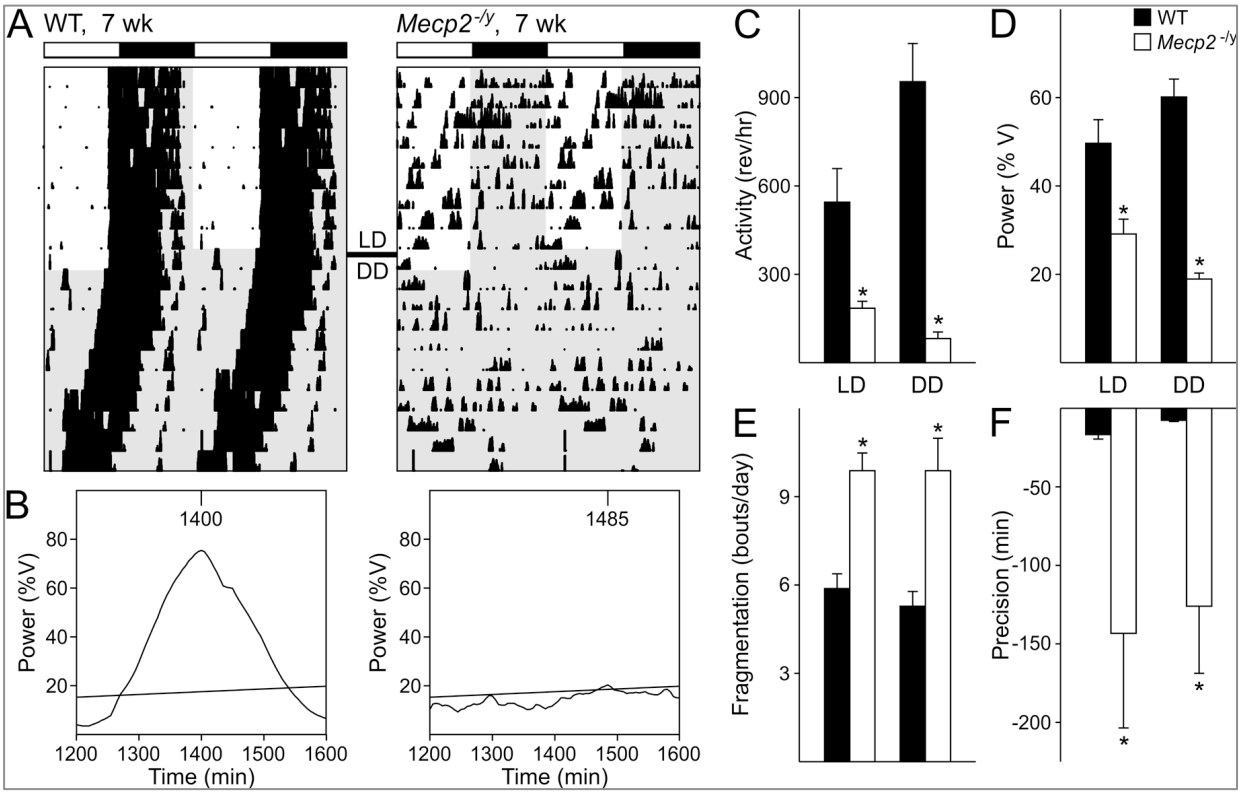

Fig 2.4 Circadian deficits in rhythms of locomotor activity in *Mecp2*$^{-/y}$ mice

A. Representative double-plotted actograms of wheel running activity from male wild-type littermates (left) and *Mecp2*$^{-/y}$ (right) mice at the age 8-10 weeks under 12:12 light/dark (LD) and constant darkness (DD) were shown. The white/black bars on top indicates the LD cycle and gray shading indicated darkness. Successive days of activity were plotted from top to bottom.

B. Chi-square (χ^2) periodograms of 10 days of activity in DD were shown from wild-type and *Mecp2*$^{-/y}$ mice with the peak of the periodogram indicating the free-running period of each genotype. Power (%V) referred to the normalized amplitude of the periodogram and the intersecting diagonal line indicated significance to $P < 0.05$.

C-F

Comparison of the amount of activity (C; wheel revolutions per hour), power (D, %V) measured by χ^2 periodogram fragmentation (E, average number of activity bouts per day), precision (F, cycle-to-cycle activity onset) between wild-type (black) and *Mecp2*$^{-/y}$ mice (white) under LD and DD condition respectively. * indicates significance to $P < 0.05$ in post hoc pairwise comparison between two genotypes after a significant effect of genotype determined by two-way ANOVA.

		WT (n=8)	Mecp2$^{-/y}$ (n=8)
LD	**Nocturnality**	89.9 ± 3.1	74.7 ± 2.9*
	Power (%V)	49.8 ± 5.2	29.2 ± 3.3*
	Alpha, α (min)	690.8 ± 52.5	361.1 ± 46.0*
	Activity (rev/hr)	547.1 ± 113.7	186.4 ± 23.7*
	Fragmentation (bouts/day)	5.9 ± 0.5	9.9 ± 0.6*
	Precision (min)	-17.1 ± 2.8	-143.6 ± 60.3*
DD	**Tau, τ (hr)**	23.5 ± 0.1	24.4 ± 0.3*
	Power (%)	60.3 ± 3.9	19.0 ± 1.2*
	Alpha, α (min)	502.1 ± 20.2	257.3 ± 32.9*
	Activity (rev/hr)	956.1 ± 129.5	86.7 ± 22.0*
	Fragmentation (bouts/day)	5.3 ± 0.5	9.9 ± 1.1*
	Precision (min)	-8.0 ± 0.7	-126.3 ± 42.9*
	LD-DD transition (min)	-32.9 ± 10.0	N/A
	CT 16 phase delay (min)	-81.6 ± 11.2	N/A

Table 2.1 Circadian parameters of activity in LD and DD between wild-type and *Mecp2*$^{-/y}$ mice at the age of 8-10 weeks

Parameters were analyzed using unpaired t-tests and * indicated significance to $P < 0.05$ between two genotypes.

mice. All together, this wheel-running activity behavior study clearly demonstrated severe deficits in circadian rhythms of locomotor activity and abnormal temporal patterning of daily activity in the *Mecp2*$^{-/y}$ mice.

Mecp2$^{-/y}$ mice exhibited a deficit in negative masking behavior

Negative masking refers to an acute suppression in response to light exposure on wheel running activity in nocturnal animals such as mice and hamster. It's believed that the same input pathway also mediates the light-induced phase shifting in circadian system involving melanopsin-expressing intrinsically photosensitive retinal ganglion cells that relay non-image-forming visual responses information through retinohypothalamic tract (RHT) (Morin 2013, Mrosovsky 1999). The actograms of wheel-running activity in *Mecp2*$^{-/y}$ mice exhibited poor entrainment under normal LD cycle indicating a potential deficit in the light induced input pathways. To confirm whether the SCN input pathways for light regulation were disrupted due to MeCP2 dysfunction, *Mecp2*$^{-/y}$ mice (n = 14) and their wild-type littermates (n = 9) were examined for negative masking behavior between two genotypes (**Fig. 2.5**). Two-way ANOVAs followed by Holm-Sidak's post hoc multiple tests revealed a significant interaction of both genotypes and treatment on the negative masking ($F_{1, 42} = 16.3$, $P < 0.0001$). Wild-type mice exhibited significant negative masking evident by suppression of their running-wheel activity during the light exposure period (486 ± 113 Rev/h, $P < 0.0001$) compared to their baseline activity (2052 ± 165 Rev/h). In contrast, *Mecp2*$^{-/y}$ mice showed a reduction in the wheel-running activity during 1-h light exposure. However, the difference was not statistically

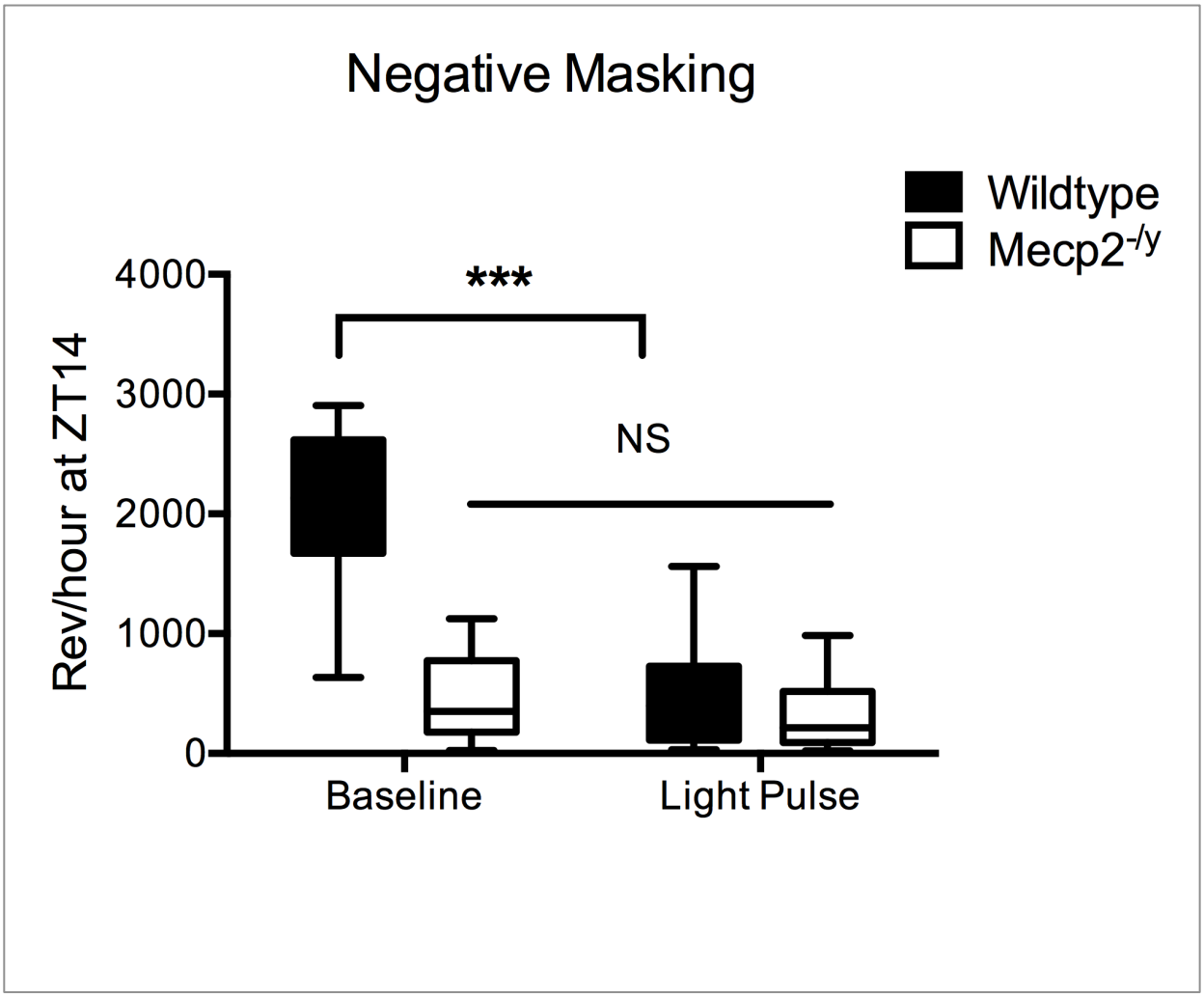

Fig 2.5 Negative masking behavioral was diminished in *Mecp2*$^{-/y}$ mice

Mecp2$^{-/y}$ (white) mice and wild-type (black) littermate controls were first entrained in a 12:12 LD cycle for at least a week and the baseline activity for each genotype was determined as the activity level (wheel revolutions per hour) measured during ZT 14-15 in the night just before 1 hour light exposure. Masking activity (Rev/hour) for each genotype was measured during 1-hour light exposure at the same ZT and compared to the baseline activity measured in the previous night. Data were presented in box-plot format. Statistical significance was determined at the level of $P < 0.05$ with two-way ANOVA analysis followed by *post hoc* multiple comparison tests. *** $P < 0.001$; NS $P > 0.05$

significant between their activity during light exposure (331 ± 103 Rev/h) and baseline (456 ± 125 Rev/h, P = 0.79) in the Mecp2-/y mice. This insignificance in negative masking could at least, partially due to low baseline activity in *Mecp2*$^{-/y}$ mice as there was a significant difference in baseline activity between *Mecp2*$^{-/y}$ mice and wild-type controls ($P < 0.0001$).

Temporal distribution of immobility-defined sleep was disrupted in *Mecp2*$^{-/y}$ mice

A common phenotype among RTT patients is poor sleep characterized by daytime napping and night awakening. To determine whether MeCP2 mutation caused the temporal pattern and amount of sleep under LD condition, sleep defined by time spent immobile was measured by video surveillance camera in combination with automated mouse tracking analysis software. As shown in **Fig 2.6A**, *Mecp2*$^{-/y}$ *mice* exhibited increased sleep latency (42.2 ± 18.6 min after lights on) compared to wild-type littermates (-4.0 ± 8.2 min after lights on, $P = 0.01$). *Mecp2*$^{-/y}$ mice did not show any alteration in the amount of total sleep time relative to their wild-type littermates during the day (WT, 445 ± 8 min; *Mecp2*$^{-/y}$, 442 ± 22 min; $P = 0.9$*)* and the night (WT, 166 ±9 min; *Mecp2*$^{-/y}$, 190 ± 42 min; $P = 0.7$) using two-way ANOVA analysis, respectively (**Fig 2.6B)**. To further examine the sleep quality in the *Mecp2*$^{-/y}$ mice for RTT model, fragmentation analysis at a higher temporal resolution was performed to determine the number of sleep bouts and the average duration of each sleep bout during the day (0-12h) and nigh (13-24h) **(Fig 2.6 C-D)**. Although sleep behavior in mice was much more fragmented and occurred during both the day and night time if compared to humans, *Mecp2*$^{-/y}$ mice showed the significant difference in both the number of sleep bouts and the average duration of sleep bout compared to the wild-type

Fig 2.6

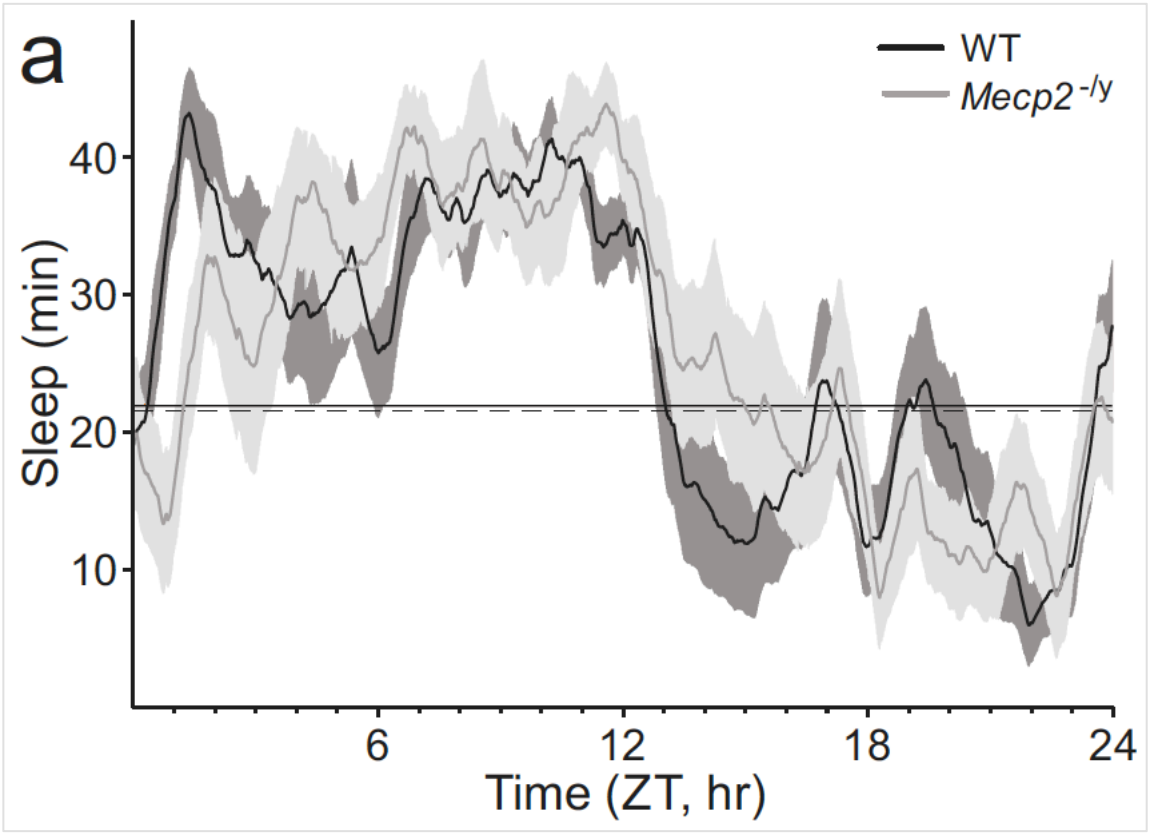
a
WT
Mecp2 -/y
Sleep (min)
40
30
20
10
6
12
18
24
Time (ZT, hr)

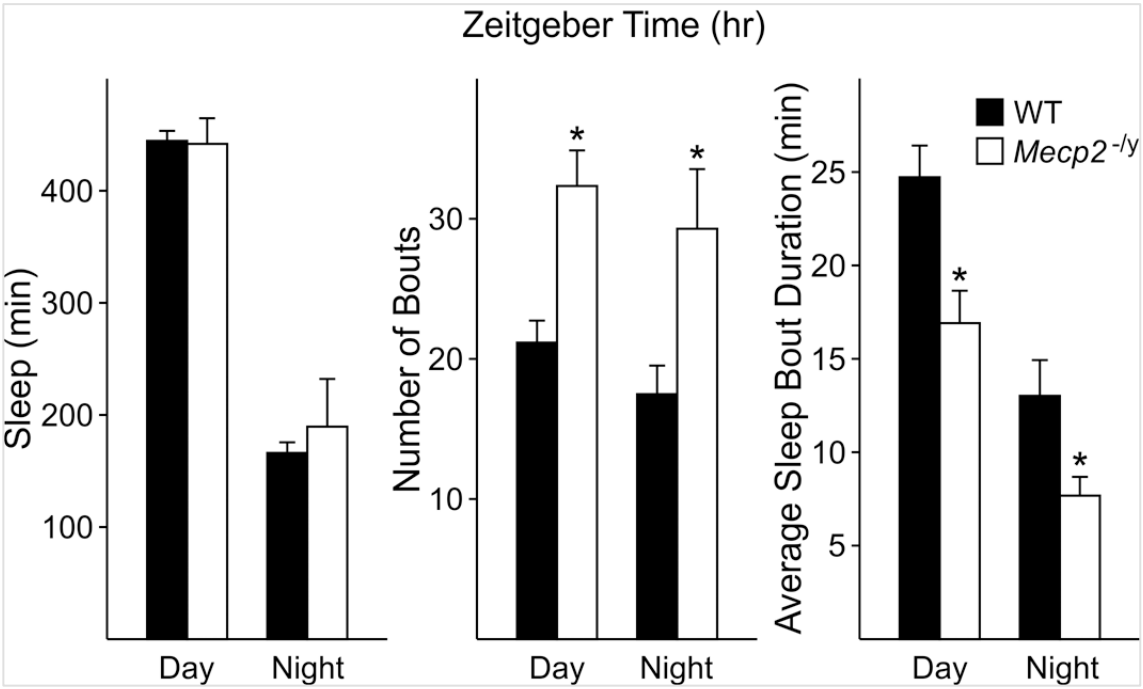
Zeitgeber Time (hr)
Sleep (min)
400
300
200
100
Day
Night
Number of Bouts
30
20
10
*
*
Day
Night
Average Sleep Bout Duration (min)
25
20
15
10
5
*
*
WT
Mecp2 -/y
Day
Night

Fig 2.6 Immobility-defined sleep behavior was affected in *Mecp2*$^{-/y}$ mice

Upper Panel: average waveforms of hourly sleep in wild-type littermates (n=8, black) and *Mecp2*$^{-/y}$ mice (n=7, white). The dark lines were the average sleep smoothed over 1 hour and the shaded area was the standard error. The straight line across was the half maximum value for each genotype. Sleep latency was determined by visually examining individual records of sleep behavior and measuring the time relative to lights-on at which each mouse achieved sleep onset (half-max of daily sleep). Mutant mice exhibited difficulty falling asleep at the beginning of rest phase and also maintaining wake during their activity onsets.

Bottom Panel: amount of time spend in sleep, average number of sleep bouts and average sleep duration of each sleep episode during the day and night, were compared between wild-type (black) and *Mecp2*$^{-/y}$ (white) mice. * indicated significance to $P < 0.05$ in *post hoc* pairwise comparisons between two genotypes after an significant effect of genotype revealed by two-way ANOVA.

littermates. There was an increase in sleep fragmentation revealed by the number of sleep bouts in the *Mecp2*$^{-/y}$ mice during the daytime (32 ± 2.5, $P < 0.0001$) and the nighttime (29 ± 4.2, $P < 0.01$) compared to wild-type mice in the day (21 ± 1.5) and the night (18 ± 2), respectively. In contrast, average duration of each sleep bout was significantly reduced in *Mecp2*$^{-/y}$ mice during the day (17 ± 1.7 min, $P < 0.001$) and night time (7.7 ± 1 min, $P < 0.01$), in relative to their wild-type littermates in the day (25 ± 1.7 min) and the night (13 ± 1.9 min), respectively. In summary, *Mecp2*$^{-/y}$ mice demonstrated significant alternations in immobility-defined sleep behavior characterized by increased sleep latency, fragmentation and reduced duration of sleep episode indicating the low sleep efficiency due to MeCP2 dysfunction.

Mecp2$^{-/y}$ mice showed a significant reduction in spontaneous firing rate (SFR) in SCN

Using the current-clamp recording technique in the whole-cell patch clamp configuration, SFR in dorsal SCN neurons were measured from WT (n=18) and *Mecp2*$^{-/y}$ mice (n=18) **(Fig 2.7)**. Recordings (1 min) were made during the day (ZT4-6) and night (ZT14-16) and the resulting data analyzed by two-day ANOVA followed by Holm-Sidak post-hoc multiple comparisons. This analysis revealed a significant effect on both the time of day ($F_{1,66} = 14.6$, $P < 0.001$) and the genotype ($F_{1,66} = 11.6$, $P < 0.01$). As expected, the SFR in wild-type SCN neurons during the daytime (5.0 ± 0.9 Hz, $P < 0.05$) were significantly higher than the night (2.4 ± 0.7 Hz). Similarly, in the *Mecp2*$^{-/y}$ mice, there were also significant difference in the SFR between the day (2.6 ± 0.8 Hz, $P < 0.05$) and nighttime (0.2 ± 0.1 Hz) indicating *Mecp2*$^{-/y}$ SCN neurons still exhibited a diurnal rhythm in spontaneous neuronal activity. Furthermore, the SFR in *Mecp2*$^{-/y}$

Fig 2.7

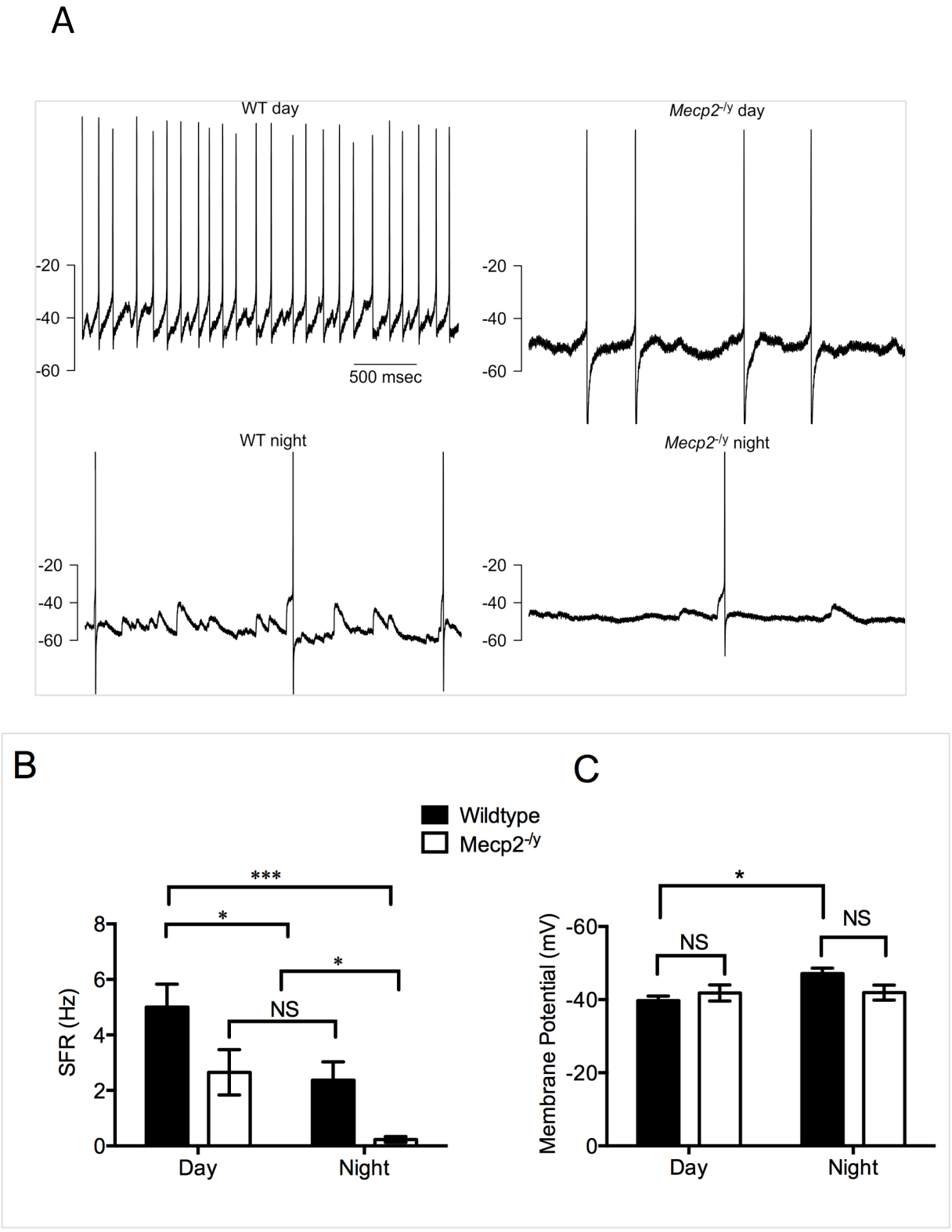
A
WT day
Mecp2-/y day
-20
-40
-60
500 msec
WT night
Mecp2-/y night
B
C
Wildtype
Mecp2-/y
***
*
*
NS
SFR (Hz)
8
6
4
2
0
Day
Night
*
NS
NS
Membrane Potential (mV)
-60
-40
-20
0
Day
Night

Fig 2.7 Spontaneous neural activity was reduced in the SCN of *Mecp2*$^{-/y}$ mice

A. Representative samples of spontaneous firing rate (SFR) recorded in dorsal SCN neurons from the wild-type and *Mecp2*$^{-/y}$ mice during the day (at ZT4-6, n=18 per genotype) and the night (ZT 16-18, n=18 per genotype) with whole-cell patch clamp.

B-C: summarized histograms of SFR (B) and membrane potentials (C) during the day and night for WT (black) and *Mecp2*$^{-/y}$ mice (white). Data was shown at means ± SEM. * indicates significant difference at the level of $P < 0.05$ as analyzed by two-way ANOVA followed by *post hoc* multiple comparisons test.

dorsal SCN neurons were significantly lower compared to the wild-type SCN neurons in both the day ($P < 0.05$) and night ($P < 0.05$), respectively **(Fig 2.7B)**. However, the reduction of SFR in *Mecp2*$^{-/y}$ SCN neurons during the day and night was not parallel with alternation in membrane properties such as conductance (Cm), input resistance (Rm) and resting membrane potential (Vm). Two-way ANOVA analysis followed by post-hoc comparison tests did not reveal any significant effects of genotype in these membrane properties ($P = 0.2$ for Cm, $P = 0.6$ for Rm, $P = 0.4$ for Vm). As expected, the resting membrane potential in wild-type SCN neurons during the night (47.1 ± 1.5 mV) was significantly hyperpolarized than the day (39.7 ± 1.3 mV, $P < 0.05$). In contrast, resting membrane potentials in *Mecp2*$^{-/y}$ SCN neurons were not altered between the day (41.8 ± 2.2 mV) and night (41.9 ± 2.1 mV; Fig **2.7C)**. These data suggest that MeCP2 mutation resulted in a significant reduction in spontaneous activity in dorsal SCN neurons and the diurnal rhythm in spontaneous firing activity was still intact in *Mecp2*$^{-/y}$ SCN neurons.

Disrupted PER2::LUC bioluminences rhythms in *Mecp2*$^{-/y}$ SCN and peripheral tissues

Previous studies already confirmed that SCN and peripheral organotypic cultures expressing bioluminescence reporter exhibited robust and sustained circadian rhythms in the clock gene-driven luciferase activity. The *ex vivo* imaging assay allowed people to record circadian parameters including period, phase of the first calculated peak and amplitude (from peak to trough) of bioluminescence rhythms to analyze molecular mechanisms (Yamazaki & Takahashi 2005). To further examine the impact of MeCP2 mutation on molecular clock components in

the SCN and peripheral oscillators, female *Mecp2*$^{-/+}$ heterozygous mice were crossed with PER2::LUC knock-in mice to generate double transgenic mice for *Mecp2*$^{-/y}$ *and Period2::Luciferase* fusion protein reporter. SCN and peripheral tissues explants including heart, lung, liver and adrenal glands were dissected from *Mecp2*$^{-/y}$ mice and wild-type littermates and cultured *ex vivo* to monitor PER2-driven bioluminescence rhythms for at least consecutive seven days. The amplitude, phase of the first calculated peak and period of PER2 rhythms from SCN, heart, lung, liver and adrenal glands explants were analyzed between *Mecp2*$^{-/y}$ and wild-type littermates **(Fig 2.8 and Table 2.2)**. SCN explants from *Mecp2*$^{-/y}$ mice exhibited a significant reduced amplitude in PER2-driven luciferase rhythms across consecutive six days (Two-way ANOVA: $F_{4,85} = 3.00$, $P < 0.05$ for significant effect of interaction for genotype and time difference; $F_{1,85} = 54.4$, $P < 0.0001$ for effect of genotype). There was also significant effect of genotype on PER2 rhythms in both lung ($F_{1,89} = 29.4$, $P < 0.0001$) and adrenal gland ($F_{1,60} = 19.4$, $P < 0.0001$) explants indicating that peripheral tissues also exhibited the reduced amplitude in PER2 rhythms due to MeCP2 mutation **(Fig 2.8C)**. Moreover, *Mecp2*$^{-/y}$ SCN explants demonstrated a phase change in PER2-driven bioluminescence rhythms. Compared to wild-type SCN (ZT 13.75 ± 0.24), there was a phase advance in the phase of the first calculated peak in *Mecp2*$^{-/y}$ SCN (ZT 12.85 ± 0.35, $P = 0.05$). However, among the peripheral tissue explants, only adrenal glands exhibited a significant phase change in PER2 rhythms. Interestingly, a phase delay was present in *Mecp2*$^{-/y}$ adrenal gland (ZT 17.04 ± 0.30, $P = 0.05$) compared to wild-type (ZT 15.40 ± 0.62, **Fig 2.8B**). The period of PER2 rhythms was not found between wild-type and *Mecp2*$^{-/y}$ SCN explants, or any of peripheral tissues.

Fig 2.8

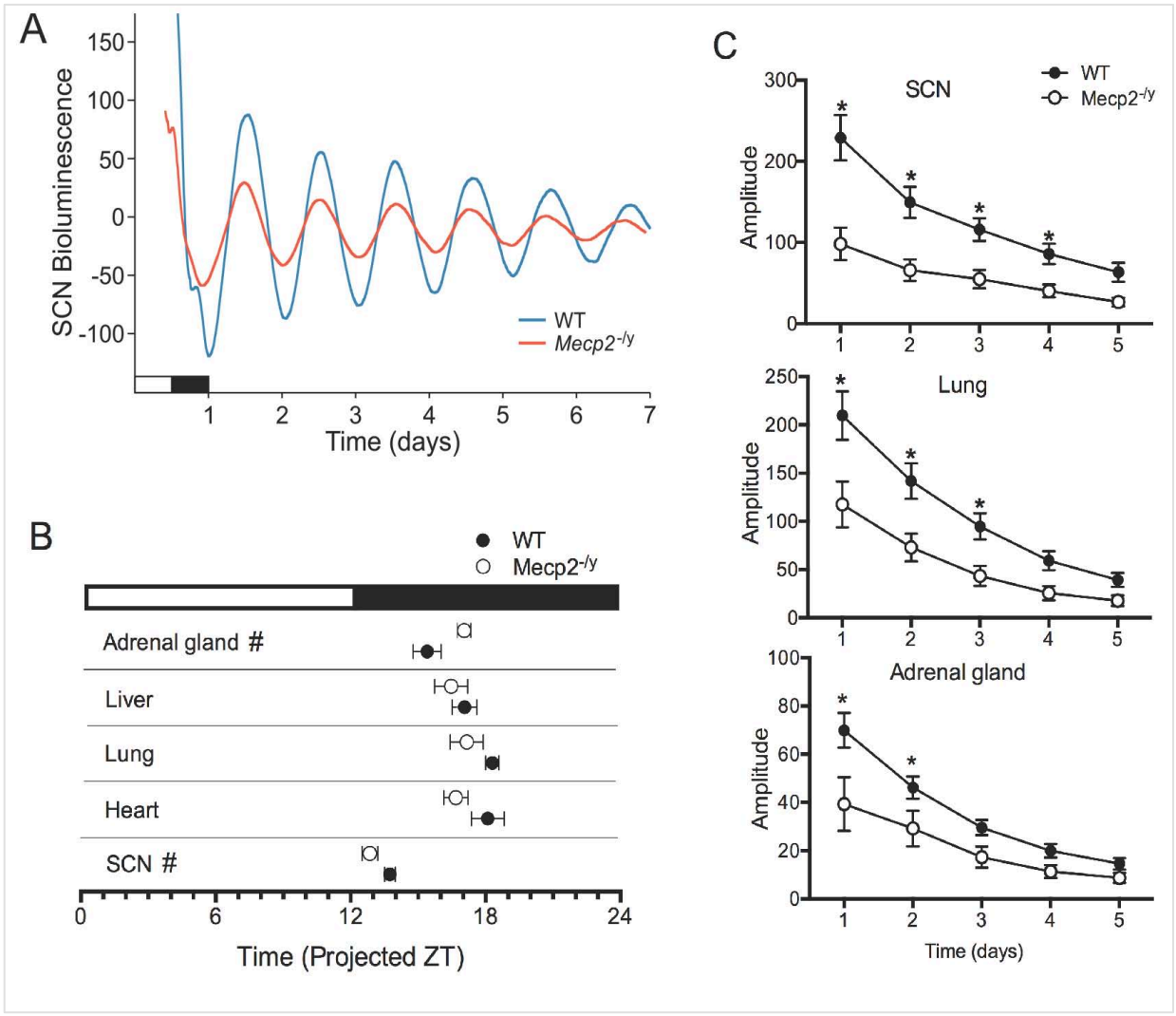
A
SCN Bioluminescence
150
100
50
0
-50
-100
1
2
3
4
5
6
7
Time (days)
WT
Mecp2-/y
B
WT
Mecp2-/y
Adrenal gland #
Liver
Lung
Heart
SCN #
0
6
12
18
24
Time (Projected ZT)
C
SCN
Amplitude
300
200
100
0
Lung
250
200
150
100
50
Adrenal gland
100
80
60
40
20
1
2
3
4
5
Time (days)

Fig 2.8 Disrupted PER2::LUC bioluminescence rhythms in the SCN and peripheral tissues of *Mecp2*$^{-/y}$ mice for 7 days.

A. Averaged sample traces of PER2 driven bioluminescence rhythms measured from wild-type (blue) and *Mecp2*$^{-/y}$ (red) SCN explants.

B. Phase relationship determined by the first calculated peak in peripheral tissues dissected from wild-type (black) and *Mecp2*$^{-/y}$ (white) mice including SCN, heart, lung, liver and adrenal glands explants. Unpaired student t tests were used for significant difference between two genotypes. # indicates significance at the level of $P = 0.05$.

C. Comparison of amplitude of PER2 bioluminescence rhythms between wild-type (black) and *Mecp2*$^{-/y}$ (white) SCN, lung and adrenal gland explants. * indicates significance difference ($P < 0.05$) at indicated time points between genotypes revealed by two-way ANOVA and *post hoc* pairwise comparison tests.

	7-8 wks WT	7-8 wks *Mecp2*$^{-/y}$
SCN	n=9	n=10
Period (hr)	25.05 ± 0.20	24.87 ± 0.15
Phase (first calculated peak)	13.75 ± 0.24	12.85 ± 0.35 *
Amplitude	228.93 ± 27.92	98.22 ± 19.96*
Heart	n=10	n=10
Period (hr)	24.17 ± 0.19	24.47 ± 0.23
Phase (first calculated peak)	18.10 ± 0.73	16.68 ± 0.54
Amplitude	29.72 ± 5.31	22.60 ± 2.46
Lung	n=11	n=9
Period (hr)	25.03 ± 0.13	24.65 ± 0.48
Phase (first calculated peak)	18.30 ± 0.30	17.17 ± 0.73
Amplitude	209.61 ± 25.13	117.63 ± 23.75*
Liver	n=10	n=10
Period (hr)	24.51 ± 0.20	24.07 ± 0.25
Phase (first calculated peak)	17.07 ± 0.54	16.47 ± 0.74
Amplitude	82.16 ± 12.66	68.42 ± 8.60
Adrenal Glands	n=9	n=6
Period (hr)	22.19 ± 0.09	22.24 ± 0.14
Phase (first calculated peak)	15.40 ± 0.62	17.04 ± 0.30*
Amplitude	64.12 ± 8.59	39.35 ± 11.10*

Table 2.2 PER2::LUC bioluminescence parameters of wild-type and *Mecp2*$^{-/y}$ *ex vivo* explants.

Amplitude, phase of the first calculated peak and period of PER2 driven bioluminescence rhythms were measured from SCN and peripheral tissues including heat, lung, liver and adrenal gland for each genotype. Unpaired student t-tests were performed to determine the statistical difference for each parameter between wild-type and *Mecp2*$^{-/y}$ explants.

* indicates $P < 0.05$.

In summary, although the PER2::LUC-driven luciferase activity rhythms still existed in the SCN and peripheral tissues from *Mecp2*$^{-/y}$ mice, the amplitude of the *Mecp2*$^{-/y}$ SCN rhythm was greatly diminished combined with a phase advance in the first peak of PER2 rhythms. In the peripheral explants, both *Mecp2*$^{-/y}$ lung and adrenal glands exhibited lower amplitude in PER2 rhythms, probably due to a weaker SCN oscillation output. In addition, adrenal glands showed a phase delay in the first peak of PER2 rhythm indicating a possible circadian misalignment in the peripheral oscillator. No significant change in the period, amplitude and phase of the first calculated peak were found in *Mecp2*$^{-/y}$ heart and liver explants compared to wild-type controls (**Table 2.2**).

Destabilization of circadian system by chronic Jet-lag increased mortality in *Mecp2*$^{-/y}$ mice

Previous study demonstrated that aged mice, exposed to a 6 hour advance of the light cycle once every week mimicking chronic jet-lag for a few weeks, died much quickly compared to the mice from the same age group housed under stable light-dark cycle (Davidson et al 2006). This study indicated that aging-related circadian deterioration, may have an adverse effect on general health specifically during the period of the phase advances of their biological clock. Current studies already demonstrated that *Mecp2*$^{-/y}$ Mice exhibited circadian deficits in their behavioral rhythms of wheel-running activity, temporal pattern of sleep, spontaneous electrical activity and PER2 rhythm in the SCN together with disorganized peripheral oscillator. To examine whether circadian destabilization could cause further disease progression and a shortened lifespan of the

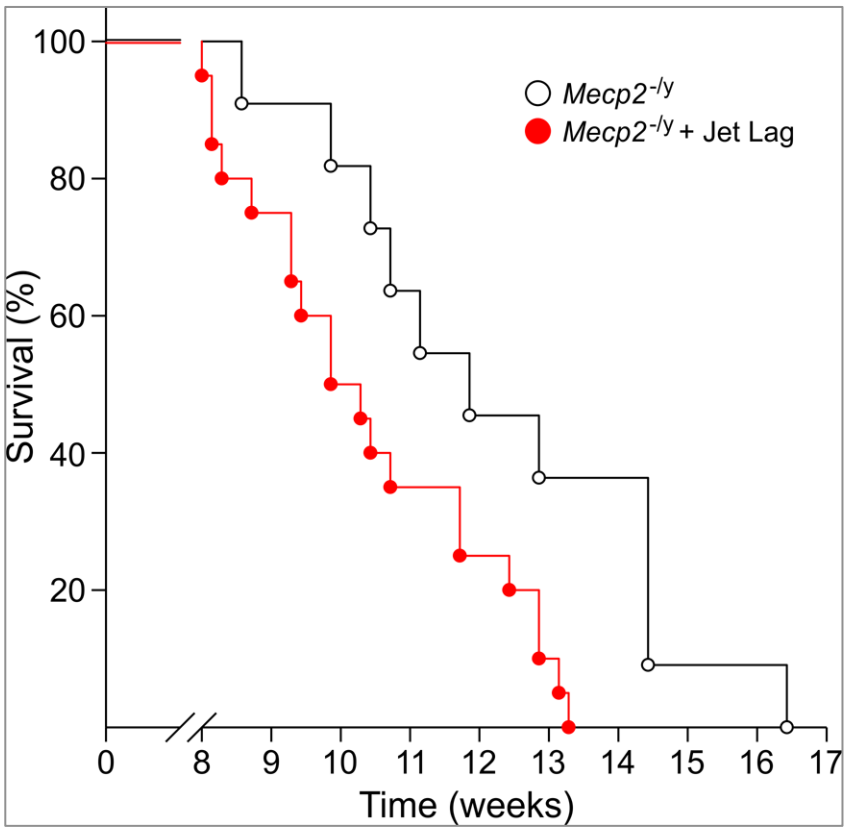

Fig 2.9 The impact of chronic jet-lag type of light condition in survival rate of *Mecp2*$^{-/y}$ mice by Kaplan Meier survival curve.

Mecp2$^{-/y}$ mice at the age of 7-8 weeks were placed either under continued constant LD light cycle or a 6-hour advance light shifting every week mimicking chronic jet-lag model. The lifespan of *Mecp2*$^{-/y}$ mice between two lighting conditions were recorded and compared using Kaplan Meier survival analysis ($P = 0.016$).

Mecp2$^{-/y}$ mice with an already disrupted circadian system, *Mecp2*$^{-/y}$ mice were placed on one of two lighting conditions starting from 7-8 weeks of age. One group of *Mecp2*$^{-/y}$ mice continued to be maintained on a stable 12:12 light-dark cycle. The other group of *Mecp2*$^{-/y}$ littermates was exposed to a 6-hour advance of the light shifting once every week until the end of experiment. *Mecp2*$^{-/y}$ mice under the jet-lag type of light condition were significantly deteriorated **(Fig 2.9)**. Kaplan-Meier survival analysis showed a significant decrease in the survival rate of *Mecp2*$^{-/y}$ mice between two lighting condition ($P < 0.05$) suggesting *Mecp2*$^{-/y}$ mice subjected to jet lag died much more quickly compared to *Mecp2*$^{-/y}$ mice with the same age housed in constant light condition. This study may raise important issues about the need of stabilizing circadian system during the long-term care and disease management of RTT individuals.

Mecp2$^{-/y}$ MEFs exhibited a reduced amplitude in clock gene expression with peripheral oscillators

To examine the effect of MeCP2 mutation on the molecular clockwork consisting of a transcription and translational negative feedback loop (TTTL), mouse embryonic fibroblasts (MEFs) dissociated from *Mecp2*$^{-/y}$ embryos and their wild-type littermates, respectively were applied to study the possible molecular mechanism underlying circadian dysfunction in *Mecp2*$^{-/y}$ mice. Following 2h synchronization with dexamethasone (0.1μM), *Mecp2*$^{-/y}$ MEFs and wild-type MEFs were collected every 6 h and subjected to RT-qPCRs to monitor *mBmal1* and *mPer2* mRNA expression during the period of 48 hours. Synchronized *Mecp2*$^{-/y}$ and wild-type MEFs showed robust rhythmic expression in *mPer2* mRNA (**Fig 2.10**). Two-way ANOVA

analysis revealed significant effects of time ($F_{7,110} = 24.57$, $P < 0.001$) and genotype ($F_{7,110} = 6.36$, $P < 0.05$) on *mPer2* mRNA levels during 48 hours post-synchronization. In addition, post-hoc multiple comparison tests indicated a significant reduction of *mPer2* expression at 24h in *Mecp2*$^{-/y}$ MEFs ($P < 0.05$). The fold change of mRNA expression calculated by the peak to trough level was analyzed and then *Mecp2*$^{-/y}$ MEFs (7.47 ± 0.93, $P < 0.001$) showed a reduced fold change in mPer2 mRNA expression compared to wild-type MEFs (12.23 ± 0.71). As BMAL1 was a negative regulator for Per2 transcription in TTTLs, it was confirmed in current study that circadian expression of mBmal1 should be in antiphase to *mPer2* mRNA oscillation. *Mecp2*$^{-/y}$ MEFs exhibited an identical rhythmic expression in *mBmal1* mRNAs similar to their wild-type controls ($F_{7,111} = 28.92$, $P < 0.0001$ for the effect of time) across indicated time points. However, there was a reduced fold change in *mBmal1* mRNA expression in *Mecp2*$^{-/y}$ MEFs (3.25 ± 0.25, $P < 0.05$) compared to WT MEFs (4.22 ± 0.30).

RTT fibroblasts exhibited alternations in clock gene expression

The majority of RTT cases resulted from missense mutations within the methyl-CpG-binding domain (MBD). Common MBD mutations included T158M, R106W and R133C et al that caused profound effects on MeCP2 structure, stability and DNA-binding properties correlating with the severity of RTT patient symptoms (Ghosh et al 2008). To examine the impact of human MeCP2 mutations in molecular clockwork, RTT patients fibroblasts (T158M and R106W) and normal human subject fibroblasts (HFF) were cultured and synchronized with dexamethasone (0.1μM) for 2h. These fibroblasts were collected every 6

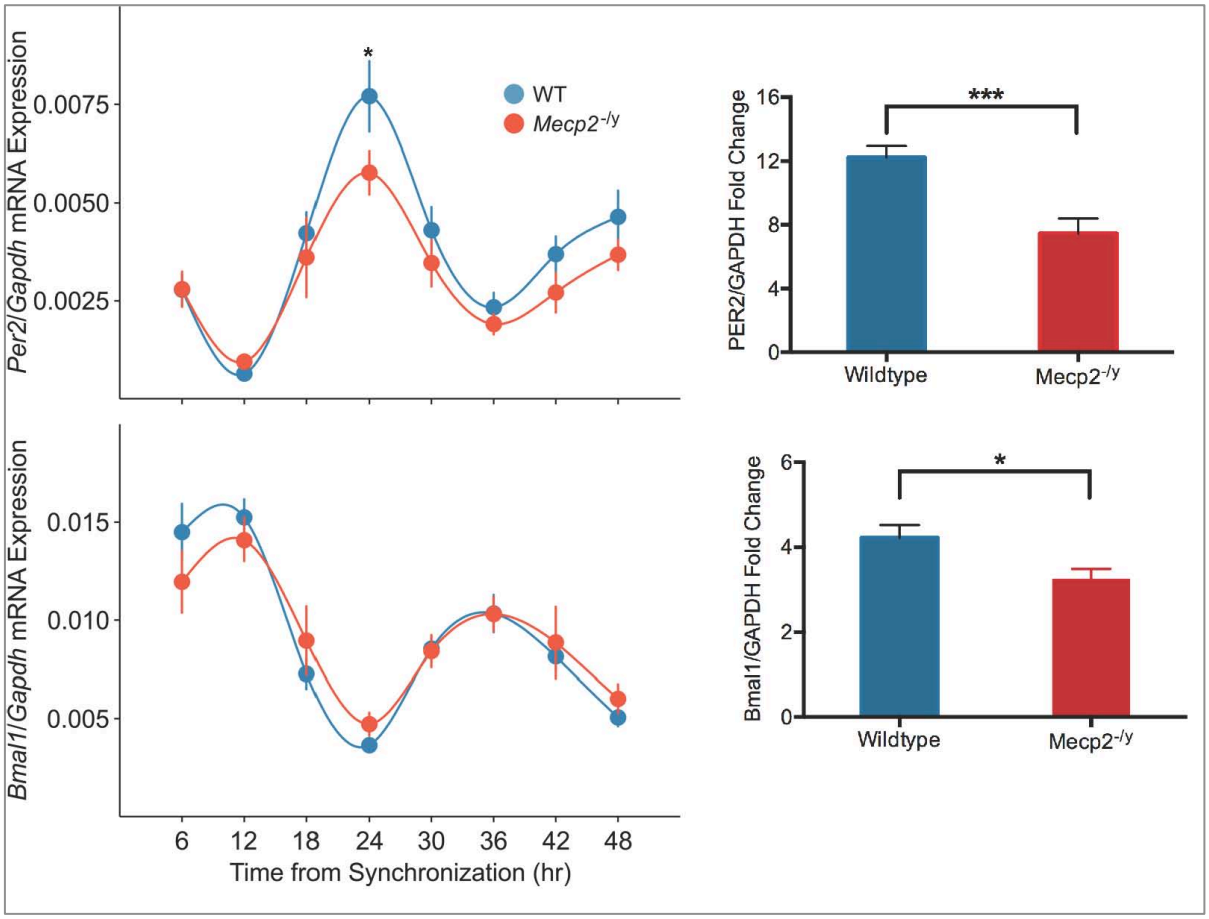

Fig 2.10 *Mecp2*$^{-/y}$ MEFs exhibited a significant reduction in clock gene expression following synchronization.

Wild-type (blue) and *Mecp2*$^{-/y}$ MEFs (red) were synchronized with dexamethasone (0.1μM) for 2 hours. Cells were subsequently collected every 6 hours following synchronization and subjected to RT-qPCRs to examine mRNA expression for *mPer2* (top) and *mBmal1* (bottom).

Left: average waveforms of *mPer2* (top) and *mBmal1* (bottom) mRNA levels between wild-type (blue) and *Mecp2*$^{-/y}$ MEFs (red) at indicated time points labeled on x axis. Two-way ANOVA analysis followed by *post hoc* multiple comparison tests were performed to determine statistical difference between genotypes. * $P < 0.05$.

Right: comparison of fold change calculated from the peak to trough level for *mPer2* (top) and *mBmal1* (bottom) expression. Unpaired student t-tests were used to calculate statistic difference in fold change of mRNA expression between genotypes.
* $P < 0.05$; *** $P < 0.001$

hours for total RNAs to examine *hPER1* and *hPER2* mRNA expression during the period of 48 hours post-synchronization using RT-qPCR. Two-way ANOVA analysis demonstrated a significant interaction of genotype and time ($F_{14,118} = 15.54$, $P < 0.0001$) and effect of time ($F_{7,118} = 23.81$, $P < 0.0001$) on rhythmic *hPER1* expression among HFF, T158M and R106W fibroblasts **(Fig 2.11)**. *Post-hoc* tests indicated that *hPer1* expression in HFF was significant different from T158M and R106W at selected time points, as indicated in **Fig 2.11**. Interestingly, control HFF and T158M fibroblasts peaked at different time in their *hPER1* mRNA expression. Similar to wild-type MEFs, control HFF cells exhibited the peak expression of *hPER1* at 24 h, however, the peak *hPER1* expression of T158M was advanced to 18 h together with a second peak at 36 h after synchronization. One-way ANOVA was performed to examine the difference in fold change of *hPER1* expression calculated by the peak level relative to trough level among three types of fibroblasts. There was a significance using one way ANOVA ($F_{2,19} = 8.5$, $P < 0.01$). However, HFF (4.16 ± 1.13) and T158M (3.53 ± 0.93, $P = 0.2$) fibroblasts exhibited similar fold change in *hPER1* expression but with the different peak time. There was a significant reduction in fold change of *hPER1* expression in R106W fibroblasts (1.77 ± 0.50) compared to either HFF ($P < 0.01$) or T158M ($P < 0.05$). In addition, the *hPER2* expression was examined and analyzed among three types of fibroblasts. Two-way ANOVA revealed a significant interaction of genotype and time ($F_{14,134} = 3.34$, $P < 0.001$) and effect of time ($F_{7,134} = 40.14$, $P < 0.0001$) on *hPer2* expression among HFF, T158M and R106W. In contrast to *hPER1* expression, T158M fibroblasts exhibited the almost identical rhythmic *hPER2* expression pattern as HFF. Post-hoc tests revealed a significant difference in *hPER2* expression between

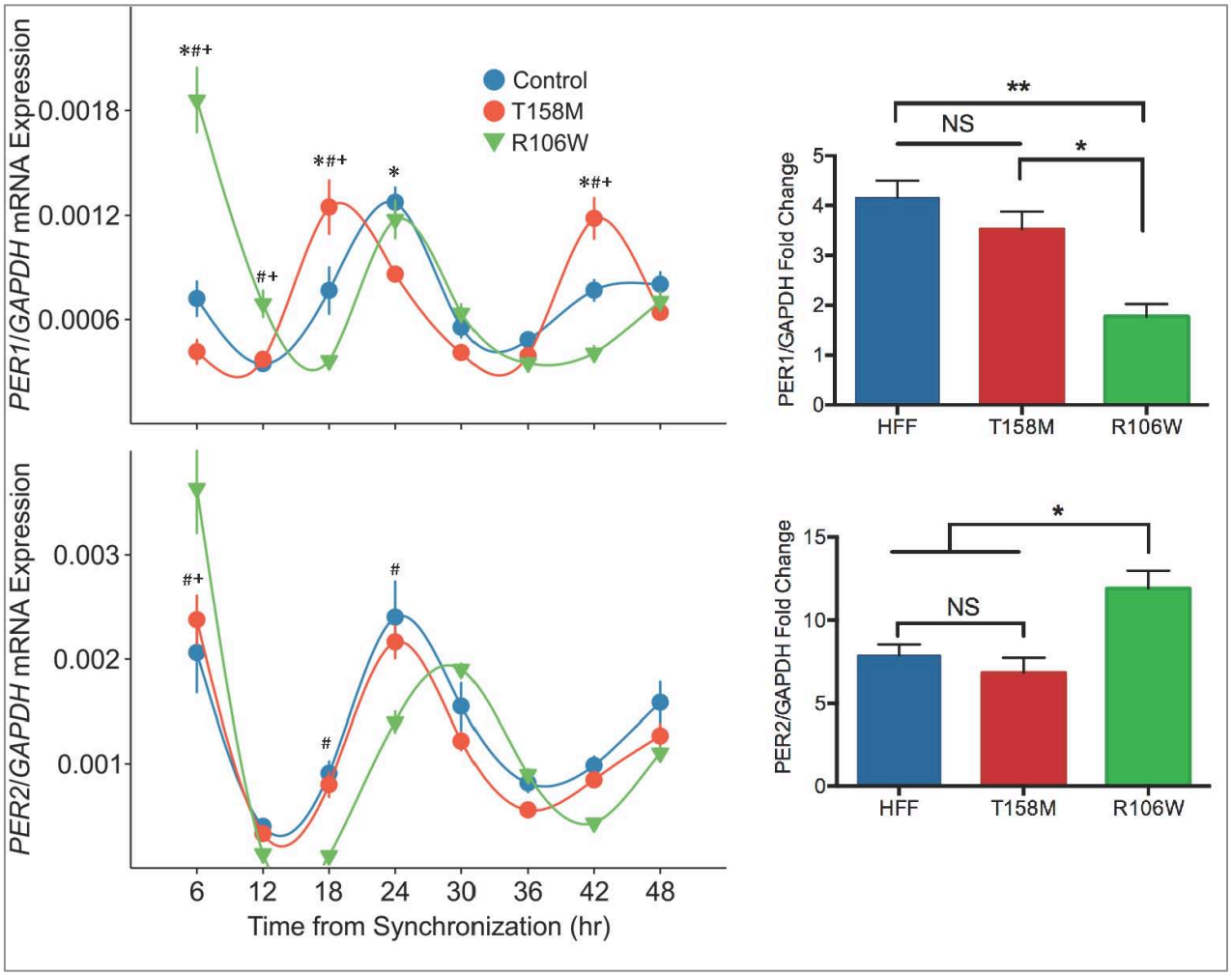

Fig 2.11 Altered clock gene expression in RTT fibroblasts following synchronization

Control fibroblast (HFF, blue) and two RTT patients fibroblasts (T158M in red; R106W in green) were synchronized with dexamethasone (0.1μM) for 2 hours. Their mRNAs were subsequently collected every 6 hours and subjected to RT-qPCRs to examine mRNA expression of *hPER1* (top) and *mPER2* (bottom) for each genotype.

Left: average waveforms of *hPER1* (top) and *hPER2* (bottom) mRNA levels for each genotype at indicated time points labeled with x axis. Two-way ANOVA analysis followed by *post hoc* multiple comparison tests were performed to determine the statistical difference among three genotypes. *indicates significant difference ($P < 0.05$) between WT and T158M, $^{\#}$ $P < 0.05$ between WT and R106W, $^{+}$ $P < 0.05$ between T158M and R106W.

Right: comparison of fold change calculated from the peak to trough level. One-way ANOVA followed by Tukey's multiple comparisons tests revealed a significant difference in fold change of mRNA expression rhythms among three genotypes as indicated. * $P < 0.05$, ** * $P < 0.01$.

HFF and R106W at indicated time points shown in **Fig 2.11**. Again, normal HFF peaked at 24h in *hPER2* expression, however, R106W delayed its peak time to 36 h. The comparison of the fold change in *hPER2* expression among there groups of cells revealed a significance using one-way ANOVA ($F_{2,18} = 7.02$, $P < 0.01$). Similar to *hPER1* expression, no significant difference was identified in *hPER2* expression fold change between control HFF (7,88 ± 2.19) and T158M (6.83 ± 2.22, $P = 0.6$). However, *hPER2* expression amplitude was significantly increased in R106W fibroblasts (11.92 ± 2.14) compared to HFF ($P < 0.05$) and T158M ($P < 0.01$) together with a delayed peak time.

Mecp2$^{-/y}$ MEFs lost rhythmic pattern of histone modification within mPer2 gene promoters

Specific histone modifications regulate gene expression and serve as good epigenetic indicators for chromatin states associated with gene activation or repression (Kimura 2013). In general, trimethylated H3K4 (H3K4me3) was found localized at transcription start sites of actively transcribed genes and essentially correlated with transcriptional activation through recruitment of RNA polymerase II and transcriptional complex. In contrast, gene silencing was mediated through two distinct mechanisms involving trimethylated H3K9 (H3K9me3) and trimethylated H3K27 (H3K27me3). Thus, H3K4me3 and H3K27me3 usually represent active and repressed gene transcription, respectively. Studies from ChIP analysis with MeCP2 and H3K4me3 antibodies indicated that MeCP2 directly binds to elements within the mPer1 and mPer2 gene promoters and MeCP2 overexpression activated both mPER1 and mPER2 expression (Alvarez-Saavedra et al 2011). The present study already demonstrated that MeCP2

dysfunction resulted in both reduced *mPer2* mRNA expression and PER2 protein. The next experiment was to perform ChIP-qPCRs with *Mecp2*$^{-/y}$ MEFs and wild-type MEFs to examine the impact of MeCP2 mutation in regulation of chromatin states in promoter region of *mPer2* gene. *Mecp2*$^{-/y}$ MEFs and wild-type MEFs were cultured, synchronized with dexamethasone (0.1 μM) for 2h and subjected to chromatin collection every 12 hours until 48h post-synchronization. Two antibodies H3K4me3 and K3K27me3 were used for immunoprecipitation followed by qPCRs. Enrichment values at post-synchronization 24h, 36 and 48h were normalized to the 12h to monitor the relative histone methylation pattern across 4 different time points between WT and *Mecp2*$^{-/y}$ MEFs**.** Two-way ANOVA combined with post-hoc tests discovered a significant interaction of genotype and time points ($F_{3,48} = 4.88$, $P < 0.01$), and effects of both time ($F_{3,48} = 4.50$, $P < 0.01$) and genotype (($F_{1,48} = 7.77$, $P < 0.01$) in H3K4me3 binding at *mPer2* promoter regions (**Fig 2.12A**). In addition, WT MEFs exhibited a significant increase in H3K4me3 enrichment indicating active gene transcription at *mPer2* promoter regions at 24h (3.30 ± 1.55) compared to 36h (0.32 ± 0.10, $P < 0.001$) or 48h (0.43 ± 0.25, $P < 0.01$). In contrast, *Mecp2*$^{-/y}$ MEFs did not show any difference in H3K4me3 enrichment at the same *mPer2* promoter regions among three time points: 24h (0.13 ± 0.07), 36h (0.05 ± 0.02) and 48h (0.12 ± 0.05, $P > 0.99$ for each comparison). Similarly, two-way ANOVA analysis also suggested a significant interaction of genotype and time points ($F_{3,48} = 8.99$, $P < 0.001$) and effects of both time (($F_{3,48} = 81.2$, $P < 0.0001$) and genotype 9($F_{1,48} = 14.5$, $P < 0.001$) in H3K27me3 binding in *mPer2* promoter gene (**Fig 2.12B**). In contrast to H3K4me3 enrichment, wild-type MEFs showed significant increase in H3K27me3 enrichment at

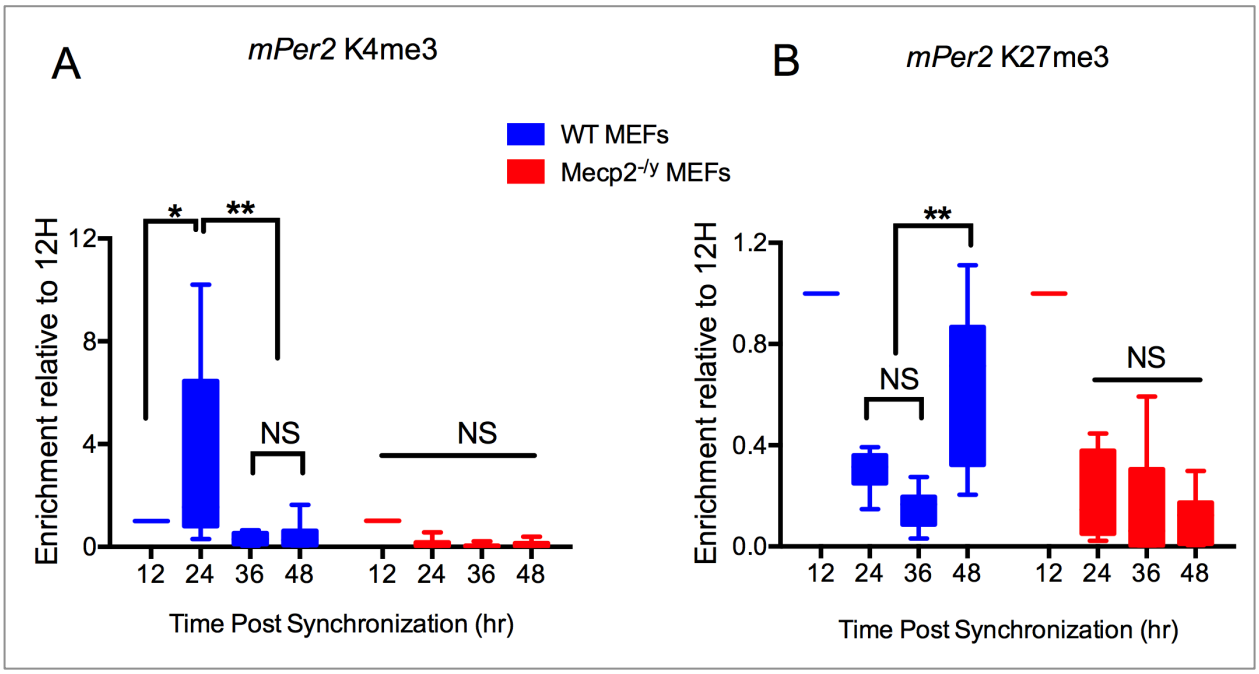

at

Fig 2.12 *Mecp2*$^{-/y}$ MEFs lost rhythmic binding pattern in histone methylation markers within *mPer2* promoter regions

WT (blue) and *Mecp2*$^{-/y}$ MEFs (red) were cultured, synchronized with dexamethasone (0.1μM) for 2 hours and subjected to chromatins collection every 12 hours until 48 hours after synchronization. ChIP-qPCRs were performed to examine histone methylation enrichment values at the promoter regions of *mPer2* gene for each genotype. ChIP analysis for binding of H3K4me3 (A) and H3K27me3 (B) included 3 regions within the mPer2 promoters relative to TSS: CRE1 (-1568), CRE2 (-2658) and CpG (-57). Enrichment values at 24h, 36 and 48h relative to input control were normalized to 12h to compare the ratios at indicated time points for each genotype. Data were presented in a box-plot format. Two-way ANOVA followed by *post hoc* multiple comparisons tests were analyzed to determine statistic significance. * $P < 0.05$, ** * $P < 0.01$.

A. Comparison of H3K4me3 enrichment representing active gene transcription at *mPer2* promoter regions during 48h post-synchronization for each genotype

B. Comparison of H3K27me3 enrichment representing repressed gene transcription at *mPer2* promoter regions during 48h post-synchronization for each genotype

mPer2 promoter regions at 48h (0.65 ± 0.13) compared to 24h (0.30 ± 0.03, $P < 0.01$) and 36h (0.15 ± 0.03, $P < 0.001$). *Mecp2*$^{-/y}$ MEFs did not show any difference in H3K27me3 binding within mPer2 promoter regions among three time points: 24h (0.19 ± 0.06), 36h (0.15 ± 0.08) and 48h (0.11 ± 0.04, $P = 0.90$ for each comparison). In summary, WT MEFs were identified with an increased binding for both H3K4me3 at post-synchronization 24h indicating active *mPer2* gene transcription and H27K27me3 at 48h correlating with transcriptional repression. However, *Mecp2*$^{-/y}$ MEFs completely lost the rhythmic binding pattern for both histone methylation markers: H3K4me3 and H27K27me3 within *mPer2* promoter regions at each indicated time point. These enrichment data were consistent with *mPer2* mRNA expression in MeCP2 mutant MEFs as *Mecp2*$^{-/y}$ MEFs exhibited an attenuated expression in *mPer2* mRNA expression at 24 h following synchronization (**Fig 2.10**).

Reduced vasointestinal polypeptide (VIP) expression in the SCN of *Mecp*$^{2-/y}$ mice

VIP is extensively expressed in SCN neurons and believed to play a critical role in synchronization of sing cell oscillation (Maywood et al 2006) and photic induction of clock gene within the SCN (Dragich et al 2010). For example, many of SCN core neurons expressing the neuropeptide VIP receive retinal input and relay this information to the rest of SCN through VIP. VIP is also found in many of the SCN efferent pathways that send projects to the paraventricular nucleus (PVN) governing a variety of daily rhythms. To examine whether MeCP2 mutation would lead to defects in VIP expression within the SCN, immunohistochemistry (IHC) were performed to compare the number of VIP positive neurons in the SCN at ZT6 between *Mecp*$^{2-/y}$

Fig 2.13

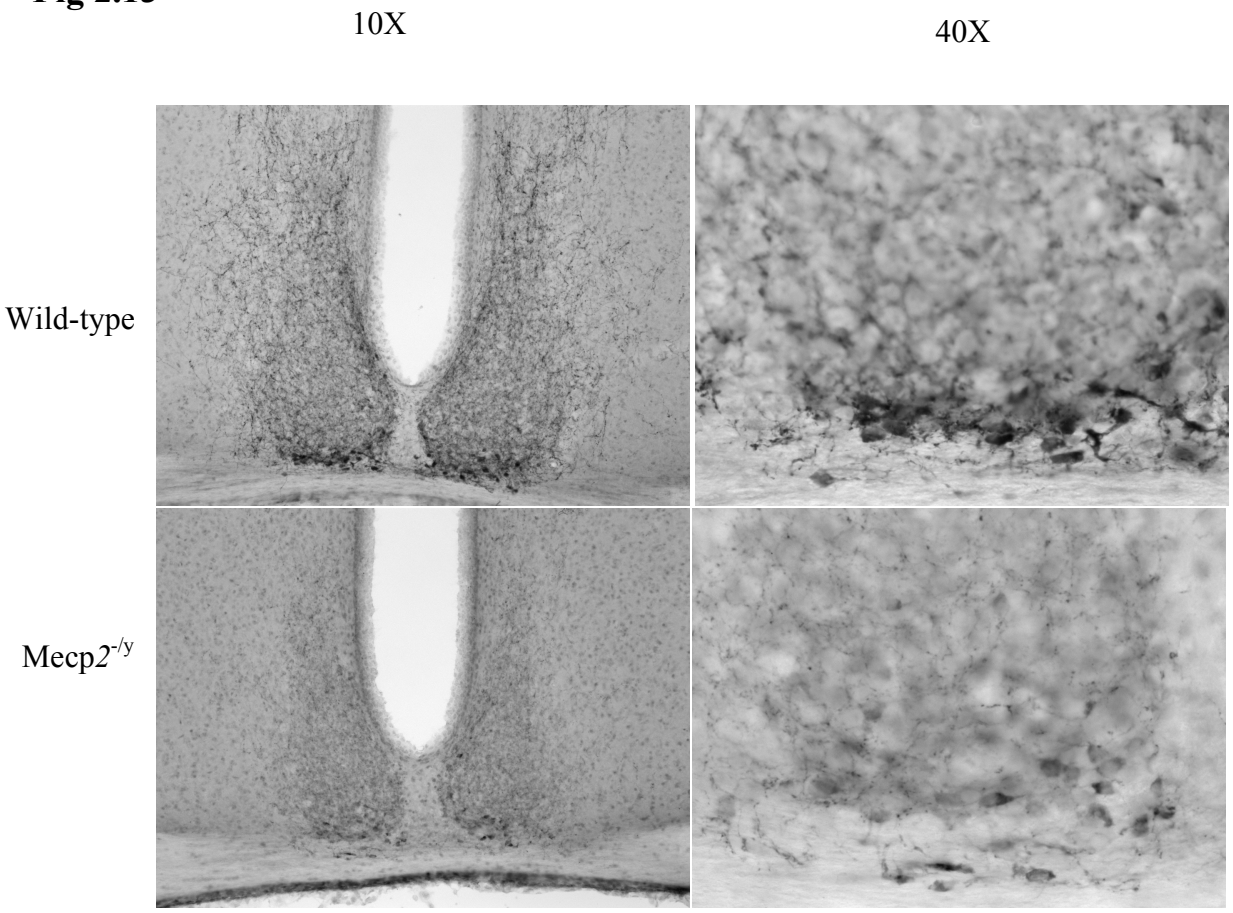
10X
40X
Wild-type
Mecp2-/y

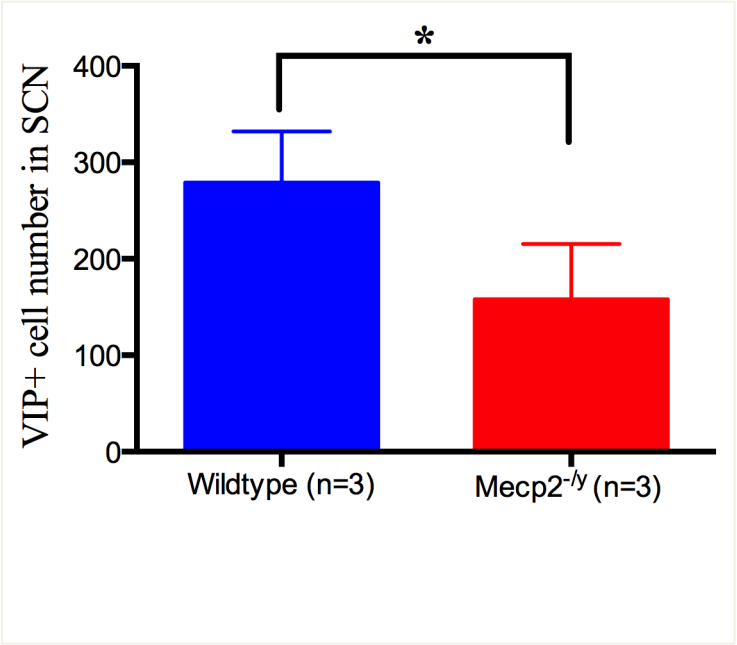
*
400
300
200
100
0
VIP+ cell number in SCN
Wildtype (n=3)
Mecp2-/y (n=3)

Fig 2.13 Disrupted VIP expression in the SCN from *Mecp*2$^{-/y}$ mice

Representative images of VIP IHC staining of coronal sections of the SCNs from wild-type (on the top) and *Mecp*2$^{-/y}$ mice (bottom) at 10x magnification (left) and high 40x magnification (right).

Bar graphs showed quantification of VIP+ cells in the SCNs from wildtype and *Mecp*2$^{-/y}$ mice (n=3 for each genotype). Unpaired student t-test was applied to determine the significance difference in the number of immunopositive cells in the SCN between two genotypes. P=0.028 for one tailed P value. P=0.056 for two tailed P value.

and wild-type SCNs **(Fig 2.13)**. Within the *Mecp*$^{2-/y}$ SCNs (158.3 ± 33.1, n=3), there was a significant reduction in the number of VIP immunopositive cells compared to the wild-type SCNs (279 ± 31, n=3) revealed by unpaired student t test ($P < 0.05$, one tailed). Even with a small sample size, these preliminary data still indicated a significant reduction in VIP expression within the SCN due to MeCP2 dysfunction.

Discussion

A growing number of clinical studies have reported an increased incidence of sleeping disturbances among RTT patients. These patients had difficulty sleeping at night and staying awake during the day and these dysfunctions in timing of their sleep wake patterns had a major impact on the quality of life of the patient population and on the family members who cared for the RTT patients (Carotenuto et al 2013, Nomura 2005, Young et al 2007). It is becoming increasingly clear that robust daily sleep-wake rhythms are essential to good health (Takahashi et al 2008). To understand the circadian control of sleep in RTT individuals and its underlying mechanism, *Mecp2*$^{-/y}$ mice as a mouse model of RTT were examined in the present study and demonstrated circadian dysfunction at the levels of behavior outputs, neuronal activity in the SCN and molecular clockwork in both SCN and peripheral oscillators. Specifically, MeCP2 mutant mice indeed showed decreased strength and poor precision of daily rhythms of activity coupled with extremely fragmented sleep behavior. The photic regulation of the circadian system was compromised in the mutant mice. Spontaneous neural activity was reduced at the level of the SCN. The molecule clockwork was disrupted both centrally in the SCN and in peripheral oscillators indicating a general disorganization of the circadian system. *Mecp2*$^{-/y}$ mice were vulnerable to destabilized circadian system as light condition mimicking chronic jet lag attenuated their lifespan. Both *Mecp2*$^{-/y}$ MEFs and RTT Fibroblasts demonstrated disrupted molecular clock gene expression and MeCP2 mutation caused a loss of rhythmic binding pattern for histone methylation markers within promoter regions of the core clock gene.

Disrupted behavioral rhythms in the *Mecp2*$^{-/y}$ mutant mice

Mecp2$^{-/y}$ mice exhibited severe circadian deficits in wheel running activity (**Fig 2.4**) and all the circadian parameters were significantly impacted by MeCP2 mutation (**Table 2.1**). Representative actograms showed arrhythmic locomotor activity in *Mecp2*$^{-/y}$ mutant mice. The strength of the diurnal and circadian rhythm of locomotor activity was significantly reduced in *Mecp2*$^{-/y}$ mice than age-matched wild-type littermates under both LD and DD condition. These mutant mice also demonstrated reduced nocturnality (percentage of activity during the night), increased fragmentation and diminished precision of activity rhythms under both LD and DD condition. Although *Mecp2*$^{-/y}$ mice were found with motor dysfunction starting at the same age suggested by a reduction of locomotor activity, poor precision of the daily activity onset and increased fragmentation under both LD and DD condition convincingly indicated that the behavior deficits observed in mutant mice were not simple due to motor dysfunction. MeCP2 mutant mice also exhibited an increase in free running period in DD condition compared to wild-type littermate and changes in the circadian period length were also indicative of a disruption in the underlying circadian pacemaker system (**Table 2.1)**. In addition, the decline in both precision and power of activity rhythms implied an intrinsically weaker central oscillator in *Mecp2*$^{-/y}$ mutant mice, which also manifested in alternation of the temporal pattern of activity rhythms. Decreased nocturnal activity was previously reported in other MeCP2 mutant mouse models. Heterozygous *Mecp2*$^{Stop/+}$ females showed particularly lower nocturnal activity and reduced overall locomotor activity (Robinson et al 2013). Mecp2$^{308/y}$ mice with relative mild phenotypes exhibited abnormal diurnal motor activity in the absence of motor skill deficits.

These mutants showed hypoactivity in the dark phase and hyperactivity in the light phase compared with wild-type littermates (Moretti et al 2005). Taken together, these data from different MeCP2 mutation models indicated that normal MeCP2 function is essential for normal temporal patterning of diurnal and circadian activity.

Mecp2$^{-/y}$ mice were not capably entrained under standard 12:12 light dark cycle and failed to demonstrate free-running endogenous rhythm under constant darkness (**Fig 2.4).** These observations indicate that MeCP2 function might be critical in light regulation pathway in the retina, which projects to the ventral SCN neurons responsible for non-image-forming visual responses. Another supportive evidence from current study is that *Mecp2*$^{-/y}$ mice exhibit deficits in the negative masking as masking behaviors share the same input pathway as light entrainment involving the projection from retina to the ventral SCN. The present study suggested that there was a reduction of wheel running activity during 1 hour light exposure in *Mecp2*$^{-/y}$ mice, however the reduced activity was not significantly different from their baseline activity indicating disrupted masking behavior in *Mecp2*$^{-/y}$ mice **(Fig 2.5)**. Taken together, these observations strongly indicated a deficit in the light regulation pathway projected to the SCN in *Mecp2*$^{-/y}$ mice.

Altered sleep behavior in the *Mecp2*$^{-/y}$ mutant mice

Video-based immobility-defined behavioral analysis was performed to assess the sleep behavior in the *Mecp2*$^{-/y}$ mutants as the assay is independent of the animal's motor function for wheel running. The immobility-defined sleep behavior analysis did not provide information

regarding the depth of sleep nor the relative progression from one type to another (NREM vs REM). However, such measurement were proved to accurately represent sleep and reached 99% correlation compared to simultaneously EEG-defined sleep if a proper immobility detection threshold was set up (Fisher et al 2012). MeCP2 mutant mice exhibited increased sleep fragmentation characterized by an increase in the number of sleep bouts and a decrease in sleep duration during the day and night (**Fig 2.6**). These data clearly indicated that although *Mecp2*$^{-/y}$ mice demonstrated the same amount of sleep time compared to wild-type littermates during the day and night, the quality of sleep was compromised due to an increased fragmentation of their sleeping pattern. Moreover, the increased sleep fragmentation observed in *Mecp2*$^{-/y}$ mice was in parallel with increased fragmentation in diurnal and circadian rhythms of locomotor activity indicating the defects in the circadian timing system in *Mecp2*$^{-/y}$ mice. Finally, *Mecp2*$^{-/y}$ mice also exhibited the increased sleep latency at the beginning of rest phase and a delayed waking time during the activity onsets (**Fig 2.6A)**. Thus, sleep fragmentation and increased sleep latency identified in *Mecp2*$^{-/y}$ mice was reminiscent of the sleep disturbances reported among RTT patients, who suffered from irregular sleep wake pattern and reduced nighttime sleep efficiency.

Reduced neural activity in the central clock of *Mecp2*$^{-/y}$ mutant mice

A wide range of studies demonstrated that the proper function of circadian timing system was crucial for normal brain activities including cognition, mood, movement, sleep, and autonomic function and many of which were disrupted in RTT patients. SCN neurons are

spontaneously active neurons that generate action potentials with a peak frequency of around 10-12 Hz during the day. During the night, SCN neurons are normally electrically silent (Colwell 2011, Ko et al 2009). In general, neurons in the SCN drive the rhythms in the outputs through the regulation of the autonomic nervous system and other neural as well as hormonal pathways to convey temporal information to control other brain regions and synchronize peripheral oscillators (Dibner et al 2010). In the present study, the impact of the MeCP2 mutation at the level of spontaneous activity in the SCN during the day and night was carefully studied for a comparison between wild-type and *Mecp2*$^{-/y}$ mice (**Fig. 2.7**). MeCP2 mutation caused a significant reduction in spontaneous firing rate (SFR) in the dorsal SCN neurons and the reduced neuronal activity in the SCN during both the day and night would weaken the temporal patterning in the SCN, the central pace maker, and its neural and hormonal outputs. These data strongly imply that the weakening of electrical output from the SCN could be part of the pathology leading to phenotypes found in *MeCP2*$^{-/y}$ mice.

SCN neurons show a diurnal rhythm in membrane potential with cells being depolarized by about 6-10mV during the day compared to the night, as shown in **Fig 2.7**. Hyperpolarized resting membrane potential is mediated mostly by a hyperpolarizing K+-dependent conductance that is active at night and inactive during the day thus contributing to the generation of rhythms in electrical activity within SCN neurons (Colwell 2011). The mutants exhibited reduced spontaneous firing rate in SCN neurons during both day and night, however, they did not show any day-night difference in resting membrane potential. Interestingly, *Mecp2*$^{-/y}$ mice still maintained the diurnal rhythms in neuronal activity within the dorsal SCN neurons **(Fig 2.7).**

Disrupted central molecular clockwork in the *Mecp2*$^{-/y}$ mutant mice

Epigenetic mechanisms involving histone modifications have recently emerged as important regulators of the central clock (Doi et al 2006, Hirayama et al 2007, Katada & Sassone-Corsi 2010), but the extent to which epigenetic mechanisms are involved in circadian regulation of molecular clockwork remains largely unknown. The core molecular mechanism responsible for generation of circadian oscillations is composed of the interacting transcription and translation feedback loops (TTFL) that drive rhythmic expression of key clock genes such as *Per2*. MeCP2 is an epigenetic factor highly expressed in the brain and crucial for many of normal brain functions. As the first experiment for potential deficits in the molecular clock system, PER2-driven luciferase activity was examined within the SCN as well as peripheral tissues explants over consecutive 7 days period (**Fig 2.8)**. *Ex vivo* monitoring with *Mecp2*$^{-/y}$ SCN explants revealed a significant decline in the amplitude of PER2-driven bioluminescence activity rhythms. In addition, MeCP2 mutation caused a phase advance (P = 0.05) at the first peak of PER2 activity rhythms within the central pacemaker (**Fig 2.8)**. These data together demonstrated a disrupted central pacemaker, the SCN, characterized by reduced PER2 expression and declined spontaneous diurnal electrical activity in the *Mecp2*$^{-/y}$ mutants. Several studies have provided evidence that the molecular clockwork in the SCN could drive the rhythms in electrical activity as an output to control behavior and physiology rhythms (Colwell 2011). Therefore current data strongly suggested that MeCP2 mutation led to a weakened and disrupted central clock. Moreover, the disrupted and weaker central pacemaker could lead to deficits in diurnal electrical activity within the SCN that are responsible for disrupted behavioral rhythms

and increased sleep fragmentation. In the contrast, all three different diseases models including the BACHD for Huntington's disease, Parkinson's disease mouse model and middle-aged mice for aging model exhibited a similar dissociation between the intact PER2 rhythms within the SCN and the reduced SCN outputs including aberrant circadian locomotor activity, reduced daytime sleep and decreased daytime neural activity rhythms (Kudo et al 2011a, Kudo et al 2011b, Nakamura et al 2011). Molecular rhythmicity in the SCN seems to remain relatively stable in the neurodegerative diseases suggesting that an intact molecular oscillator in the SCN may not be sufficient enough for a normally functionally circadian system. Current data using *Mecp2*$^{-/y}$ mice might further suggest that the neural activity rhythms driven by the molecular clock system seem to be necessary for the generation of robust rhythms in clock gene expression. However, this current study cannot exclude the possibility that MeCP2 mutation may directly cause the reduction in the spontaneous electrical activity within the SCN, as previous study already indicated that the mutants showed altered neural activity in other brain regions including cortex, hippocampus, and brain stems (Calfa et al 2011, Dani & Nelson 2009, Samaco & Neul 2011).

Disorganized peripheral oscillators in the *Mecp2*$^{-/y}$ mutant mice

The current study clearly revealed the disrupted molecular clockwork in peripheral oscillators. Both lung and adrenal gland explants exhibited significant reduction in the amplitude of PER2-driven bioluminescence rhythms and adrenal glands displayed a phase delay at the first peak of PER2 rhythms (**Fig 2.8).** In addition, using RT-qPCRs, *Mecp2*$^{-/y}$ MEFs

demonstrated significant reduction in core clock gene expression including *mBmal1* and *mPer2* mRNA expression compared to wild-type MEFs following synchronization (**Fig 2.9).** These experiments indicated that MeCP2 mutation led to disorganized and desynchronized peripheral oscillators, probably caused by the weakened and disrupted central clockwork. All together, the present study suggested an integral role of MeCP2 in the circadian timing system and also provided a mechanistic explanation for the sleep/wake disturbances observed in RTT patients.

Molecular mechanism underlying the regulation of MeCP2 in core clock gene expression

Current data also suggested how MeCP2 regulated circadian regulation of clock gene transcription through histone modification. ChIP-qPCR experiments using *Mecp2*$^{-/y}$ and control MEFs were performed to study the potential underlying epigenetic mechanism (**Fig 2.11**). Control MEFs demonstrated an increase in H3K4me3 binding at *mPer2* promoter regions at post-synchronization 24 h, indicating an active *mPer2* transcription at the same time. In contrast, there was an increase in H3K27me3 enrichment within the same promoter regions at post-synchronization 48 h representing transcriptional suppression of *mPer2.* In the absence of MeCP2, rhythmic enrichment of histone methylation markers including H3K4me3 and H3K27me3 within *mPER2* promoter genes at each indicated time point was completely abolished suggesting *Mecp2*$^{-/y}$ dysfunction failed to generate the rhythmic chromatin remodeling pattern at the promoter regions of core clock gene, *mPer2*. Taken together, these data strongly indicated the potential molecular mechanism of MeCP2 in the regulation of core clock gene expression that was involved in epigenetic regulation such as histone methylation.

Reduced VIP expression in the SCN

The neuropeptide VIP is critical in the SCN circuit and acts as endogenous neurotransmitter mediating interneuronal synchrony within the SCN (Hastings et al 2014, Kudo et al 2013, Vosko et al 2007). Mice deficient in VIP or its VPAC2 receptor exhibited a grossly disordered circadian behavior and physiology (Colwell et al 2003). At the molecular level, the loss of VIP or the VPAC2 receptor caused the loss of circadian rhythms in core clock gene-driven bioluminescence and the loss of synchronization of the cellular oscillators (Maywood et al 2006). Previous data suggested that VIP plays an important role for robust rhythms in clock gene expression within the SCN and some peripheral organs (Loh et al 2011). The preliminary data with IHC suggested that MeCP2 dysfunction caused the defects in VIP expression within the SCN **(Fig 2.13)**. *Mecp2*$^{-/y}$ mice exhibited the significantly decreased number of VIP-positive cells in the SCN compared to wildtype controls (one tailed $P < 0.05$). It's not known yet whether the total number of neurons decreases in the SCN from *Mecp2*$^{-/y}$ mice as the mutants usually display the smaller and densely packed neurons together with a reduced brain volume. Further study is needed to examine the difference in the total number of neurons within the SCN and the intensity of VIP expression between wildtype and *Mecp2*$^{-/y}$ SCN.

Impact of current study

RT-qPCRs with fibroblasts dissociated from RTT patients revealed a disrupted clock gene expression for *hPER1* and *hPER2* mRNAs indicating the disorganized molecular clockwork in RTT patients (**Fig 2.10)**. The disruption of circadian rhythms evidenced by sleep disturbances

reported in RTT patients could have profound consequences on clinical care of RTT individuals. In addition, chronic jet lag experiments with *Mecp2*$^{-/y}$ mice suggested that mutant mice were more vulnerable to destabilized circadian system that led to accelerated mortality and shortened lifespan in *Mecp2*$^{-/y}$ mice compared to the mutants at the same age housed under stable light condition **(Fig 2.8).** RTT individuals exhibited a prolonged survival with approximately 60% surviving to early middle age (**Fig 2.3**). Currently there is no cure for RTT and the treatment for RTT is based entirely on symptom control. In addition to RTT classical neurological phenotypes, symptoms from other systems are very common among RTT individuals such as breathing abnormalities, cardiac dysfunction, mood disorders and gastrointestinal dysfunction et al. Thus it becomes critical to understand how to maintain a stable circadian system during the long-term care and disease management for RTT patients. At last, studies with Huntington's disease mouse model already suggested that interventions that stabilized the deteriorating daily rhythms with scheduled meal times could delay the progression of motor dysfunction and reduce the cognitive symptoms in the mutant line (Pallier & Morton 2009). It is not known yet whether the treatment strategies such as light therapy, scheduled meals, scheduled exercise and sleep will be also effective to boost the already disrupted circadian rhythms in the RTT mouse models (Schroeder & Colwell 2013). It would be very interesting to examine whether these treatment strategies subjected to stabilize and boost the circadian system would eventually ameliorate and rescue the RTT-related phenotypes in the MeCP2 mutant mice.

References

Aguilar-Arnal L, Sassone-Corsi P. 2013. The circadian epigenome: how metabolism talks to chromatin remodeling. *Current opinion in cell biology* 25: 170-6

Albrecht U. 2012. Timing to perfection: the biology of central and peripheral circadian clocks. *Neuron* 74: 246-60

Albrecht U, Eichele G. 2003. The mammalian circadian clock. *Current opinion in genetics & development* 13: 271-7

Alvarez-Saavedra M, Antoun G, Yanagiya A, Oliva-Hernandez R, Cornejo-Palma D, et al. 2011. miRNA-132 orchestrates chromatin remodeling and translational control of the circadian clock. *Human molecular genetics* 20: 731-51

Anderson A, Wong K, Jacoby P, Downs J, Leonard H. 2014. Twenty years of surveillance in Rett syndrome: what does this tell us? *Orphanet journal of rare diseases* 9: 87

Asher G, Gatfield D, Stratmann M, Reinke H, Dibner C, et al. 2008. SIRT1 regulates circadian clock gene expression through PER2 deacetylation. *Cell* 134: 317-28

Borbely AA. 1982. A two process model of sleep regulation. *Human neurobiology* 1: 195-204

Calfa G, Hablitz JJ, Pozzo-Miller L. 2011. Network hyperexcitability in hippocampal slices from Mecp2 mutant mice revealed by voltage-sensitive dye imaging. *J Neurophysiol* 105: 1768-84

Carotenuto M, Esposito M, D'Aniello A, Rippa CD, Precenzano F, et al. 2013. Polysomnographic findings in Rett syndrome: a case-control study. *Sleep & breathing = Schlaf & Atmung* 17: 93-8

Chapleau CA, Lane J, Larimore J, Li W, Pozzo-Miller L, Percy AK. 2013. Recent Progress in Rett Syndrome and MeCP2 Dysfunction: Assessment of Potential Treatment Options. *Future neurology* 8

Chen RZ, Akbarian S, Tudor M, Jaenisch R. 2001. Deficiency of methyl-CpG binding protein-2 in CNS neurons results in a Rett-like phenotype in mice. *Nat Genet* 27: 327-31

Colwell CS. 2011. Neuroscience: Sleepy neurons? *Nature* 472: 427-8

Colwell CS, Michel S, Itri J, Rodriguez W, Tam J, et al. 2003. Disrupted circadian rhythms in VIP- and PHI-deficient mice. *American journal of physiology. Regulatory, integrative*

and comparative physiology 285: R939-49

d'Orsi G, Demaio V, Scarpelli F, Calvario T, Minervini MG. 2009. Central sleep apnoea in Rett syndrome. *Neurological sciences : official journal of the Italian Neurological Society and of the Italian Society of Clinical Neurophysiology* 30: 389-91

Dani VS, Nelson SB. 2009. Intact long-term potentiation but reduced connectivity between neocortical layer 5 pyramidal neurons in a mouse model of Rett syndrome. *The Journal of neuroscience : the official journal of the Society for Neuroscience* 29: 11263-70

Davidson AJ, Sellix MT, Daniel J, Yamazaki S, Menaker M, Block GD. 2006. Chronic jet-lag increases mortality in aged mice. *Current biology : CB* 16: R914-6

Davidson AJ, Yamazaki S, Menaker M. 2003. SCN: ringmaster of the circadian circus or conductor of the circadian orchestra? *Novartis Foundation symposium* 253: 110-21; discussion 21-5, 281-4

Dibner C, Schibler U, Albrecht U. 2010. The mammalian circadian timing system: organization and coordination of central and peripheral clocks. *Annual review of physiology* 72: 517-49

Doi M, Hirayama J, Sassone-Corsi P. 2006. Circadian regulator CLOCK is a histone acetyltransferase. *Cell* 125: 497-508

Dragich JM, Kim YH, Arnold AP, Schanen NC. 2007. Differential distribution of the MeCP2 splice variants in the postnatal mouse brain. *The Journal of comparative neurology* 501: 526-42

Dragich JM, Loh DH, Wang LM, Vosko AM, Kudo T, et al. 2010. The role of the neuropeptides PACAP and VIP in the photic regulation of gene expression in the suprachiasmatic nucleus. *The European journal of neuroscience* 31: 864-75

Ellaway C, Peat J, Leonard H, Christodoulou J. 2001. Sleep dysfunction in Rett syndrome: lack of age related decrease in sleep duration. *Brain & development* 23 Suppl 1: S101-3

Fisher SP, Godinho SI, Pothecary CA, Hankins MW, Foster RG, Peirson SN. 2012. Rapid assessment of sleep-wake behavior in mice. *Journal of biological rhythms* 27: 48-58

Frank E, Sidor MM, Gamble KL, Cirelli C, Sharkey KM, et al. 2013. Circadian clocks, brain function, and development. *Annals of the New York Academy of Sciences* 1306: 43-67

Ghosh RP, Horowitz-Scherer RA, Nikitina T, Gierasch LM, Woodcock CL. 2008. Rett syndrome-causing mutations in human MeCP2 result in diverse structural changes that impact folding and DNA interactions. *The Journal of biological chemistry* 283: 20523-34

Golombek DA, Rosenstein RE. 2010. Physiology of circadian entrainment. *Physiological reviews* 90: 1063-102

Guenole F, Baleyte JM. 2011. Meta-analysing the effectiveness of melatonin for sleep-disturbed individuals with autism spectrum conditions: should Rett syndrome be included? *Developmental medicine and child neurology* 53: 1063; author reply 64

Hagebeuk EE, van den Bossche RA, de Weerd AW. 2013. Respiratory and sleep disorders in female children with atypical Rett syndrome caused by mutations in the CDKL5 gene. *Developmental medicine and child neurology* 55: 480-4

Hastings MH, Brancaccio M, Maywood ES. 2014. Circadian pacemaking in cells and circuits of the suprachiasmatic nucleus. *Journal of neuroendocrinology* 26: 2-10

Hastings MH, Goedert M. 2013. Circadian clocks and neurodegenerative diseases: time to aggregate? *Current opinion in neurobiology* 23: 880-7

Hirayama J, Sahar S, Grimaldi B, Tamaru T, Takamatsu K, et al. 2007. CLOCK-mediated acetylation of BMAL1 controls circadian function. *Nature* 450: 1086-90

Itri JN, Michel S, Vansteensel MJ, Meijer JH, Colwell CS. 2005. Fast delayed rectifier potassium current is required for circadian neural activity. *Nature neuroscience* 8: 650-6

Itri JN, Vosko AM, Schroeder A, Dragich JM, Michel S, Colwell CS. 2010. Circadian regulation of a-type potassium currents in the suprachiasmatic nucleus. *Journal of neurophysiology* 103: 632-40

Jagannath A, Peirson SN, Foster RG. 2013. Sleep and circadian rhythm disruption in neuropsychiatric illness. *Current opinion in neurobiology* 23: 888-94

Katada S, Sassone-Corsi P. 2010. The histone methyltransferase MLL1 permits the oscillation of circadian gene expression. *Nature structural & molecular biology* 17: 1414-21

Kimura H. 2013. Histone modifications for human epigenome analysis. *Journal of human genetics* 58: 439-45

Kirby RS, Lane JB, Childers J, Skinner SA, Annese F, et al. 2010. Longevity in Rett syndrome: analysis of the North American Database. *The Journal of pediatrics* 156: 135-38 e1

Ko GY, Shi L, Ko ML. 2009. Circadian regulation of ion channels and their functions. *Journal of neurochemistry* 110: 1150-69

Kudo T, Loh DH, Truong D, Wu Y, Colwell CS. 2011a. Circadian dysfunction in a mouse model of Parkinson's disease. *Experimental neurology* 232: 66-75

Kudo T, Schroeder A, Loh DH, Kuljis D, Jordan MC, et al. 2011b. Dysfunctions in circadian behavior and physiology in mouse models of Huntington's disease. *Experimental neurology* 228: 80-90

Kudo T, Tahara Y, Gamble KL, McMahon DG, Block GD, Colwell CS. 2013. Vasoactive intestinal peptide produces long-lasting changes in neural activity in the suprachiasmatic nucleus. *Journal of neurophysiology* 110: 1097-106

Loh DH, Dragich JM, Kudo T, Schroeder AM, Nakamura TJ, et al. 2011. Effects of vasoactive intestinal peptide genotype on circadian gene expression in the suprachiasmatic nucleus and peripheral organs. *Journal of biological rhythms* 26: 200-9

Loh DH, Kudo T, Truong D, Wu Y, Colwell CS. 2013. The Q175 mouse model of Huntington's disease shows gene dosage- and age-related decline in circadian rhythms of activity and sleep. *PloS one* 8: e69993

Masri S, Sassone-Corsi P. 2013. The circadian clock: a framework linking metabolism, epigenetics and neuronal function. *Nature reviews. Neuroscience* 14: 69-75

Maywood ES, Reddy AB, Wong GK, O'Neill JS, O'Brien JA, et al. 2006. Synchronization and maintenance of timekeeping in suprachiasmatic circadian clock cells by neuropeptidergic signaling. *Current biology : CB* 16: 599-605

Mohawk JA, Green CB, Takahashi JS. 2012. Central and peripheral circadian clocks in mammals. *Annual review of neuroscience* 35: 445-62

Moretti P, Bouwknecht JA, Teague R, Paylor R, Zoghbi HY. 2005. Abnormalities of social interactions and home-cage behavior in a mouse model of Rett syndrome. *Human molecular genetics* 14: 205-20

Morin LP. 2013. Nocturnal light and nocturnal rodents: similar regulation of disparate functions? *Journal of biological rhythms* 28: 95-106

Mrosovsky N. 1999. Masking: history, definitions, and measurement. *Chronobiology international* 16: 415-29

Nagoshi E, Saini C, Bauer C, Laroche T, Naef F, Schibler U. 2004. Circadian gene expression in individual fibroblasts: cell-autonomous and self-sustained oscillators pass time to daughter cells. *Cell* 119: 693-705

Nakamura TJ, Nakamura W, Yamazaki S, Kudo T, Cutler T, et al. 2011. Age-related decline in circadian output. *The Journal of neuroscience : the official journal of the Society for Neuroscience* 31: 10201-5

Nomura Y. 2005. Early behavior characteristics and sleep disturbance in Rett syndrome. *Brain & development* 27 Suppl 1: S35-S42

Pallier PN, Morton AJ. 2009. Management of sleep/wake cycles improves cognitive function in a transgenic mouse model of Huntington's disease. *Brain research* 1279: 90-8

Roane HS, Piazza CC, Sgro GM, Volkert VM, Anderson CM. 2001. Analysis of aberrant behaviour associated with Rett syndrome. *Disability and rehabilitation* 23: 139-48

Robinson I, Reddy AB. 2014. Molecular mechanisms of the circadian clockwork in mammals. *FEBS letters*

Samaco RC, Neul JL. 2011. Complexities of Rett syndrome and MeCP2. *The Journal of neuroscience : the official journal of the Society for Neuroscience* 31: 7951-9

Saper CB, Sehgal A. 2013. New perspectives on circadian rhythms and sleep. *Current opinion in neurobiology* 23: 721-3

Schroeder AM, Colwell CS. 2013. How to fix a broken clock. *Trends in pharmacological sciences* 34: 605-19

Schwartz JR, Roth T. 2008. Neurophysiology of sleep and wakefulness: basic science and clinical implications. *Current neuropharmacology* 6: 367-78

Takahashi JS, Hong HK, Ko CH, McDearmon EL. 2008. The genetics of mammalian circadian order and disorder: implications for physiology and disease. *Nature reviews. Genetics* 9: 764-75

Takahashi K, Yamanaka S. 2006. Induction of pluripotent stem cells from mouse embryonic and adult fibroblast cultures by defined factors. *Cell* 126: 663-76

Vosko AM, Schroeder A, Loh DH, Colwell CS. 2007. Vasoactive intestinal peptide and the mammalian circadian system. *General and comparative endocrinology* 152: 165-75

Yamazaki S, Takahashi JS. 2005. Real-time luminescence reporting of circadian gene expression in mammals. *Methods in enzymology* 393: 288-301

Yoo SH, Yamazaki S, Lowrey PL, Shimomura K, Ko CH, et al. 2004. PERIOD2::LUCIFERASE real-time reporting of circadian dynamics reveals persistent circadian oscillations in mouse peripheral tissues. *Proceedings of the National Academy of Sciences of the United States of America* 101: 5339-46

Young D, Nagarajan L, de Klerk N, Jacoby P, Ellaway C, Leonard H. 2007. Sleep problems in Rett syndrome. *Brain & development* 29: 609-16

Chapter 3

Effects of 7,8-dihydroxyflavone in a mouse model of Rett Syndrome

Abstract

Alternations in the neurotrophin brain-derived-neurotrphic-factor (BDNF)-TrkB signaling pathway were reported in the disease progression of Rett syndrome (RTT) and restoration of BDNF was believed to be a potential therapeutic intervention for RTT treatment. A small molecule, 7,8-Dihydroxyflavone (7,8-DHF) was recently identified to be a potent TrkB receptor agonist that potentially crossed the blood-brain barrier (BBB) and mimicked certain BDNF functions. The present study here was focused on whether 7,8-DHF displayed therapeutic effects to rescue RTT-related phenotypes in MeCP2 mutant mice. Systematic administration of 7,8-DHF activated the phosphorylation of TrkB receptors and generated robust downstream Akt phorphorylation in wild-type mouse cortex and hippocampus tissues within 2 hrs after intrapertoneal injection, although the increase in p-TrkB was not yet statistically significant due to small sample size. Chronic systematic administration of 7,8-DHF did not significantly improve the life span of the *Mecp2*$^{-/y}$ mutants, when administered through intraperitoneal injection or drinking water. At the physiological level, *Mecp2*$^{-/y}$ mice exhibited a significant reduction in spontaneous firing rate of layer V pyramidal neurons in prefrontal cortex and this decrease was not accompanied by a change in the intrinsic properties of the recorded neurons. At last, incubation of acute cortical slices with 7,8-DHF significantly increased the spontaneous firing rate of L5 pyramidal neurons from *Mecp2*$^{-/y}$ cortical slices. Treatment with 7,8-DHF also tended to increase the spontaneous firing frequency in wild-type cortical neurons, although this effect was not yet statistically significant, probably due to a small sample size. Taken together, these data suggested that 7,8-DHF rescued the physiological impact due to the loss of MeCP2 and raised the possibility that it could be therapeutically useful for the treatment of RTT.

Introduction

Brain-derived neurotrophic factor (BDNF) is the most widely distributed neurotrophin in the center nervous system. BDNF binding to its specific transmembrane receptor tryopomyosin-receptor-kinase B (TrkB) leads to dimerization and autophosphorylation of the tyrosine sites, in turn activates phosphorylation of phosphoinositide (PI3K), MEK-ERK, and phospholipase C1 (PLC1). The MEK-ERK pathway is important in controlling neurite growth, cellular differentiation and neuronal survival during development. Moreover, MEK-ERK signaling continues to support synaptic plasticity, neuronal structural and function in the adult brain. In addition, PI3K activation triggers AKT to enhance cell survival. Activation of PLC1 triggers the synthesis of inositol-1,4,5-triphosphate (InsP3) and diacylglycerol (DAG), and subsequently activates calcium-dependent protein kinases that are critical for synaptic plasticity (Li & Pozzo-Miller 2014).

The proof-of-principle that restoring normal BDNF levels was beneficial to MeCP2 mutant mouse model as well as RTT patients, came from *in vitro* culture and *in vivo* animal studies with genetic, physiological and pharmacological manipulations. The AKT/mTOR signaling pathway was also reduced in both *Mecp2*-null mice and heterozygous female mice suggesting the absence of MeCP2 could lead to an impaired protein synthesis (Ricciardi et al 2011). Furthermore, conditional *Bdnf* knockout in postmitotic neurons exhibited similar phenotypes comparable to *Mecp2* mutant mice, including reduced brain and neuronal some size as well as stereotypic hindlimb-clasping motor dysfunction. Additionally, *Mecp2* mutant mice gradually reduced BDNF expression throughout the brain and lowered BDNF level correlated with the progression of disease phenotypes (Chang et al 2006). BDNF overexpression in

cultured hippocampal neurons was able to reverse impaired dendritic morphology caused by MeCP2 dysfunction (Larimore et al 2009). Using conditional knockout animals, BDNF overexpression in postnatal excitatory forebrain neurons of *Mecp2* knockout mice significantly rescued major RTT-related neurological deficits leading to extended lifespan, improved locomotor function, increased brain weight and restoration of spontaneous firing rate in cortical pyramidal neurons (Chang et al 2006).

The key challenge for BDNF-related therapy is drug delivery to the CNS. BDNF is a moderately sized, charged protein with a short *in vivo* half-life, and therefore unable to cross the blood-brain-barrier (BBB) via peripheral administration. In order to function properly, BDNF must be administered directly into the CNS. However, that usually caused intolerable adverse effects and failure of infusion therapy (Nagahara & Tuszynski 2011). Lacking a safe and reliable delivery system for BDNF treatment in humans has limited its application as an efficient therapeutic approach for a variety of neurological disorders, including Rett Syndrome. Therefore, improving endogenous BDNF expression and/or enhancing BDNF/TrkB signaling pathways are considered to be more practical therapeutic alternatives for clinical application. Although tremendous efforts were made to generate agonists to activate TrkB signaling, including the use of monoclonal antibodies and peptide mimetics, no exogenous agents have been successfully developed to fully mimic BDNF function or act as the potent and selective *in vivo* TrkB agonists.

Recently, a small molecule TrkB agonist, 7,8-dihydrocyflavon (7,8-DHF) as one of the flavone derivatives has received much attention for treatment of various neurological diseases. Flavonoids are a large group of polyphenolic compounds containing a basic flavan nucleus with two aromatic rings (the A and the B rings) interconnected by a three-carbon-atom heterocyclic

ring (the C ring). Flavonoids represent one of the largest and the most diverse class of plant secondary metabolites. These compounds are naturally present in vegetable, fruits and beverages, and thus are considered as important components of the daily diet. Flavonoids have been known for a long time to have the ability to exert diverse biological effects (bioflavonoids). In particular, they were reported as antioxidants and preventive agents against cancer (Harborne & Williams 2000). Accumulating evidence suggested that flavonoids had the potential to improve human memory and cognitive performance as they were capable to protect vulnerable neurons, enhanced existing neuronal function and stimulated neuronal regeneration (Spencer 2008). In addition, flavonoids were able to exert effects on long-term potentiation (LTP), one of the major mechanisms underlying learning and memory, and consequently on memory and cognitive performance through their interactions with the signaling pathways including PI3kinase/AKT (Vauzour et al 2007) and MAPK (Maher et al 2006).

Recent studies discovered that 7,8-dihydrocyflavon (7,8-DHF) was a selective TrkB agonist based on standard chemical screening. 7,8-DHF was able to cross the BBB after systemic administration (Jang et al 2010). Further study showed that 7,8-DHF recapitulated the physiological actions of BDNF as it strongly bound to TrkB, provoked receptor dimerization and autophosphorylation leading to activation of TrkB downstream signaling pathways including MAPK and PI3K-AKT pathways. Pharmacokinetics experiments indicated that 7,8-DHF was able to penetrate the BBB as well. The oral bioavailability of 7,8-DHF was about 5% and its half-life was around 134 minutes detected in the plasma after oral gavage of 50mg/kg (Liu et al 2013). Systemic administration of 7,8-DHF activated TrkB receptors through activation of phosphorylated TrkB in the rodent brain (Andero et al 2012, Andero et al 2011, Jang et al 2010). In addition, 7,8-DHF and its synthetic derivative, 4'-dimethlamino-7,8-dihydroxyflavone

(4'-DMA-7,8-DHF) were reported to display neuroprotective effects in a few of neurological disorders such as: Rett Syndrome, Alzheimer's disease (AD), Huntington's disease (HD) and immobilization-induced stress with mutant mouse models (Andero et al 2012, Jiang et al 2013, Johnson et al 2012, Zhang et al 2014). These studies demonstrated that the small molecule TrkB agonists, such as 7,8-DHF and 4'-DMA-7,8-DHF, were able to protect primary cortical neurons from Aβ-induced toxicity, promote synaptogenesis and synaptic plasticity, and prevent memory deficits in AD mouse model. Similarly, these TrkB agonists were reported to promote neurogenesis (Zhang et al 2014), dramatically improve motor deficits, ameliorate brain trophy and extend survival in HD mice (Jiang et al 2013).

To determine whether 7,8-DHF could potentially be used as a therapeutic intervention for a mouse model of Rett Syndrome, western blot was first performed to test whether systematic injection of 7,8-DHF could activate TrkB receptor and downstream Akt signaling pathway with wild-type mouse cortex and hippocampus tissue. To confirm previous findings of the 7,8-DHF rescuing effects, *Mecp2*$^{-/y}$ mice were systematically administered with 7,8-DHF to examine whether the treatment could improve the shorter life span of the mutants. At last, cortical slices dissected from *Mecp2*$^{-/y}$ mice and wildtype littermate controls were examined whether the treatment of 7,8-DHF could rescue spontaneous electrical activity in prefrontal cortical neurons with the whole cell patch clamp recordings.

Materials and Methods

Animals

Animals were housed in the University of California, Los Angeles (UCLA) animal care facility and all the procedures were performed in accordance with guidelines approved by the Animal Research Committee (ARC) at UCLA. All the experiments were conducted on *Mecp2*$^{-/y}$ male mice and their C57BL/6 wild-type littermates. Female heterozygous founder mice (Strain name: B6.Cg-Mecp2$^{tm1.1Jae}$/Mmucd) were obtained from Mutant Mouse Regional Resource Center (MMRRC) at UC Davis and used to establish *Mecp2*^{1lox} mutant mice colony that carry germline-recombined *Mecp2* mutant allele at UCLA. This line was maintained by backcrossing heterozygous *Mecp2*$^{+/-}$ females with male C57/BL6 wild-type mice. Near the end of gestation, males were removed from the breeding cages so that dams were housed individually. Dams were kept with their delivered pups until the end of weaning. Weaned animals were housed in cages with up to 5 same sex littermates and maintained on a 12 h light/12h darkness cycle with lights on at 07:00.

Genotyping

Standard genomic DNA purification procedure was performed to collect mouse genomic DNA samples. PCR and agarose gel electrophoresis were applied to determine wild-type and *Mecp2* mutant allele using the following primers: Nsi-5 (5'-CAC CAC AGA AGT ACT ATG ATC-3'), 2lox-3 (5'-CTA GGT AAG AGC TCT TGT TGA-3'), and Nsi-3 (5'-ATG CTG ACA AGC TTT CTT CTA-3'). Genotype was determined by gel electrophoresis characterized by 180-bp band for wild-type allele and 300-bp band for the *Mecp2* mutant allele.

Systematic treatment with 7,8-DHF

Mecp2$^{-/y}$ mice were treated with 7,8-DHF to examine whether the drug could improve the lifespan of mutant animals. Two groups of mutant mice were studied: *Mecp2*$^{-/y}$ mice in experimental group treated with 7,8-DHF and *Mecp2*$^{-/y}$ mice in control group treated with the vehicle. For intraperitoneal (i.p.) injection experiment, 7,8-DHF was dissolved in dimethyl sulfoxide (DMSO) to generate a stock solution at the concentration of 12.5 mg/ml. Then phosphate buffered saline (PBS) was gradually added into the DMSO solution until the final concentration reached 0.5 mg/ml in 30% DMSO/PBS (v/v). Based on animal's body weight, low dose (5 mg/kg) or high dose (25 mg/kg) of 7,8-DHF in the total volume of 200-300 μl DMSO/PBS was provided to animals through i.p. injection. Control group *Mecp2*$^{-/y}$ mice received the same volume of vehicle (30% DMSO/PBS) injection. *Mecp2*$^{-/y}$ mutant animals were treated with i.p. injection twice a week starting at roughly 3 weeks of age until the end of their life term. For chronic 7,8-DHF in drinking water experiments, 160 mg 7,8-DHF was gradually added in 1L water in a continuously stirring condition while simultaneously monitoring the pH value of the solution. 1N sodium hydroxide (NaOH) solution was slowly dropped into the mixed solution to gradually adjust pH to reach a range of 7.2-7.6 that allowed 7,8-DHF to reach this best solubility. The 7,8-DHF containing water with 1% sucrose was filtered, covered with foil paper and stored at 4 $^{\circ}$C before it was given to *Mecp2* mutant mice as drinking water. Water with 1% sucrose only was provided to control group animals for comparison. Water bottles with 7,8-DHF solution and vehicle were replaced every 3-4 days and the mutant mice were monitored daily. Animal's body mass and drinking volume were recorded every 3-4 day to monitor water intake as well. Kaplan-Meier survival curves were generated to assess the statistical significance in the difference between two groups.

Western Blot

Previous study reported that TrkB activation induced by 7,8-DHF in mouse brain reached the maximum level at 1-2 h after intraperitoneal injection (Liu et al 2010). Mouse brains were collected on ice immediately from euthanized animals at 2h after i.p. injection with either low dose or high dose of 7,8-DHF. The cortex and hippocampus tissues were immediately dissected and frozen on dry ice directly. Standard Western blot was performed with some modifications: mouse brain tissues were homogenized and lysed at 4°C in 100 µl of homogenization buffer per 20 mg of brain tissue containing 10mM Sodium-β-glycerophosphate, 50 mM Tris (pH 7.4), 150 mM sodium chloride (NaCl), 1mM ethylenediaminetetraacetic acid (EDTA, pH 8.0), 1% Triton X-100, 1.5 mM sodium orthovanadate (Na_3VO_4), 50mM sodium fluoride (NaF), 10 mM Sodium-pyrophosphate, 10 mM sodium glycerophosphate, 1 mM phenylmethylsulfonyl fluoride (PMSF) and freshly prepared proteinase inhibitor cocktail in a ratio of 1:1000 (Roche). Then brain samples were centrifuged (30 min, 13,000×*g*) twice at 4°C and supernatant fractions were collected. After protein concentration was determined with BCA protein assay kit (Pierce), all brain samples were diluted with lysis buffer at a final concentration of 1 µg/µl and then mixed with 4x sample loading buffer containing bromophenol blue, 10% glycerol and 10 mM β-mercaptoethanol. Subsequently, brain protein samples were heated for 5 min at 100°C for denaturation. A total of 10 µg protein per sample was loaded on 7.5% Tris-HCl acrylamide gels and then separated by sodium dodecyl sulfate polyacrylamide gel electrophoresis (SDS-PAGE) using the 20-cm Protean II xi cell system (Bio-Rad). Afterwards, protein samples were transferred onto a nitrocellulose membrane which was subsequently blocked in the presence of 5% nonfat milk powder, and then incubated overnight with primary antibodies at 4 °C. The following primary antibodies were used for blotting: rabbit polyclonal

anti-p-TrkB (Tyr706) in 5% BSA/TBS/tween-20 (1:200; Santa Cruz), rabbit polyclonal total TrkB (145 kDa) in 5% milk/TBS/tween-20 (1:1,000; Biovision), rabbit monoclonal anti-phospho-Akt (Ser473) in 5% milk/TBS/tween-20 (1:5000; sigma) and mouse monoclonal anti-beta actin (1:6000, Sigma). Secondary goat anti-mouse or anti-rabbit IgG-horseradisch antibodies (CalBiochem) were used for immune protein detection with the ECL plus chemiluminescence system (Perkin Elmer) together with X-Omat Blue films (Kodak). The intensity of immunoblotted target proteins was quantified with ImageJ software (NIH).

Slice preparation

Mecp2$^{-/y}$ mice and wild-type littermates in C57BL/6J strain at the age of 4–5 weeks were deeply anesthetized with isoflurane and decapitated according to protocols approved by the UCLA Chancellor's Animal Research Committee. Specifically, animal brains were quickly removed and transferred into 4°C in a sodium-free cutting solution containing the following (in mM): 135 *N*-methyl-D-glucamine, 26 HEPES, 10 D-glucose, 4 MgCl2, 1.2 KH2PO4, 1 KCl, and 0.5 CaCl2 (bubbled with 100% O2, pH 7.4, 290–300 mOsm). Coronal sections of 350 μm were cut at frontal neocortex in the same sodium-free solution using a Leica V1200S vibratome and transferred to an interface holding chamber, which contains standard artificial cerebrospinal fluid (ACSF) at 32°C containing the following (in mM): 126 NaCl, 26 HEPES, 10 D-glucose, 2.5 KCl, 2 MgCl2, 2 CaCl2, 1.25 NaH2PO4 (100% O2, pH 7.4, 290-300 mOsm). For spontaneous firing activity, the ACSF was modified as the follows: 3.5 mM KCl, 0.5 mM $MgCl_2$ in place of $MgSO_4$ and 1 mM $CaCl_2$. Osmolality was adjusted to 316-320 mOsm. After 30 min, the slices were subsequently maintained at room temperature (22–24°C) prior to recordings. Brain slices were transferred to a standard submerged recording chamber (Warner Instruments) at 32-34°C

and perfused at 3 ml/min with standard ACSF. The recording chamber was mounted on an upright microscope (Olympus-BX51WI, Olympus, Japan), equipped with 5x and 40x water immersion type objectives.

Whole-cell recordings

Somatic whole-cell recordings were obtained from visually identified L5 pyramidal cells, as described before (Dani et al 2005). Glass capillaries electrodes (4- to 6-MΩ resistance) were pulled from borosilicate patch pipettes (King Precision Glass). The recordings were always started 5 min after establishing the whole-cell configuration. Passive membrane properties and firing behavior of neurons were studied in current-clamp mode by injecting hyperpolarizing and depolarizing current steps through the recording electrodes. A current step of −100 pA was started, and then gradually increased the magnitude in steps of 30 pA. For the recordings of current-clamp mode, the intracellular solution contained (in mM): 140 K-gluconate, 8 KCl, 2 MgCl2, 4 Na2-ATP, 0.3 Na2-GTP, 10 HEPES, pH 7.25–7.30 adjusted with KOH (275–285 mOsm). For intrinsic excitability studies, DNQX (25 μM), D-AP5 (50 μM) and picrotoxin (100 μM) were added to block ionotropic glutamatergic and GABAergic transmission. All drugs were purchased from Sigma-Aldrich. Only cells with high seal resistance of >1 GΩ and a series resistance of <25 MΩ were included in the analysis. Series- and input-resistance were controlled before and after each recording, and the cells were discarded if one or both parameters changed more than 20% throughout the whole experiment. Data were acquired by using a Multiclamp 700B computer-controlled amplifier (Axon Instruments, Union City, CA, Molecular Devices) at 10 kHz and low-pass filtered at 4 kHz, and digitized at 4 kHz using a Digidata-1440.

Statistical analyses

All statistical analyses were performed using Prism 6.0c (GraphPad Software; La Jolla, CA). Except for survival curve, all of the data were presented as mean ± SEM. Statistical analysis was performed by either Student's t-test or one-way ANOVA followed by the Dunnett's *post hoc* multiple comparison tests. Kaplan Meier survival curves were generated and a log rank test was used to assess the statistical significance in the difference between the experimental group and control group. The level of significant difference was set for $P < 0.05$.

Results

7,8-DHF activated TrkB and downstream signaling pathway in wild-type mouse brain

To explore whether peripheral administration of 7,8-DHF could mimic BDNF and effectively activate TrkB receptors in mouse cortex and hippocampus, wild-type C57/BL6 mice were treated with either 7,8-DHF (5mg/kg or 25 mg/kg) or vehicle (30% DMSO/PBS) through intraperitoneal (i.p.) injection. Previous study suggested that activated TrkB phosphorylation induced by 7,8-DHF reached the peak level at 2 hours after i.p. injection and the drug displayed a robust neuroprotective effect with a dose of 5 mg/kg (Jang et al 2010). Thus 7,8-DHF with two different doses was administered to examine its dosage effect: low dose of 5mg/kg and high dose of 25 mg/kg. Immediately at 2 hour after i.p. injection, mouse cortex and hippocampus tissues were collected and prepared for immunoblotting to examine the TrkB phosphorylation and downstream Akt signaling pathway. As there was not much difference in the drug's effect between two dosages, low dose and high dose experiments were combined for the statistic analysis. As shown in **Fig 3.1 & Fig 3.2**, 7,8-DHF increased phosphorylation of TrkB compared to control brain tissues, which only received DMSO injection (169 ± 17% in combined 7,8-DHF group relatively to DMSO group; n=2)**.** The total of TrkB expression did not change between control and 7,8-DHF treated brain tissues (108 ± 8% in DMSO group, 103 ± 2% in low dose 7,8-DHF group and 116 ± 1% in high dose group; n=2 for each group). In addition, intraperitoneal injection of 7,8-DHF induced robust downstream Akt phosphorylation signaling pathway (283 ± 55% in combined 7,8-DHF group relatively to control DMSO group, n=4) and 7,8-DHF induced increase in p-Akt was statistically significant compared to control group (One tailed Student's t-test, $P < 0.05$). At last, there was no difference in beta-actin (β-actin) level between control and 7,8-DHF treatment groups (107 ± 0% in the treatment group compared to

Fig 3.1

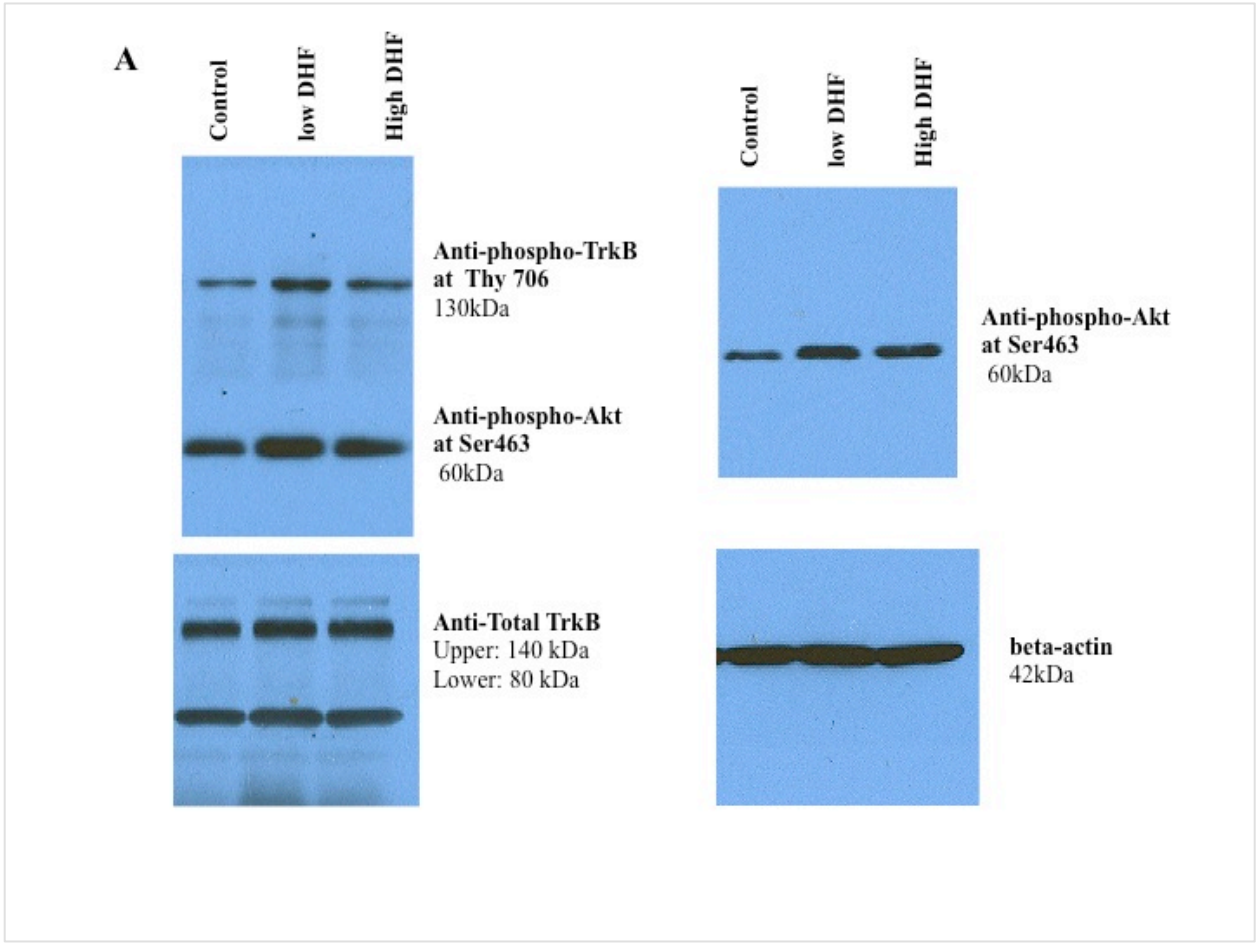

Fig 3.1 7,8-DHF activated TrkB receptors and downstream PI3/Akt signaling pathway in wild-type cortex and hippocampus tissues.

Representative immunoblotting for TrkB signaling. Wild-type C57/BL6 littermates were intraperitoneal injected with either DMSO, low dose of 7,8-DHF (5 mg/kg) or high dose of 7,8-DHF (25 mg/kg) at the age of 4-5 weeks. Mice were euthanized and cortex and hippocampus samples were collected at 2 h after peripheral administration. Western blotting conducted with the following antibodies as indicated: anti-phosphorylated TrkB, anti-phosphorylated Akt and anti-TrkB to examine TrkB receptors and Akt phosphorylation.

Fig 3.2

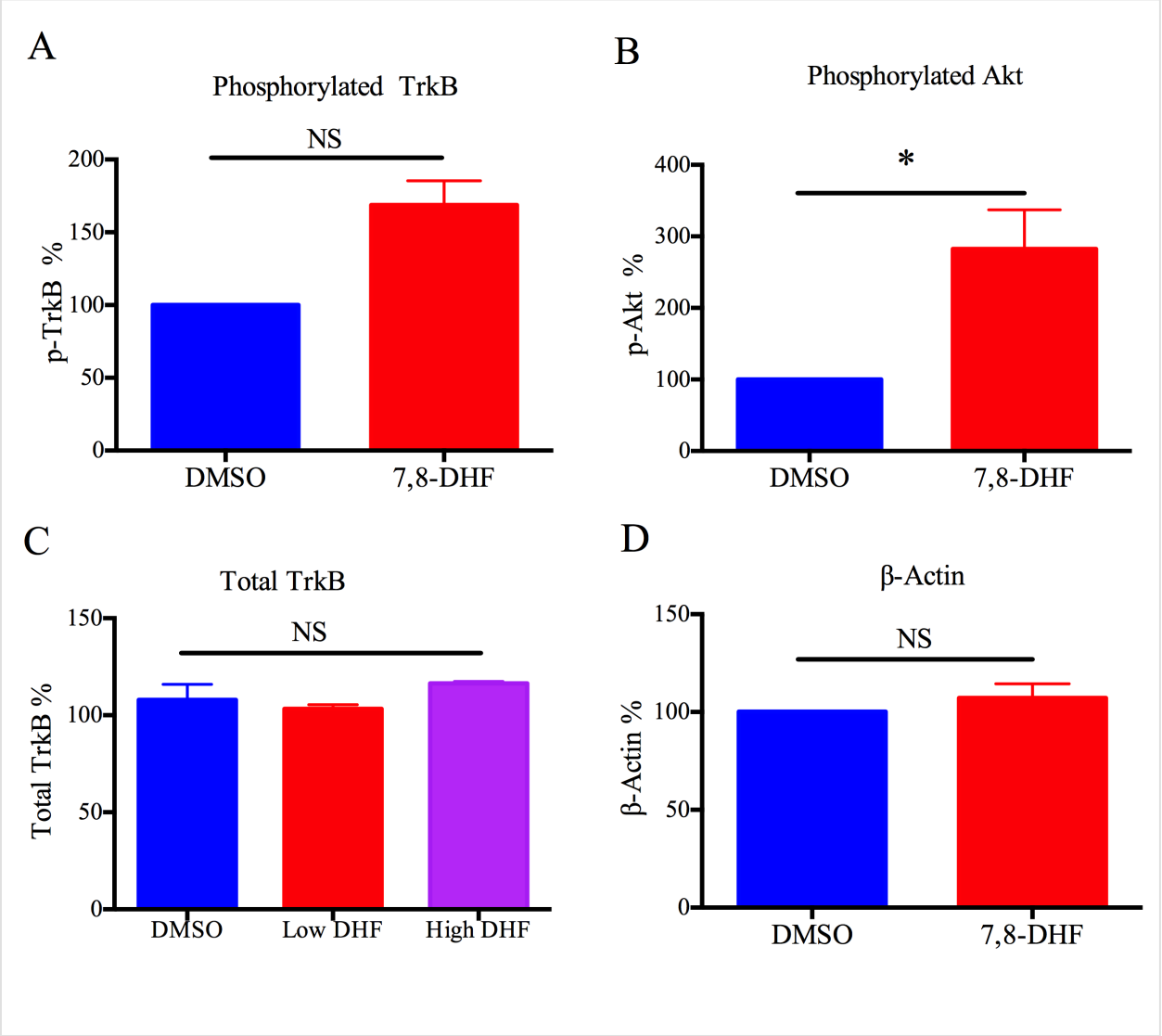

Fig. 3.2 Summarized quantification of immunoblotted protein intensity

Values were expressed as mean ± SE and normalized as relatively expression to control DMSO group (as 100%) from the same experiments to minimize the variation between immunoreaction.
A: phosphorylated TrkB (n=2 for each group)
B: phosphorylated Akt (n=4 for each group),
C: total TrkB (n=2 for each group) **D**: β-actin (n=2 for each group).

Student's t-tests (one tailed) were used for a comparison between control and treated groups for **A, B** & **D**. One-way ANOVA was used to analyze significance among three groups (**C**). * indicates significant difference at the level of $P < 0.05$. NS indicates $P > 0.05$.

DMSO group, n=2) as β-actin was used as loading control. I did many preliminary experiments to optimize western blot protocol for TrkB phosphorylation using mouse brain tissues. Eventually I was able to get clean and specific protein bands for phosphorylated Trk B at Tyr 706 and phosphorylated Akt at Ser 473. However, due to a small sample size (n=2 for each group, **Fig 3.2**), the phosphorylated TrkB from 7,8-DHF treated animals was not statistically significant from control group with Student's t-test. There was a significant increase in phosphorylated-Akt from 7,8-DHF treated group compared to control levels revealed by one tailed Student's t-test ($P < 0.05$). Taken together, these data suggested that treatment of 7,8-DHF with even low dose of 5 mg/kg might be sufficient to induce TrkB phosphorylation and downstream Akt phosphorylation in the cortex and hippocampus of mouse brain at 2 hours after peripheral injection.

Treatment with 7,8-DHF did not improve the lifespan of *Mecp2*$^{-/y}$ mice

Mecp2$^{-/y}$ mice exhibited a short life span and usually died at the age of 10-12 weeks. To examine whether peripheral administration of 7,8-DHF could extend or rescue the short life span that was common characteristic phenotype of *Mecp2* mutants, *Mecp2*$^{-/y}$ mice were treated with either 7,8-DHF (5 mg/kg) or vehicle (DMSO) at roughly 3 weeks of age through i.p. injection. To minimize stressful effects induced by animal handling, intraperitoneal injection was given to the mice twice a week and continued until the end of experiments. *Mecp2*$^{-/y}$ mice treated with 7,8-DHF (n=10, average survival time 80 ± 6 days) did not survive better compared to DMSO-treated *Mecp2*$^{-/y}$ littermates (n=9, 82 ± 6 days), as measured by Kaplan-Meier survival curves **(Fig 3.3A**, $P > 0.8$, log rank test). To further confirm the therapeutic efficacy of 7,8-DHF in RTT mouse model reported in previous study (Johnson et al 2012), 7,8-DHF was

administered to *Mecp2*$^{-/y}$ mice in drinking water immediately after weaning around 3 weeks of age. Compared to the control *Mecp2*$^{-/y}$ mice receiving only water (n=19, average survival time 88 ± 6 days), *Mecp2*$^{-/y}$ mice treated with 7,8-DHF in drinking water (n=17, average survival time 86 ± 5 days) did not live any longer (**Fig 3.3B**, $P > 0.4$, log rank test). In contrary to previous finding (Johnson et al 2012), these data suggested that chronic systematic administration of 7,8-DHF did not exert significant beneficial effect on the lifespan of *Mecp2*$^{-/y}$ mice, when administered through intraperitoneal injection or drinking water.

Fig 3.3 7,8-DHF treatment did not improve the life span of *Mecp2*$^{-/y}$ mice

A. Lifespan as measured by Kaplan-Meier survival curves showing the proportion of *Mecp2*$^{-/y}$ mice that survived (y axis) at each day after birth (x axis) for *Mecp2*$^{-/y}$ mice i.p. injected with 7,8-DHF (blue curve) and *Mecp2*$^{-/y}$ mice injected with DMSO (red curve). *Mecp2*$^{-/y}$ mice were treated with either 7,8-DHF (5 mg/kg) or DMSO twice every week following weaning until the end of studies. 7,8-DHF did not significantly extend the life expectancy of *Mecp2*$^{-/y}$ mice (7,8-DHF group, n=10; DMSO group n=9; $P > 0.8$, log rank test).

B. Lifespan as measured by Kaplan-Meier survival curves for *Mecp2*$^{-/y}$ mice administered with 7,8-DHF in drinking water (blue curve) and *Mecp2*$^{-/y}$ mice treated only with water (red curve). There were not significant difference in the lifespan of *Mecp2*$^{-/y}$ mice between treated group and control group (7,8-DHF group, n=19; control water group n=17; $P > 0.4$, log rank test).

Fig 3.3

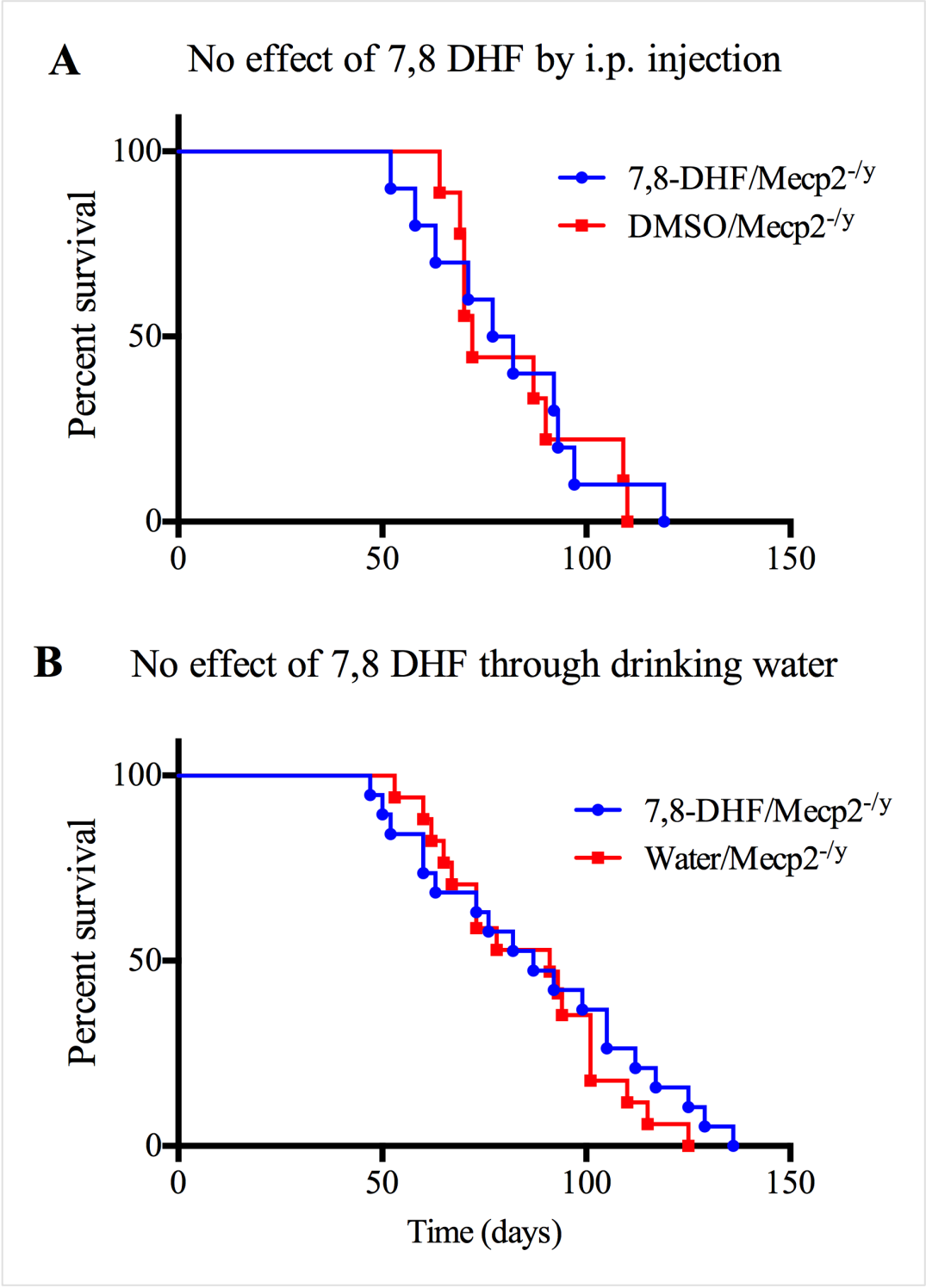
A
No effect of 7,8 DHF by i.p. injection
Percent survival
100
50
0
0
50
100
150
7,8-DHF/Mecp2-/y
DMSO/Mecp2-/y
B
No effect of 7,8 DHF through drinking water
Percent survival
100
50
0
0
50
100
150
Time (days)
7,8-DHF/Mecp2-/y
Water/Mecp2-/y

Reduced spontaneous activity in L5 pyramidal neurons in prefrontal cortex from *Mecp2*$^{-/y}$ mice

It was reported that *Mecp2*-mutant mice exhibited reduced cortical spontaneous activity in the layer 5 pyramidal neurons in the primary somatosensory cortex. The comprised neuronal function occurred even at 2 weeks of age in *Mecp2* mutant mice even before the appearance of classical behavioral symptoms and became progressive as difference in cortical firing rate between mutant and WT animals was more than doubled at 4-5 weeks of age (Dani et al 2005). Theses data indicated physiological abnormality preceded the onset of RTT-like symptoms in *Mecp2* mutant mice. As RTT brain displayed regional abnormalities in the frontal cortex including morphology alternations and volumetric reduction, L5 pyramidal neurons in prefrontal cortex from *Mecp2*$^{-/y}$ mice were examined for their physiological analyses. To confirm previous findings that cortical neuronal activity was disrupted due to loss of MeCP2 (Dani et al 2005), spontaneous action potential firing activity in layer V pyramidal neurons in prefrontal cortex dissected from *Mecp2*$^{-/y}$ and wild-type littermate controls at the age of 4-5 weeks was recorded and compared between two genotypes using whole-cell current-clamp recordings at physiological temperature 31-33°C **(Fig 3.4)**. As previously described (Dani et al 2005), modified ACSF solution containing reduced Ma^{2+}, Ca^{2+} and slightly elevated K^{+} was used for spontaneous firing recording and resting membrane potentials (interspike potential) was adjusted to -60 mV by injection of a small depolarizing current. *Mecp2*$^{-/y}$ neurons (1.6 ± 0.4 Hz, n=32) exhibited more than two-fold reduction in the mean firing rate compared to wild-type neurons (3.2 ± 0.4 Hz, n=22) revealed by student's t test (two tailed $P < 0.05$**)**. Thus, dysfunction of MeCP2 resulted in a significant decrease in the firing rate of L5 pyramidal neurons in prefrontal cortex from *Mecp2*$^{-/y}$ mice at the age of 4-5 weeks compared to their wild-type littermates.

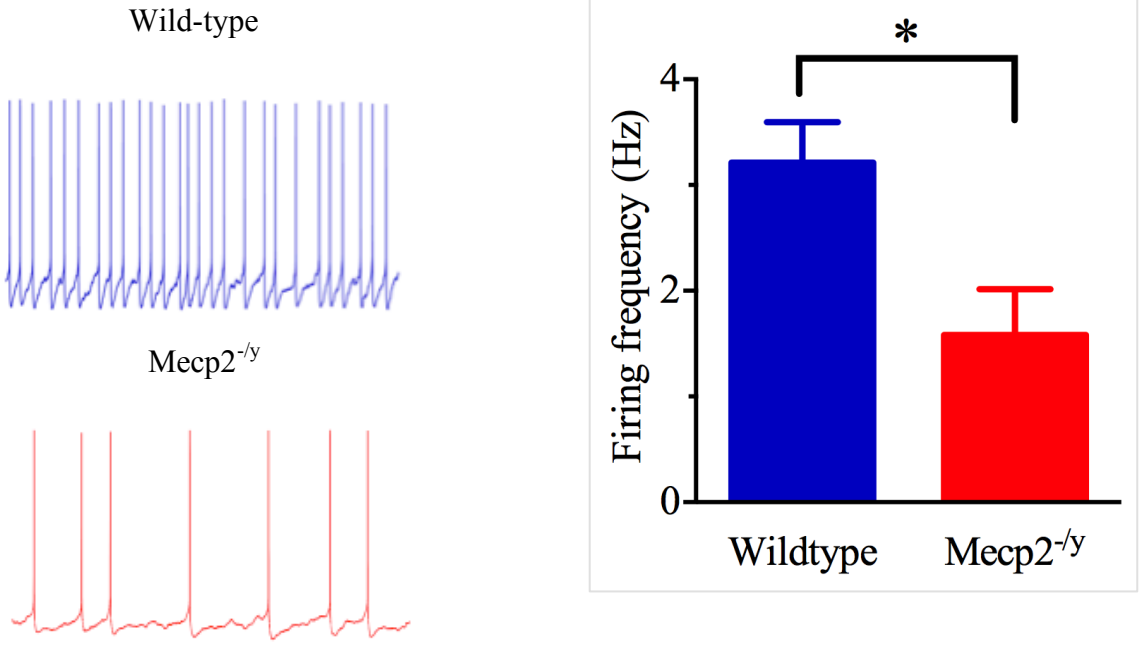

Fig 3.4 Reduced spontaneous firing rate of L5 pyramidal neurons in prefrontal cortex of *Mecp2*$^{-/y}$ mice, compared to wild-type littermate controls at the age of 4-5 weeks

Representative traces (left) for spontaneous firing frequency recorded at 31-33°C from a wild-type cortical neuron (top) and *Mecp2*$^{-/y}$ neuron (bottom).

Summarized bar graph (right) showed the average spontaneous firing rate of wild-type neurons (blue, n=32) and *Mecp2*$^{-/y}$ neurons (red, n=22). Unpaired Student's t-test revealed a significant reduction (> 2 fold) in mean firing frequency of mutant neurons, compared to wild-type neurons.

* indicates significant difference at the level of $P < 0.05$.

MeCP2 dysfunction did not affect intrinsic properties in prefrontal cortical neurons

Reduced neuronal activity in the cortex could attribute to reduced intrinsic electrical excitability of L5 pyramidal neurons or change in presynaptic transmission inputs onto these neurons. To examine whether intrinsic properties were altered in the *Mecp2*$^{-/y}$ mutant neurons, whole-cell current clamp recordings were performed in the presence of excitatory and inhibitory synaptic transmission blockers: picrotoxin (100 μM); D-AP5 (50 μM) and DNQX (25 μM) with standard ACSF to monitor electrical responses of L5 pyramidal neurons upon current injection. Action potentials were elicited in response to a series of depolarizing current steps with 30 pA increment and 1s duration and the resulting firing frequency were plotted as a function of injecting current amplitude (**Fig 3.5)**. Tow-way ANOVA followed by post hoc multiple comparison tests revealed there was no difference in the mean spike frequency upon current injection between two genotypes ($F_{5,60} = 0.17$, $P = 1.0$ for effect of interaction; $F_{1,60} = 0.20$, $P = 0.2$ for effect of genotype). In addition, the mean voltage threshold for triggering first spike upon current injection was identical to each other between wild-type (-36.7 ± 2.1mV, n=6) and *Mecp2*$^{-/y}$ cortical neurons (-38.8 ± 2.6 mV, n=6; $P > 0.05$). The input resistance measured routinely throughout the whole period of each recording was not altered between two genotypes (data not shown). These data together indicated that intrinsic electrical properties of L5 pyramidal neurons in the prefrontal cortex were not affected by MeCP2 mutation.

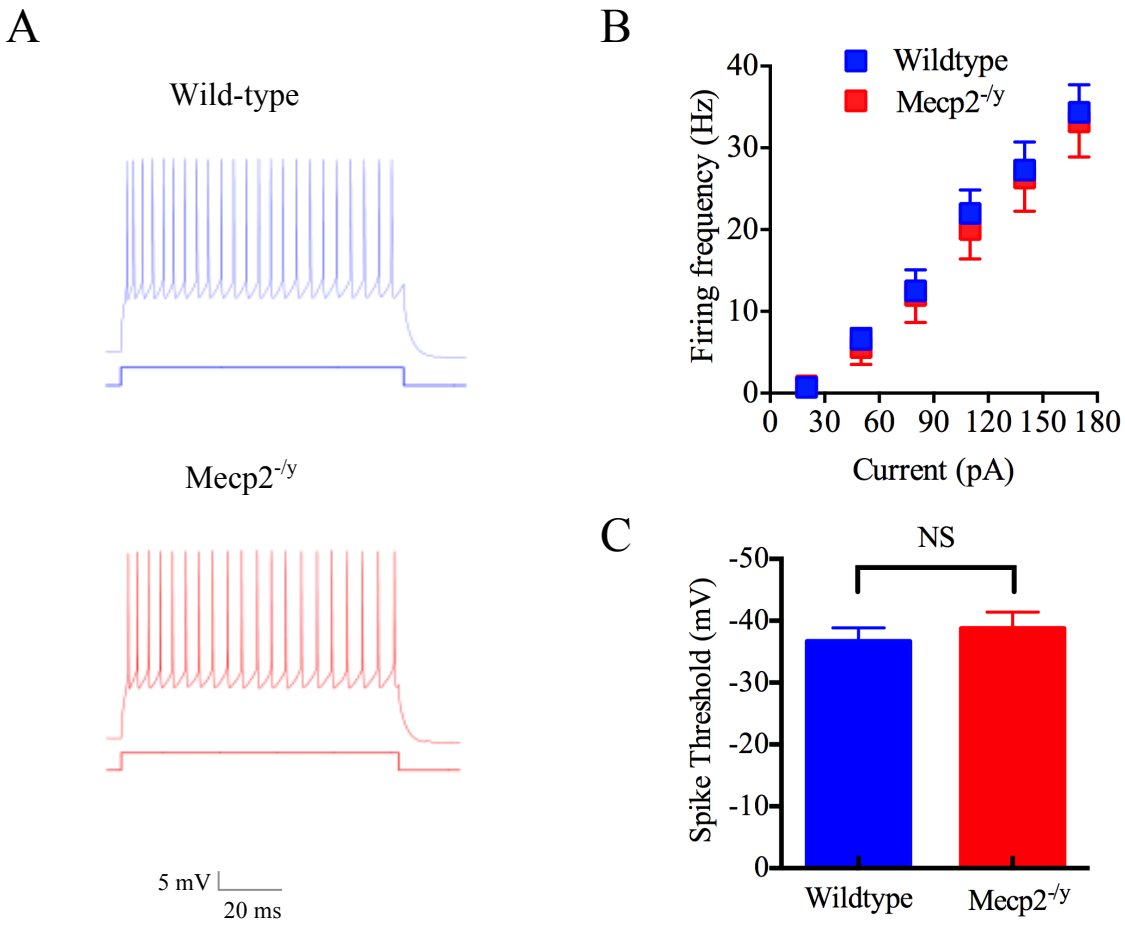

Fig 3.5 No change in intrinsic electrical properties of L5 pyramidal neurons in prefrontal cortex from *Mecp2*$^{-/y}$ mice at the age of 4-5 weeks

A. Representative sample traces of action potential in response to a depolarizing current step of 120 pA in a wild-type neuron (top) and mutant neuron (bottom).

B. No difference in the average firing frequency plotted as a function of injected current amplitudes between wild-type (blue) and mutant neurons (red) revealed by two-way ANOVA.

C. The mean voltage threshold for the first peak was not altered by MeCP2 mutation, analyzed by unpaired Student's t –test. NS indicates $P > 0.05$.

Differential effects of 7,8-DHF on spontaneous firing activity of L5 pyramidal neurons in prefrontal cortex from *Mecp2*$^{-/y}$ mice and wild-type littermates

The small molecule, 7,8-DHF was characterized to mimic BDNF through binding with TrkB receptor and triggering the downstream intracellular signaling cascades (Jiang et al 2013). 7,8-DHF was shown to exert neuroprotective effects against excitotoxicity and ischemic damage, rescue memory and cognitive deficits in aged animals (Chen et al 2011, Choi et al 2010, Devi & Ohno 2012). At the electrophysiology level, 7,8-DHF was found to modulate synaptic transmission and intrinsic neuronal excitability in the layer 2/3 of the mouse visual cortex (Marongiu et al 2013). To examine the rescuing effect of 7,8-DHF on spontaneous firing rate of L5 pyramidal neurons in prefrontal cortex of MeCP2 mutants, cortical slices dissected from *Mecp2*$^{-/y}$ mice and wild-type littermates were incubated for at least 30 minutes with 50μM 7,8-DHF to determine the drug's effect on spontaneous activity for both genotypes using whole-cell patch-clamp recordings in current clamp mode. As shown in **Fig 3.6**, a significant increase in the spontaneous firing frequency was observed in *Mecp2*$^{-/y}$ cortical neurons after treatment with 7,8-DHF (3.3 ± 0.5 Hz, n=6) compared to untreated *Mecp2*$^{-/y}$ cortical neurons (1.8 ± 0.5 Hz, n=6), as revealed by unpaired Student's t-test (one tailed $P < 0.05$). In the contrary, incubation with 7,8-DHF caused an increase in the spontaneous firing rate in wild-type cortical neurons (3.9 ± 0.5 Hz, n=8) compared to untreated wild-type neurons (2.8 ± 0.3, n=8); however, unpaired Student's t-test suggested this increase in the spontaneous firing rate was not yet statistically significant compared to untreated wild-type neurons (one tailed P =0.051). I believe the increase with wild-type neurons will eventually reach the statistical significance if include a large sample size. These data clearly indicated a differential effect of 7,8-DHF on spontaneous firing activity between wild-type and *Mecp2*$^{-/y}$ cortical neurons.

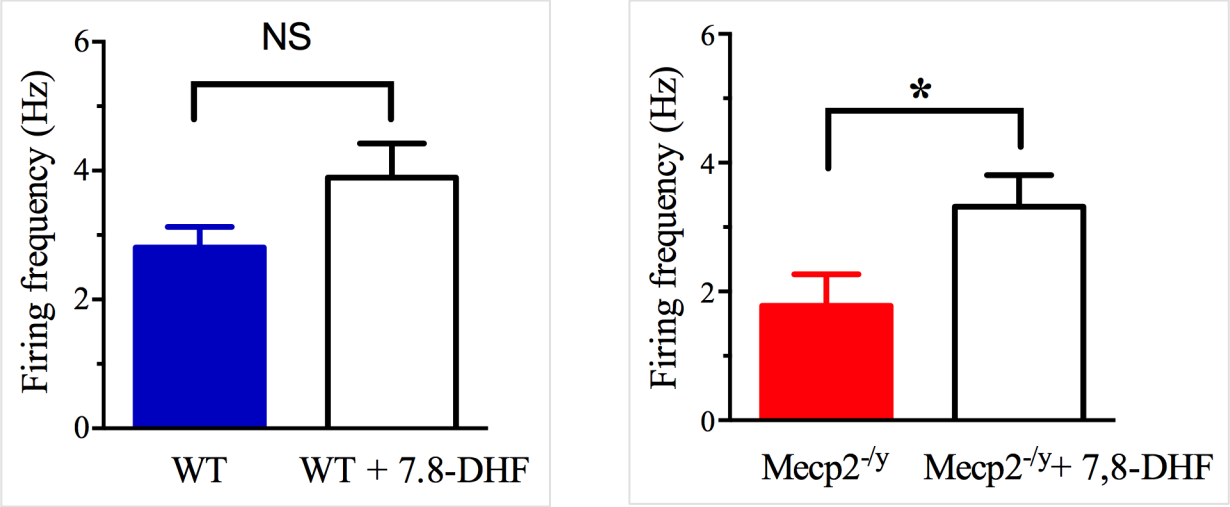

Fig 3.6 7,8-DHF enhanced spontaneous firing frequency of *MeCP2*$^{-/y}$ cortical neurons

Prior to treatment with 7,8-DHF, spontaneous firing activity was recorded on L5 pyramidal neurons from either wild-type controls or *MeCP2*$^{-/y}$ cortical slices as a baseline. Subsequently, 7,8-DHF (50 µM) was added into modified ACSF and perfused with cortical neurons for at least 30 min and spontaneous firing rate was recorded again to compare the drug's treatment effects on both genotypes.

A. Wild-type neurons (n=8) exhibited an increase in spontaneous firing frequency after 30 min incubation with 7,8-DHF. However, this increase was not yet statistically significant analyzed by unpaired Student's t-test (one tailed $P = 0.051$).

B. Spontaneous firing frequency in *MeCP2*$^{-/y}$ cortical neurons (n=6) was significantly increased after 30 min incubation with 7,8-DHF revealed by unpaired Student's t test (one tailed $P < 0.05$). * indicates significant difference $P < 0.05$.

Discussion

7,8-DHF is a recently identified TrkB receptor agonist with potent neurotrophic activities mimicking BDNF signaling. The present study was originally proposed to examine whether 7,8-DHF could display therapeutic effects to improve and rescue RTT-related phenotypes with MeCP2 mutant mouse model for RTT. Current data demonstrated that systematic administration of 7,8-DHF activated the phosphorylation of TrkB receptors and generated robust downstream Akt signaling in cortex and hippocampus tissues from wild-type C57B/L mice. At the neurophysiological level, MeCP2 dysfunction caused a significant reduction in spontaneous firing activity of pyramidal neurons in prefrontal cortex and this decrease was not caused by a change in the intrinsic properties of the recorded neurons, as suggested by previous studies. Incubation of acute cortical slices with 7,8-DHF significantly enhanced the spontaneous firing rate in L5 pyramidal neurons of *Mecp2*$^{-/y}$ mice. However, systematic administration of 7,8-DHF did not improve the life span of *Mecp2*$^{-/y}$ mice, at least through either intraperitoneal injection or drinking water.

Recovering BDNF expression in mutant *Mecp2*$^{-/y}$ mice appeared to ameliorate many of RTT-like phenotypes (Chang et al 2006, Kline et al 2010); however, BDNF is very limited for therapeutic approaches for RTT because of its inability to cross the BBB and a short half-life. 7.8-DHF was considered as a small molecule and potent TrkB agonist (Jang et al 2010). It was reported that both intraperitoneal injection and adding 7,8-DHF in drinking water induced robust TrkB phosphorylation, downstream Akt and MAPK signaling pathway indicating that either this compound or its metabolites were capable to cross the blood-brain barrier and activate TrkB receptors in the mouse cortex and hippocampus. The present study highlighted the previous

findings that systematic administration of 7,8-DHF with a low dose of 5 mg/kg was able to activate downstream PI3/Akt phosphorylation in wild-type mouse cortex and hippocampus. Although, the increase in phosphorylated TrkB expression following 7,8-DHF injection was not statistically significant yet, probably due to a small sample size (n=2)**.** In summary, the western blot experiments strongly indicated that 7,8-DHF induced TrkB activation and robust downstream phosphor-Akt expression in mouse cortex and hippocampus tissues within 2 hours after intraperitoneal injection (**Fig 3.1 & 3.2)**

The neurophysiological consequences of MeCP2 dysfunction were illustrated in a few of previous studies (Chang et al 2006, Dani et al 2005, Dani & Nelson 2009, Wood et al 2009). These studies demonstrated a significant reduction in spontaneous action potential firing rate in the layer V pyramidal neurons of primary somatosensory cortex in MeCP2 mutant mice using whole cell patch recordings. Being consistent with those previous findings, the current study using whole-cell current–clamp recordings discovered that 1) spontaneous firing activity in prefrontal cortex pyramidal neurons was significantly reduced in *MeCP2*$^{-/y}$ mice, compared to their wild-type littermates **(Fig 3.4)**; 2) the intrinsic electrical properties of MeCP2 mutant cortical neurons were not affected by the absence of MeCP2 **(Fig 3.5)**. Reduced circuit excitability could arise from decreased excitatory or increased inhibitory presynaptic transmission onto these pyramidal neurons. Previous studies also demonstrated such alternations including reduced excitatory synaptic transmission and increased inhibitory synaptic signaling in the somatosensory cortex due to the loss of MeCP2 function. It was believed that MeCP2 dysfunction induced a shift of the homeostatic balance between excitation and inhibition (E/I) leading to enhanced inhibition in the cortex (Dani et al 2005, Wood et al 2009).

As shown in **Fig 3.6,** incubation of acute cortical slices with 7,8-DHF for 30 min induced a significant increase in spontaneous firing rate in MeCP2 mutant cortical neurons revealed by one-tailed unpaired Student's t-test. 7,8-DHF also increased the spontaneous firing frequency in wild-type neurons; however, this increase was not yet able to reach statistical significance level compared to untreated wild-type neurons (P = 0.051). These data at least suggested a differential effect of 7,8-DHF on spontaneous firing rate of cortical neurons between two genotypes. MeCP2 mutant neurons, relative to wild-type neurons appeared to be more sensitive in response to 7,8-DHF. The precise mechanism of 7,8-DHF effects has been clarified at the cellular level. It was recently reported that 7,8-DHF exerted modulatory effects on synaptic transmission and intrinsic neuronal properties using whole cell patch clamp recordings from layer 2/3 pyramidal neurons of mouse visual cortex. Specifically, 7,8-DHF increased neuronal excitability and caused a selective reduction in the strength of GABAergic inhibition, but did not change the glutamatergic transmission in pyramidal neurons of mouse visual cortex (Marongiu et al 2013). In consideration of the fact that MeCP2 deficiency resulted in a change in E/I balance in favor to inhibition in the cortex particularly, I would speculate that 7,8-DHF may have a great therapeutic potential to reverse the phenotypes such as: reduced spontaneous neuronal excitability and imbalanced synaptic transmission, that were characteristic features of cortical synaptic dysfunction caused by MeCP2 mutation.

At last, the lifespan experiments to examine the rescuing effects of 7,8-DHF on the survival of *Mecp2*$^{-/y}$ mutants were not successful and I was unable to replicate the positive findings from previous study (Johnson et al 2012). Results from Johnson et al 2012 demonstrated that administration of 7,8-DHF in drinking water significantly decreased the severity of disease phenotypes and progression in *Mecp2*$^{-/y}$ mice, including improvement in life span and body

weight, and rescue of motor dysfunction and breathing abnormalities. In their studies, *Mecp2*$^{-/y}$ mice were treated with the drug in drinking water starting at 4 weeks of age and 7,8-DHF significantly extended the lifespan of mutant mice from 66 ± 2 days to 80 ± 4 days ($P < 0.003$, log rank test). I followed the same protocols for systematic administration of 7,8-DHF through drinking water and conducted experiments with the same mutant strain (Mecp2$^{tm1.1Jae}$) in my study; however, I did not observe any improvement in the life span of *Mecp2*$^{-/y}$ mice between 7,8-DHF treated group and control group **(Fig 3.3)**. In addition, data from intraperitoneal injection experiments showed that the average survival time of *Mecp2*$^{-/y}$ mice treated with 7,8-DHF was 80 ± 6 days and that treated with DMSO injection was 82 ± 6 days. For 7,8-DHF added in drinking water experiments, the average survival time of *Mecp2*$^{-/y}$ mice treated with 7,8-DHF in drinking water was 88 ± 6 days and that in water only group was 86 ± 5 days. B y comparing these survival numbers, it brought to my attention that the average lifespan in non-treatment *Mecp2*$^{-/y}$ mice group from my studies (86 ± 5 days, n=17) was almost the same as that in 7,8-DHF treatment group (80 ± 4 days, n=32) after I combined treatment data together into one treatment group and one control group. However, the mean lifespan in non-treated *Mecp2*$^{-/y}$ group from my study was significantly longer than that from Johnson et al 2012 (66 ± 2 days, n=35). It suggested that *Mecp2*$^{-/y}$ mice from control non-treated group (Johnson et al 2012) displayed a much shorter lifespan (66 ± 2 days). In addition, I applied two different treatment methods: intraperitoneal injection and adding into drinking water for systematic administration of 7,8-DHF in the current study. Neither one display any beneficial effect to improve the survival rate of *Mecp2*$^{-/y}$ mutant mice. In addition, Andrew Pieper's lab from University of Texas Southwestern Medical Center also conducted the same experiments to examine the rescuing effects of 7,8-DHF on the lifespan of *Mecp2*$^{-/y}$ mice, but did not find any

positive results (personal communication). Although, a few of studies indicated that 7,8-DHF and its synthetic derivative displayed beneficial effects in mouse models of stress, depression, aging and neurodegenerative diseases including Parkinson's disease, Alzheimer's disease, Huntington's disease and amyotropical lateral sclerosis (ALS) (Jang et al 2010, Jiang et al 2013, Korkmaz et al 2014, Liu et al 2010, Liu et al 2013, Zhang et al 2014), it might still need additional experiments using different *Mecp2* mutant models or alternative administration methods, such as oral gavage or osmatic pump, to validate the *in vivo* effects of 7,8-DHF and its derivatives on major RTT-related phenotypes in animal models.

References

Andero R, Daviu N, Escorihuela RM, Nadal R, Armario A. 2012. 7,8-dihydroxyflavone, a TrkB receptor agonist, blocks long-term spatial memory impairment caused by immobilization stress in rats. *Hippocampus* 22: 399-408

Andero R, Heldt SA, Ye K, Liu X, Armario A, Ressler KJ. 2011. Effect of 7,8-dihydroxyflavone, a small-molecule TrkB agonist, on emotional learning. *Am J Psychiatry* 168: 163-72

Chang Q, Khare G, Dani V, Nelson S, Jaenisch R. 2006. The disease progression of Mecp2 mutant mice is affected by the level of BDNF expression. *Neuron* 49: 341-8

Chen J, Chua KW, Chua CC, Yu H, Pei A, et al. 2011. Antioxidant activity of 7,8-dihydroxyflavone provides neuroprotection against glutamate-induced toxicity. *Neuroscience letters* 499: 181-5

Choi DC, Maguschak KA, Ye K, Jang SW, Myers KM, Ressler KJ. 2010. Prelimbic cortical BDNF is required for memory of learned fear but not extinction or innate fear. *Proceedings of the National Academy of Sciences of the United States of America* 107: 2675-80

Dani VS, Chang Q, Maffei A, Turrigiano GG, Jaenisch R, Nelson SB. 2005. Reduced cortical activity due to a shift in the balance between excitation and inhibition in a mouse model of Rett syndrome. *Proceedings of the National Academy of Sciences of the United States of America* 102: 12560-5

Dani VS, Nelson SB. 2009. Intact long-term potentiation but reduced connectivity between neocortical layer 5 pyramidal neurons in a mouse model of Rett syndrome. *The Journal of neuroscience : the official journal of the Society for Neuroscience* 29: 11263-70

Devi L, Ohno M. 2012. 7,8-dihydroxyflavone, a small-molecule TrkB agonist, reverses memory deficits and BACE1 elevation in a mouse model of Alzheimer's disease. *Neuropsychopharmacology : official publication of the American College of Neuropsychopharmacology* 37: 434-44

Harborne JB, Williams CA. 2000. Advances in flavonoid research since 1992. *Phytochemistry* 55: 481-504

Jang SW, Liu X, Yepes M, Shepherd KR, Miller GW, et al. 2010. A selective TrkB agonist with potent neurotrophic activities by 7,8-dihydroxyflavone. *Proceedings of the National Academy of Sciences of the United States of America* 107: 2687-92

Jiang M, Peng Q, Liu X, Jin J, Hou Z, et al. 2013. Small-molecule TrkB receptor agonists improve motor function and extend survival in a mouse model of Huntington's disease. *Hum Mol Genet* 22: 2462-70

Johnson RA, Lam M, Punzo AM, Li H, Lin BR, et al. 2012. 7,8-dihydroxyflavone exhibits therapeutic efficacy in a mouse model of Rett syndrome. *J Appl Physiol (1985)* 112:

704-10

Kline DD, Ogier M, Kunze DL, Katz DM. 2010. Exogenous brain-derived neurotrophic factor rescues synaptic dysfunction in Mecp2-null mice. *The Journal of neuroscience : the official journal of the Society for Neuroscience* 30: 5303-10

Korkmaz OT, Aytan N, Carreras I, Choi JK, Kowall NW, et al. 2014. 7,8-Dihydroxyflavone improves motor performance and enhances lower motor neuronal survival in a mouse model of amyotrophic lateral sclerosis. *Neuroscience letters* 566: 286-91

Larimore JL, Chapleau CA, Kudo S, Theibert A, Percy AK, Pozzo-Miller L. 2009. Bdnf overexpression in hippocampal neurons prevents dendritic atrophy caused by Rett-associated MECP2 mutations. *Neurobiol Dis* 34: 199-211

Li W, Pozzo-Miller L. 2014. BDNF deregulation in Rett syndrome. *Neuropharmacology* 76 Pt C: 737-46

Liu X, Chan CB, Jang SW, Pradoldej S, Huang J, et al. 2010. A synthetic 7,8-dihydroxyflavone derivative promotes neurogenesis and exhibits potent antidepressant effect. *J Med Chem* 53: 8274-86

Liu X, Qi Q, Xiao G, Li J, Luo HR, Ye K. 2013. O-methylated metabolite of 7,8-dihydroxyflavone activates TrkB receptor and displays antidepressant activity. *Pharmacology* 91: 185-200

Maher P, Akaishi T, Abe K. 2006. Flavonoid fisetin promotes ERK-dependent long-term potentiation and enhances memory. *Proceedings of the National Academy of Sciences of the United States of America* 103: 16568-73

Marongiu D, Imbrosci B, Mittmann T. 2013. Modulatory effects of the novel TrkB receptor agonist 7,8-dihydroxyflavone on synaptic transmission and intrinsic neuronal excitability in mouse visual cortex in vitro. *European journal of pharmacology* 709: 64-71

Nagahara AH, Tuszynski MH. 2011. Potential therapeutic uses of BDNF in neurological and psychiatric disorders. *Nat Rev Drug Discov* 10: 209-19

Ricciardi S, Boggio EM, Grosso S, Lonetti G, Forlani G, et al. 2011. Reduced AKT/mTOR signaling and protein synthesis dysregulation in a Rett syndrome animal model. *Hum Mol Genet* 20: 1182-96

Spencer JP. 2008. Food for thought: the role of dietary flavonoids in enhancing human memory, learning and neuro-cognitive performance. *Proc Nutr Soc* 67: 238-52

Vauzour D, Vafeiadou K, Rice-Evans C, Williams RJ, Spencer JP. 2007. Activation of pro-survival Akt and ERK1/2 signalling pathways underlie the anti-apoptotic effects of flavanones in cortical neurons. *J Neurochem* 103: 1355-67

Wood L, Gray NW, Zhou Z, Greenberg ME, Shepherd GM. 2009. Synaptic circuit abnormalities

of motor-frontal layer 2/3 pyramidal neurons in an RNA interference model of methyl-CpG-binding protein 2 deficiency. *The Journal of neuroscience : the official journal of the Society for Neuroscience* 29: 12440-8

Zhang Z, Liu X, Schroeder JP, Chan CB, Song M, et al. 2014. 7,8-dihydroxyflavone prevents synaptic loss and memory deficits in a mouse model of Alzheimer's disease. *Neuropsychopharmacology : official publication of the American College of Neuropsychopharmacology* 39: 638-50

Nagahara AH, Tuszynski MH. 2011. Potential therapeutic uses of BDNF in neurological and psychiatric disorders. *Nature reviews. Drug discovery* 10: 209-19

Ricciardi S, Boggio EM, Grosso S, Lonetti G, Forlani G, et al. 2011. Reduced AKT/mTOR signaling and protein synthesis dysregulation in a Rett syndrome animal model. *Human molecular genetics* 20: 1182-96

Spencer JP. 2008. Food for thought: the role of dietary flavonoids in enhancing human memory, learning and neuro-cognitive performance. *The Proceedings of the Nutrition Society* 67: 238-52

Vauzour D, Vafeiadou K, Rice-Evans C, Williams RJ, Spencer JP. 2007. Activation of pro-survival Akt and ERK1/2 signalling pathways underlie the anti-apoptotic effects of flavanones in cortical neurons. *Journal of neurochemistry* 103: 1355-67

Zhang Z, Liu X, Schroeder JP, Chan CB, Song M, et al. 2014. 7,8-dihydroxyflavone prevents synaptic loss and memory deficits in a mouse model of Alzheimer's disease. *Neuropsychopharmacology : official publication of the American College of Neuropsychopharmacology* 39: 638-50